

HRV Analysis and Personal Identification Using Bathtub ECG in Different Water Temperatures

XU Jianbo

A DISSERTATION
SUBMITTED IN FULFILLMENT OF THE REQUIREMENTS
FOR THE DEGREE OF DOCTOR OF PHILOSOPHY
IN COMPUTER SCIENCE AND ENGINEERING

Graduate Department of Computer and Information Systems

The University of Aizu

2022



© Copyright by XU Jianbo, March 2022

All Rights Reserved.

The dissertation titled

*HRV Analysis and Personal Identification Using Bathtub ECG in
Different Water Temperatures*

by

XU Jianbo

is reviewed and approved by:

Main referee

Professor

CHEN Wenxi

2022/2/14
Wenxi Chen



Senior Associate Professor

ZHU Xin

Xin Zhu 2022/2/14



Associate Professor

HISADA Yasuhiro

HISADA Yasuhiro 2022/2/14



Professor

PAIK Incheon

Incheon Paik 2022/2/14



THE UNIVERSITY OF AIZU

March 2022

Contents

List of Figures	vi
List of Tables	viii
List of Abbreviations	ix
Abstract	x
Acknowledgment	xii
Chapter 1 Introduction	1
1.1 Historical Overview of HRV	1
1.2 Influencing Factors of HRV	2
1.3 HRV Analysis Techniques	2
1.3.1 Linear Analysis	2
1.3.1.1 Time Domain	2
1.3.1.2 Frequency Domain	3
1.3.1.3 Time-Frequency Domain	3
1.3.2 Non-linear Analysis	3
1.3.3 Statistical Analysis	3
1.3.3.1 Clustering Analysis	7
1.3.3.2 Variance Analysis	7
1.4 Personal Identification	7
1.4.1 Non-biometric Methods	7
1.4.2 Biometric Methods	8
1.5 ECG-based Personal Identification	12
1.6 Artificial Neural Network	14
1.6.1 Convolutional Neural Network	14
1.6.2 Recurrent Neural Network	15
1.7 Motivation of This Study	15
1.8 Structure of This Dissertation	16
Chapter 2 Measurement of Bathtub ECG	18
2.1 Historical Overview of Bathtub ECG	18
2.2 Measurement System	20
Chapter 3 HRV Analysis	24
3.1 Introduction	24
3.1.1 HRV and Age/Gender	25
3.1.2 HRV and Diseases	25

3.1.3	HRV and Stress	25
3.1.4	HRV and Sleep	26
3.1.5	HRV and Other Factors	26
3.2	Motivation	27
3.3	Method	27
3.3.1	ECG Processing	27
3.3.2	HRV Parameters	30
3.3.3	Statistical Analysis	33
3.4	Results and Discussion	33
3.5	Conclusion	35
Chapter 4 Personal Identification		40
4.1	Introduction	40
4.2	Improvement of Personal Identification Rate	41
4.2.1	Methods and Materials	42
4.2.1.1	Subjects and ECG Recordings	42
4.2.1.2	Data Processing and Analysis	42
4.2.1.3	Data Structure and CNN Model Design	44
4.2.2	Results and Discussion	47
4.2.3	Conclusions and Future Work	51
4.3	RNN-based Personal Identification	56
4.3.1	Methods and Materials	58
4.3.1.1	Data Processing and Analysis	58
4.3.1.2	Data Structure and Classification Model Design	60
4.3.2	Results and Discussion	62
4.3.3	Conclusion and Future Work	62
4.4	Number of Heartbeats and Personal Identification Rate	64
4.4.1	Motivation	64
4.4.2	Methods and Materials	66
4.4.2.1	Features Extraction	66
4.4.2.2	Identification	66
4.4.3	Results and Discussion	69
4.4.4	Conclusion and Future Work	75
Chapter 5 Results and Discussion		77
Chapter 6 Conclusions and Future Work		80
6.1	Conclusions	80
6.2	Future Work	80

List of Figures

Fig. 1.1	Non-biometric methods.	9
Fig. 1.2	Behavioral biometrics methods.	10
Fig. 1.3	Physical biometrics methods.	11
Fig. 1.4	Structure of this dissertation.	17
Fig. 2.1	A bathtub system with electrodes for monitoring ECG [1].	19
Fig. 2.2	Typical recording of ECG signal obtained by the bathtub system (red lines) and by the conventional methods (blue lines) [1].	20
Fig. 2.3	Connection of four limb leads.	21
Fig. 2.4	ECG monitor: OpenBCI Ganglion Biosensing Board.	21
Fig. 2.5	ECG collection system.	21
Fig. 2.6	Bath water and bath room temperature monitor.	22
Fig. 2.7	Profiles of bath water temperature from one subject during bathing under five conditions.	23
Fig. 3.1	Flowchart for the ECG processing, HRV feature calculation, and statistical analysis.	28
Fig. 3.2	Spectrum analysis result.	29
Fig. 3.3	Noise removed HRV signal.	31
Fig. 3.4	Output of ECG processing in each step.	32
Fig. 3.5	Comparison of the cleaned RRI and resampled RRI.	34
Fig. 3.6	Feature trends for 20 HRV features in three analysis domains under three WT conditions.	36
Fig. 3.7	Analysis of significant differences for 20 HRV features in three analysis domains under three WT conditions: A = (36–38) °C, B = (38–40) °C, and C = (40–42) °C.	37
Fig. 4.1	Main components of the normal ECG waveform.	42
Fig. 4.2	Process of the ECG decomposition and reconstruction.	43
Fig. 4.3	Comparison of RRI in different WTs (A to J represents each subject, L represents low water temperature, H represents high water temperature).	45
Fig. 4.4	Comparison of R peaks amplitude in different WTs (A to J represents each subject, L represents low water temperature, H represents high water temperature).	46
Fig. 4.5	28 1D QRS complexes to 2D QRS imaging.	47
Fig. 4.6	CNN model.	48
Fig. 4.7	Varieties of accuracy based on different training epoch.	51
Fig. 4.8	Confusion matrix of test result based on low WT.	52
Fig. 4.9	Confusion matrix of test result based on high WT.	53

Fig. 4.10	ROC curve of low WT based on different training epoch. . .	54
Fig. 4.11	ROC curve of high WT based on different training epoch. . .	55
Fig. 4.12	Components of one layer in the whole RNN architecture. . .	57
Fig. 4.13	Flowchart of data processing and personal identification. . .	59
Fig. 4.14	Magnitude response.	60
Fig. 4.15	Noise removal and signal smoothing process.	61
Fig. 4.16	1-D QRS complex to 2-D binary image.	67
Fig. 4.17	CNN model.	68
Fig. 4.18	Confusion matrix of the validation result based on first recog- nition stage.	70
Fig. 4.19	Variety of mean recognition rate based on different testing ECG length.	73
Fig. 4.20	Variation in recognition rate for each subject.	74

List of Tables

Tab. 1.1	HRV time domain measures.	4
Tab. 1.2	HRV frequency domain measures.	5
Tab. 1.3	HRV nonlinear domain measures.	6
Tab. 3.1	The statistic results of the HRV features based on different bathtub WT.	38
Tab. 4.1	Test result based on low WT.	49
Tab. 4.2	Test result based on high WT.	50
Tab. 4.3	Varieties of AUC based on different training epoch.	51
Tab. 4.4	Detailed parameters of LSTM networks.	60
Tab. 4.5	Dataset and validation accuracy.	63
Tab. 4.6	Validation result.	71

List of Abbreviations

HR	Heart Rate
HRV	Heart Rate Variability
RRI	R R Interval
ECG	Electrocardiogram
DFT	Discrete Fourier Transform
DWT	Discrete Wavelet Transform
PSD	Power Spectral Density
IIR	Infinite Impulse Response
ANN	Artificial Neural Network
CNN	Convolutional Neural Network
RNN	Recurrent Neural Network
DL	Deep Learning
FFT	Fast Fourier Transform
AR	Autoregressive
ULF	Ultra Low Frequency
VLF	Very Low Frequency
LF	Low Frequency
HF	High Frequency
TP	Total Power
ROC	Receiver Operating Characteristic
AUC	Area Under Curve

Abstract

This study aims to explore the heart rate variability (HRV) and personal identification using the electrocardiogram (ECG) at different water temperatures (WTs) during bathing. There are ten subjects in the experiment, including five males and five females. The ECG is collected at five WT conditions, which are 37 ± 0.5 °C, 38 ± 0.5 °C, 39 ± 0.5 °C, 40 ± 0.5 °C and 41 ± 0.5 °C, respectively. Three ECG recordings are collected using the non-contacts electrodes at each preset WT condition for each subject. Each recording is 18 minutes long, the sampling rate is 200 Hz. Finally, we collect 150 ECG recordings and 150 WT recordings during bathing. To perform the HRV analysis, 1-minute ECG segment is used each time. Twenty HRV features which including the time domain, frequency domain, and the non-linear domain measures are calculated. The variety of the measured HRV features is analyzed using the k-means clustering analysis method based the preset WT conditions during bathing. What's more, the mean, standard deviation (SD), and significant differences of the measured HRV features based on the WT conditions are calculated. The experimental result shows that with increasing WT, the HRV features of pLF, LF/HF, HR, and SD1/SD2 are monotonously and significantly ($p < 0.05$) increased, and the D_2 , HF power, total power, pHF, mean RRI, SDNN, RMSSD, SDDSD, AURRI, SD1, and SD2 are monotonously and significantly ($p < 0.05$) decreased. Therefore, we confirm that the WT has an important impact on the HRV. To accurately and quickly perform personal identification using ECG at different WTs, firstly, we explore how to improve the personal identification performance. We notice that increasing the diversity of training samples can greatly improve the identification rate. Compare to the previous study, the accuracy based on low WT is increasing from 12.17% to 90.49%, and the accuracy based on high WT is increasing from 13.33% to 90.00%. Both of the two accuracy increased approximately 6 times. Because the ECG has strong time-dependent characteristics, then we design an recurrent neural network (RNN)-based accurate personal identification system. The robust and best identification rate is more than 96.31%. Finally, we investigate the impact of the number of heart beats on personal identification rate. When the number of selected QRS is 20 or greater, the robust identification rate is more than 98.00%.

概要

この研究は、異なる水温（WT）でそれぞれ入浴中の心電図（ECG）を計測し、心拍変動（HRV）と個人識別を調査することを目的としています。実験に参加する被験者は、男性 5 人と女性 5 人の 10 人です。心電図は、 $37\pm 0.5^{\circ}\text{C}$ 、 $38\pm 0.5^{\circ}\text{C}$ 、 $39\pm 0.5^{\circ}\text{C}$ 、 $40\pm 0.5^{\circ}\text{C}$ 、 $41\pm 0.5^{\circ}\text{C}$ の 5 つの WT 条件で収集します。各被験者の設定した WT 条件で非接触電極を使用して 3 回心電図を記録しました。1 回の記録時間は 18 分、サンプリングレートは 200Hz です。最終的に入浴中に心電図記録 150 回と WT 記録 150 回を収集しました。HRV 解析には、毎回 1 分間の心電図セグメントが使用されます。時間域、周波数域、非線形域を含む 20 種類の HRV 特徴量を算出しました。測定された HRV 機能の多様性は、あらかじめ設定された入浴中の WT 条件に基づいて k-means クラスタリング分析法を使用して分析されます。さらに、WT 条件に基づいて、測定された HRV 各特徴量の平均値、標準偏差（SD）、有意差を算出しました。実験結果は、WT の上昇に伴い、pLF、LF / HF、HR、SD1 / SD2 の HRV 機能が単調かつ有意に ($p < 0.05$) 増加し、 D_2 、HF パワー、総パワー、pHF、平均 RRI、SDNN、RMSSD、SDSD、AURRI、SD1、SD2 が単調かつ有意に ($p < 0.05$) 減少します。このことから、WT が HRV に重要な影響を与えていると考えられます。異なる WT で計測した ECG を使用して個人識別を正確かつ迅速に行うために、まず個人識別のパフォーマンスを向上させる方法を検討します。その結果、学習サンプルの多様性を高めることで、識別率を大幅に向上させることができることがわかりました。従来手法と比較して、低 WT では 12.17% から 90.49% に、高 WT では 13.33% から 90.00% に精度が向上していることがわかります。両方とも約 6 倍の精度が向上しました。心電図は時間に依存する特性が強いため、リカレントニューラルネットワーク（RNN）に基づく正確な個人識別システムを設計しました。その結果、最高の識別率は 96.31% 以上です。最後に、心拍の個数が個人識別の識別率に与える影響について調査します。選択された QRS の数が 20 以上の場合、ロバスト識別率は 98.00% 以上になります。

Acknowledgment

I am very grateful to everyone who gave me guidance, support, and assistance during my doctoral study in the past three years.

Firstly, I wish to express my sincere appreciation to my supervisor, Prof. CHEN Wenxi. He not only provided me plenty of professional guidance throughout my doctoral study of three years and sparked my interest in the topic selection and the paper writing with great continuous patience at every stage, but also encouraged scientific rigour while promoting a relaxed and helping environment, taught me many very useful skills to do research, and gave me plenty of advice to let me know the appropriate manners to communicate, cooperate and get along with others. All those words are treasure to me, because they will always be shining in my mind like the navigation light when I am struggling in the darkness and then offer me great power to conquer the challenges appeared in both my future research career and my life.

Secondly, I gratefully acknowledge the constructive comments and suggestions from the other review committee members, Prof. ZHU Xin, Prof. HISADA Yasuhiro, and Prof. PAIK Incheon. I have revised my dissertation very carefully by taking all the comments and suggestions into account. Much appreciation for these comments that have much improved the quality of this dissertation. Many thanks for the time and the patience of all referees.

Thirdly, I really also appreciate so much to Mrs. Huang, the wife of Prof. Wenxi Chen that provided me much help during my daily life. I would also like to thank the lab members and Rika Mashiko who provided me a lot help, and also many thanks to the administrative staffs such as MIYUKI Yamahira, YOKOYAMA Tomoe, KIYOTAKA Otake, GOTO Hiroshi, MORI Yuka, UENO Ayami et al. at SAD and OSIP of the University of Aizu who help me a lot in the campus study and life during my stay in Japan.

Finally, I would like to show my highest gratitude to my family members who giving me continuous support and great love.

Chapter 1

Introduction

This chapter mainly introduces the related knowledge about heart rate variability (HRV) and personal identification.

1.1 Historical Overview of HRV

Humans have been studying the HRV thousands of years ago. The pulse is caused by changes in the pressure that blood exerts on arterial vessels when the heart ejects blood. Heart rate refers to the number of times the heart beats (systolic and diastolic) per unit time (1 minute), that is, the number of times the heart beats per minute. In a resting state, the pulse rate and heart rate are almost same for a healthy person. In some special cases, such as a pregnant woman or a person with heart diseases, high blood pressure, asthma, or pregnancy, the pulse rate will change. According to the existing historical records, humans began to use the pulse to diagnose diseases from about 800 BC to 200 BC. A Chinese famous physician of Bian Que (扁鹊, about 500 BC, also known as Qin Yueren, 秦越人) diagnosed some diseases based on the variation of the pulse rate [2]. He used his fingers to press the pulse of the patient to observe the pulse changes, and to identify the rise and fall of viscera functions and the stagnation of blood, fluid, and essence. At the same time, Bian Que also comprehensively used the methods of looking, smelling and asking to diagnose diseases. Specifically, "looking" means to observe the patient's development, complexion, tongue coating, face, etc. with the eyes, and to detect the internal organs lesions through the external body surface. "Smelling" means listening and smelling, listening to the patient's voice, coughing, wheezing, etc., sniffing the patient's odor, if there is no bad breath, body odor, etc., through the level, strength, turbidity, and urgency of the patient's language breath. Distinguish between the deficiency and the actual cold and heat of the disease. "Asking" is to inquire the patient's symptoms, medical history, etc.; to understand the medical history and family medical history, etiology, disease process, treatment process, symptoms, diet, etc. through inquiries. Subsequently, an ancient Greek physician and scientist named Herophilos (about 335 BC to 280 BC) used a water clock to measure the pulse rate [3]. A British doctor named John Floyer (1649–1734) invented a pulse watch, which can be used to accurately measure pulse rate in clinical practice [4]. Rev. Stephen Hales (1677–1761) was the first to report that the beat-to-beat interval and arterial pressure level varied during the respiratory cycle [5]. Carl Ludwig (1816–1895) invented a device named smoked

drum kymograph in 1847, which can be used to measure the mechanical activity. He was the first person to record the amplitude and periodic oscillations of arterial pressure waves that change during respiration. His experiment result showed that the pulse rate regularly increased during inspiration and slowed during expiration [6]. At the end of the 19th century and the beginning of the 20th century, Willem Einthoven (1860-1927) used a galvanometer to accurately measure the changes in current and recorded the electrical activity of the heart continuously for the first time [7]. With the development and standardization of the electrocardiogram (ECG), it has become possible to evaluate the successive changes in the heart rhythm. In the early 1960s, Norman Jeff Holter invented a portable ECG recording instrument, which can continuously record 24 hours of ECG. This invention allows humans to further explore the relationship between heart rate (HR) changes and cardiac disease [8]. Beginning in the early 1970s, Hyndman et al. used power spectrum analysis methods to study the physiological basis of the various frequency components that make up the periodic changes of the HR [9]. In 1987, Goldberger and West evaluated the nonlinear dynamic characteristics of HRV [10]. Thanks to these pioneering studies of predecessors, the field of HRV has expanded rapidly. In recent years, both linear (time, frequency, and time-frequency domain) and non-linear HRV analysis techniques have been used to quantify HRV.

1.2 Influencing Factors of HRV

HRV is an important indicator of physical and mental health. The instantaneous HRV rhythm represents a dynamic balance between the sympathetic nervous system (SNS) and parasympathetic nervous system (PNS) branches of the autonomic nervous system (ANS) [11]. Therefore, the quantitative analysis of HRV is considered an effective method for the diagnosis of many cardiac diseases in clinical applications. However, HRV is affected by many internal and external factors. The internal factors mainly include mental stress, gender, age, and disease, while the external factors mainly include sleep, drugs, alcohol, smoking, and diet.

1.3 HRV Analysis Techniques

The HRV analysis techniques mainly include linear and non-linear techniques, and the linear HRV analysis technique divided into the time domain, frequency domain, and time-frequency domain techniques.

1.3.1 Linear Analysis

1.3.1.1 Time Domain

Essentially, the HRV analysis is to calculate the variations of the R-R intervals or the normal-normal intervals. SDNN: the standard deviation of all NN intervals; SDANN: the standard deviation of the averages of NN intervals in all 5-minute segments of the entire recording; RMSSD: the square root of the mean of the sum of the squares of differences between adjacent NN intervals; MSDNN: Mean of the standard deviations of all NN intervals for all 5-minute segments of the entire

recording; SDD: Standard deviation of differences between adjacent NN intervals; NN50: Number of pairs of adjacent NN intervals differing by more than 50 ms in the entire recording; pNN50: NN50 count divided by the total number of all NN interval; The time domain measures mainly include the statistical measures and geometric measures, they are easy to calculate, as is shown in Tab. 1.1.

1.3.1.2 Frequency Domain

Although the time domain HRV analysis techniques can measure the total variability of HRV, there is a notable exception that they can not measure the specific components of HRV. Since the late 1960s, with the rapid development of signal processing technology, researchers began to study the frequency components of HRV. Power spectral density (PSD) analysis decomposes the total variance of a series of continuous beats into its frequency components, that is, how power is distributed as a function of frequency; The spectral power for a given frequency can then be quantified by determining the area under the curve within a specified frequency range. The two most common spectral analysis approaches are Fast Fourier Transform analysis (FFT) and autoregressive (AR) modeling. The HRV parameters in frequency domain is shown in Tab. 1.2.

1.3.1.3 Time-Frequency Domain

When the spectral characteristics change rapidly, the conventional power spectrum methods like FFT and AR modeling that are not appropriate to analyze the biomedical signals. On the other hand, time-frequency analysis has more ideal time-varying spectral characteristics based on instantaneous frequency. The time-frequency approach can be used to analyze the variation of the ANS behavior both in steady-state and non steady-state.

1.3.2 Non-linear Analysis

With the development of digital signal processing technology, some non-linear analysis technologies are also used to measure the HRV, such as the SD1: the standard deviation of the PP perpendicular to the line of identity; SD2: the standard deviation of the PP along to the line of identity; En(0.2): approximate entropy computed with the threshold r set to $0.2 \cdot SD_{NN}$; En(r_{max}): approximate entropy computed with the threshold r set to value which maximizes entropy; En(r_{chon}): approximate entropy computed with the threshold r set to value computed with the formula proposed by Chon; D2: correlation dimension, and so on. The details are shown in Tab. 1.3.

1.3.3 Statistical Analysis

Statistical analysis refers to the establishment of a specific mathematical model through mathematical principles and methods, which could scientifically, accurately, and objectively perform mathematical statistics and analysis of the quantitative changes of a specific research object, and finally forming a quantitative conclusion, and then revealing the development trend of the research object, relationships, and changes. Statistical analysis is the science of collecting, exploring,

Table 1.1: HRV time domain measures.

Variable	Unit	Description
SDNN	ms	Standard deviation of all NN intervals
SDANN	ms	Standard deviation of the averages of NN intervals in all 5-minute segments of the entire recording
RMSSD	ms	The square root of the mean of the squares of differences between adjacent NN intervals
MSDNN	ms	Mean of the standard deviations of all NN intervals for all 5-minute segments of the entire recording
SDSD	ms	Standard deviation of differences between adjacent NN intervals
NN50	—	Number of pairs of adjacent NN intervals differing by more than 50 ms in the entire recording; three variants are possible counting all such NN intervals pairs or only pairs in which the first or the second interval is longer
pNN50	%	NN50 count divided by the total number of all NN intervals
HRV	—	Total number of all NN intervals divided by the height of the histogram of all NN intervals measured on a discrete scale with bins of 7.8125 ms (1/128 seconds)
triangular index		
TTNN	ms	Baseline width of the minimum square difference triangular interpolation of the highest peak of the histogram of all NN intervals
Differential index	ms	Difference between the widths of the histogram of differences between adjacent NN intervals measured at selected heights (e.g., at the levels of 1,000 and 10,000 samples)
Logarithmic index	—	Coefficient of the negative exponential curve $k \cdot e^{-t}$, which is the best approximation of the histogram of absolute differences between adjacent NN intervals

Table 1.2: HRV frequency domain measures.

Variable	Unit	Description	Frequency range
5-mins Total Power	ms ²	The variance of NN intervals over the temporal segment	0.4 Hz
VLF	ms ²	Power in VLF range	0.04 Hz
LF	ms ²	Power in LF range	0.04–0.15 Hz
LF norm	—	LF power in normalized units LF/(total power-VLF)×100	
HF	ms ²	Power in HF range	0.15–0.4 Hz
HF norm	—	HF power in normalized units HF/(total power-VLF)×100	
LF/HF	—		
24-hours Total Power	ms ²	Variance of all NN intervals	0.4 Hz
ULF	ms ²	Power in the ULF range	0.003 Hz
LF	ms ²	Power in the VLF range	0.003–0.04 Hz
VLF	ms ²	Power in the LF range	0.04–0.15 Hz
HF	ms ²	Power in the HF range	0.15–0.4 Hz
	—	Slope of the linear interpolation of the spectrum in a log-log scale	0.04 Hz

VLF: very low frequency band; LF: low-frequency band; HF: high-frequency band; ULF: ultra low frequency band.

Table 1.3: HRV nonlinear domain measures.

Variable	Unit	Description
SD1	ms	The standard deviation of the PP perpendicular to the line of identity
SD2	ms	The standard deviation of the PP along to the line of identity
En(0.2)		Approximate Entropy computed with the threshold r set to 0.2*SDNN
En(rmax)		Approximate Entropy computed with the threshold r set to value which maximizes entropy
En(r chon)		Approximate Entropy computed with the threshold r set to value computed with the formula proposed by Chon
D2		Correlation Dimension
a1		Short term fluctuation slope in Detrended Fluctuation Analysis
a2		Long-term fluctuation slope in Detrended Fluctuation Analysis
l mean	Beats	Mean line length in RP
l max	Beats	Maximum line length in RP
REC	%	Recurrence rate
DET	%	Determinism
ShEn		Shannon Entropy
FuEn		Fuzzy Entropy
ApEn		Approximate Entropy

and presenting large amounts of data to discover underlying patterns and trends. In this study, we use the clustering analysis and variance analysis technologies.

1.3.3.1 Clustering Analysis

Cluster analysis refers to the analysis process of grouping a collection of physical or abstract objects into multiple classes composed of similar objects. It is an important human behavior. The goal of cluster analysis is to collect data to classify on the basis of similarity. Clustering comes from many fields, including mathematics, computer science, statistics, biology, and economics. Many clustering techniques have been developed based on different application fields. These technical methods are used to describe data, measure the similarity between different data sources, and classify data sources into different clusters. Clustering is a process of classifying data into different classes or clusters. Therefore, the similarities are big in the same cluster. From a statistical point of view, cluster analysis is a method of simplifying data through data modeling. Traditional statistical cluster analysis methods include systematic clustering, decomposition, addition, dynamic clustering, ordered sample clustering, overlapping clustering and fuzzy clustering. Cluster analysis tools using k-means, k-center points and other algorithms have been added to many well-known statistical analysis software packages, such as SPSS, SAS, etc.

1.3.3.2 Variance Analysis

R.A. Fisher invented the analysis of variance (ANOVA) and used to test the significance of the difference between the means of two or more samples. The basic idea of variance analysis is to determine the influence of controllable factors on the research results by analyzing and studying the contribution of different sources of variation to the total variation. According to the different types of data design, there are two methods of analysis of variance as follows: 1. To compare the mean of multiple samples in a group design, the analysis of variance with a completely random design should be used, that is, one-way analysis of variance. 2. For the comparison of the mean values of multiple samples in the random block design, the analysis of variance of the compatibility group design should be used, that is, the two-factor analysis of variance.

1.4 Personal Identification

There are many personal identification methods. They can be divided into two aspects, non-biometric and biometric methods.

1.4.1 Non-biometric Methods

The non-biometric techniques include ID cards, keys, personal identification numbers (PINs), and passwords [12], as shown in Fig. 1.1. They are also called traditional identification methods. The PINs code is a security code used to verify the identity of a person. It is widely used for any digital content that needs to be accessed, which can include communication equipment, car locks, home locks,

and so on. Like a password, a PINs can also encrypt and protect the database so that other people cannot access your data. Therefore, the PINs should be kept secret because it is a credential to access important services, such as financial transactions. The obvious difference between the PINs and the password is that the PIN is limited to numbers (0-9), and the password can contain numbers, uppercase and lowercase letters, punctuation, and so on. For each number in the PIN, you have only 10 options available, but the password can have more options. The more options for each character, the harder the password is to crack. So, the password is safer than the PINs.

Although they have been used for personal identification and can protect systems and databases by restricting access, with the advancement of forgery technology, they are now easily cracked. Traditional passwords, PINs and ID cards have many shortcomings. For example, in the process of use, passwords and PINs are particularly dependent on the user's memory and are easy to forget, keys and IDs are also easily lost and stolen.

1.4.2 Biometric Methods

Because of the insecurity and inconvenience of the non-biometric, biometric techniques have been attracting attention in recent years. The biometric feature has some its own intrinsic characteristics, which are: Uniqueness: The characteristics of any two people should be sufficiently different. Universality: A characteristic that everyone should have. Collectability: Features can be measured easily and quantitatively. Persistence: The features should be immutable enough for a period of time (relative to the matching criteria) [13–18].

According to the above inherent characteristics of biometrics, the biometric methods can be divided into behavioral biometrics and physical biometrics [19–24]. The gait, voice and signature which are associated with the behavior or dynamic measurements of an individual that can be taken as the behavioral biometrics, as shown in Fig. 1.2. The fingerprint, face, ear, DNA, iris, retina and hand geometry which are associated with the shape or measurements of the human body that can be taken as the physical biometrics [25–28], as shown in Fig. 1.3.

Traditional authentication technology depends on what you have and know, while biometric authentication depends on your identity. Compared with traditional identity verification technology, biometric technology is more difficult to be stolen, forgotten, borrowed or forged. Therefore, the authentication process based on biometrics is safer. Each biometric feature has its own advantages. Firstly, because biometrics cannot be lost or forgotten (passwords can be lost or forgotten), they are inherently more reliable than password-based authentication. Secondly, password-based authentication can be passed by anyone who knows the password, and the person who sets the password does not need to be present. However, biometrics are more difficult to copy, share and distribute. The biometric identification system requires that the person being verified must be present at the specified place at the specified time. In some cases, biometric technology can be used in conjunction with passwords (or tokens) to enhance the security provided by the authentication system. In addition, cracking a biometric system requires more professional knowledge and experience. It not only costs more time and money, but also often leaves more visit records and traces in the cracking process,

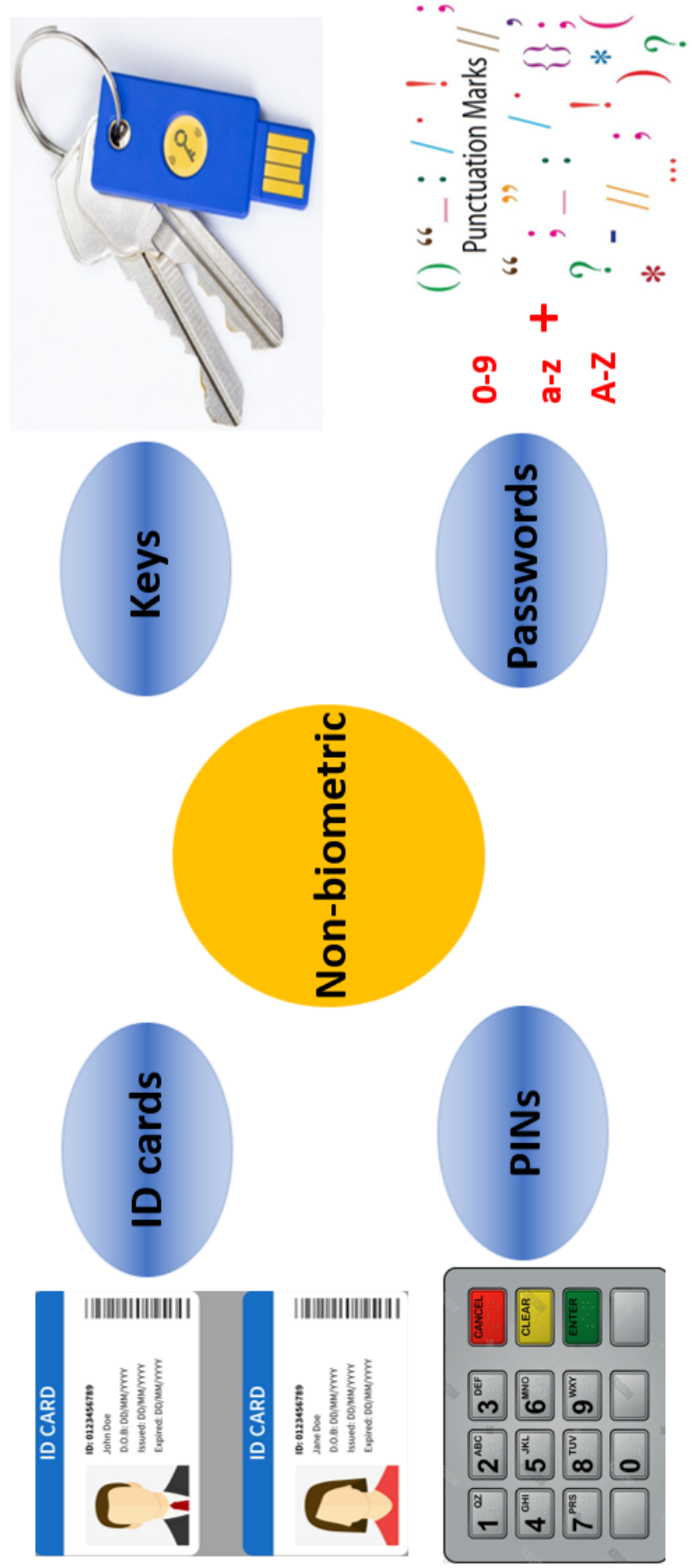


Figure 1.1: Non-biometric methods.

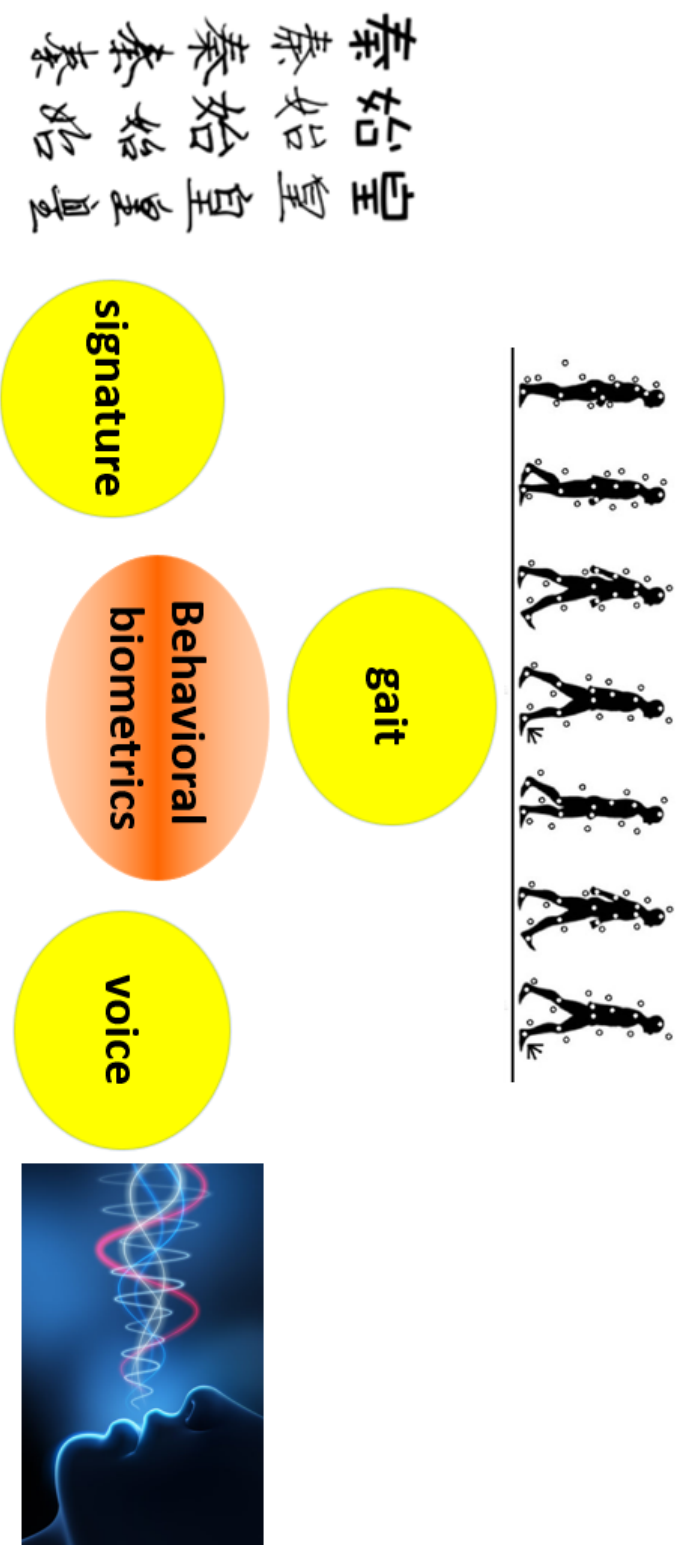


Figure 1.2: Behavioral biometrics methods.

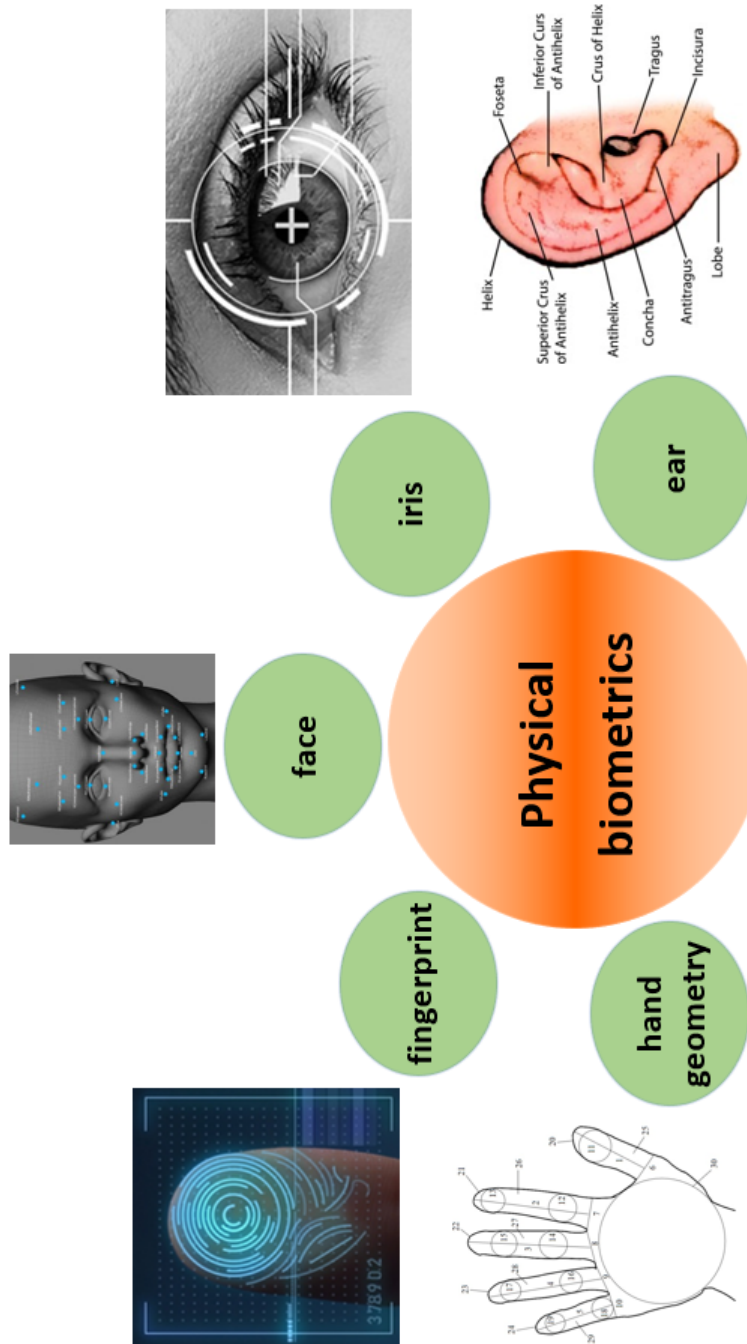


Figure 1.3: Physical biometrics methods.

which greatly increases the cost and risk of the crime. Therefore, the authentication scheme based on biometrics is a powerful alternative to the traditional authentication scheme.

However, with the advancement of various forgery technologies, each biometric feature slowly exposed its own shortcomings. Some biometric features are exposed on the surface of the human body. With the emergence of various forgery technologies, they are now easily forged and becoming more and more insecure. For example, the fingerprints could be copied, facial features are easily forged by 3-D models, iris could be photographed, sounds are recorded by a tape recorder, and hand geometry or veins on the back of the hand can be also copied. According to application requirements, appropriate biometrics should be used for a given authentication application.

1.5 ECG-based Personal Identification

Among the current biometric technologies, DNA and ECG are the safest, and they are extremely difficult to forge. Therefore, their applications are becoming more and more extensive, and they are playing an increasingly important role in civil, commercial and government applications. However, because DNA is difficult to extract, DNA-based biometric technology is currently mainly used in government applications for criminal and forensic investigations. Because ECG is easy to collect, in recent years, ECG-based biometric technology has become a research hotspot in academia and industry. Like DNA, the ECG is also regarded as an emerging biometric technology.

The ECG shows the process of the electrical activity of the heart. It exists in all the living person, and is usually used for medical diagnostic purposes in clinical practice. A normal ECG waveform includes three important parts, which are P wave, QRS complex and T wave [29–35]. Among them, the QRS complex contains more discriminative information. Many previous studies have proposed the use of QRS complex for personal identification [36–39].

L. Biel et al. used the ECG to perform personal identification in 2001 [40]. They collected the ECG signal using the standard 12-lead method when the subjects were rest. Then, they extracted some ECG features and performed personal identification in the predetermined group. The multivariate analysis method was used during the identification process. Their experiment result confirmed that it was feasible to perform personal identification with the features that extracted from one lead. And only three electrodes attached on the subject was enough when collected the ECG.

M. Kyoso and A. Uchiyama designed an identification system using the ECG signal in 2001 [41]. First, they extracted some important ECG features from the patients and registered them in the system. Then they performed personal identification by comparing the new ECG features and the previously registered ECG feature. The important ECG features and their combinations were used to test the system.

Z. Zhang and D. Wei proposed an ECG-based human identification system using the Bayes' theorem in 2006 [36]. They collected 502 ECG recordings from 502 subjects. Each recording was segmented into two parts: half of the data was

used for training, half of the data was used for testing. The variables dimension of the extracted ECG features were reduced using the principal component analysis method. The Bayes theorem was used to performed personal identification. The experiment result showed that the Bayes theorem method could achieve better performance than the Mahalanobis distance.

A. D. Chan et al. used the Wavelet distance measure to perform personal identification with ECG signal in 2008 [42]. The subject was holding two electrodes on the pads of his thumbs using his thumb and index fingers during the data collection process. There were 50 subjects in the experiment. Each subject collected one ECG recording per day. Three ECG recording were collected for each subject. One recording was used to train and the the other two recordings were used to test. Three quantitative measures of correlation coefficient, percent residual difference, and a novel distance measure based on wavelet transform were used to perform classification. The final classification accuracy was 89%. They confirmed that the accuracy based on the wavelet distance measure was higher than that the other two methods by almost 10%.

T.-W. D. Shen et al. designed a one-lead ECG-based identification system for a normal population in 2010 [43]. They collected 168 short-term ECG recordings using Lead-I when the subjects were in rest state. And 50 ECG recordings were randomly selected to train and test the system. The templates and new ECG databases were generated by the signal averaging method during the denoising process. Then the distance classification and template matching methods were used to test the system performance. The identification rate was 98% based on single algorithm and 100% based on the combined system model that added the prescreening process. The final accuracy was 95.3% using the 168 ECG recordings based on the combined model.

Z. Zhao and L. Yang proposed an ECG-based identification system using the matching pursuit and support vector machine in 2011 [44]. The important information of the ECG signal was decomposed into different atoms by sparse decomposition method with Gabor dictionary. Then, they used the support vector machine to perform identification and achieved 95.3% identification rate with 20 subjects.

F. Zeng et al. designed a statistical-based ECG identification algorithm using the matching reduced binary pattern theory in 2012 [45]. The experiment result showed high identification rate and low computational complexity using the public normal sinus rhythm and MIT-BIH arrhythmia databases. The main contributions of this algorithm was that it didn't need waveform complex information and denoising during the whole identification process.

Z. Zhao et al. proposed an ECG-based identification system using the ensemble empirical mode decomposition (EEMD) in 2013 [46]. To reduce the effects of noise and heart rate variability, they performed noise elimination, heartbeat normalization, and quality measurement during the preprocessing process. The K-nearest neighbors (KNN) was taken as the classifier. The Welch spectral analysis was used to extract the significant heartbeat features and then decompose the ECG into a number of intrinsic mode functions (IMFs). The principal component analysis was used to reduce the dimensionality of the feature space. The system achieved 95% identification rate with 90 subjects from three MIT-BIH ECG databases that were the PTB, the long-term ST, and the ST change database.

1.6 Artificial Neural Network

WS. McCulloch et al. published a paper titled a logical calculus of the ideas immanent in nervous activity, which has since inspired people's interest in studying the Artificial Neural Network (ANN) in 1943 [47]. The ANN has been a research hotspot since it emerged in the field of artificial intelligence (AI) in 1980s.

As we all know, the brain has super learning and thinking abilities. It can analyze incomplete, unclear, and vague information and make its own judgments based on these information. Simply put, an ANN is a computer program that simulates the way of processes information of the human brain. It collects knowledge by detecting patterns and relationships in the data, and abstracts the human brain neuron network from the perspective of information processing, establishes a certain simple model, and forms different networks according to different connection methods. Specifically, an ANNs is composed of processing units called neurons. Multiple processing units are connected to multiple artificial neurons through different weight coefficients to form an ANNs. The number of processing units, weight coefficients, and neurons can all be considered adjustable, which reflects that the nature of neural networks is actually a complex parameterized system.

1.6.1 Convolutional Neural Network

Convolutional Neural Network (CNN) is one of the representative algorithms of deep learning, and the research on it began in the 1980s.

Alexander Waibel et al. invented the first CNN, which was time delay neural network (TDNN) in 1987 [48]. TDNN was a CNN which was applied to speech recognition field. Its input was the preprocessed speech signal using FFT. Its hidden layer consisted of two one-dimensional convolution kernels that were used to extract the shift-invariant features in the frequency domain. In 1988, W. Zhang et al. invented the shift-invariant ANN (SIANN) which was a two-dimensional CNN in the field of medical images detection in 1988 [49]. Y. LeCun et al. independently constructed a CNN for image classification, it was the original version of LeNet in 1989 [50]. It consisted of two convolutional layers, two fully connected layers, a total of 60,000 learning parameters, which were much larger than TDNN and SIANN. It was structurally close to modern CNNs.

Subsequently, Y. LeCun et al. designed a CNN named LeNet-5 dedicated to handwritten digits recognition in 1989 [51]. The LeNet-5 added a pooling layer compare to the LeNet which was used to filter the input features, but it still followed LeNet's learning strategy. Both of the LeNet-5 and its subsequent variants defined the basic structure of modern CNNs. The shift-invariant features of the input images could be effectively extracted depended on the alternately construction of the convolution-pooling layers in the LeNet-5. The success of LeNet-5 has aroused people's attention to the application of CNNs. Microsoft developed an optical character recognition (OCR) system using CNN in 2003 [52]. Other applied research based on CNNs has also been developed, including portrait recognition and gesture recognition [53, 54].

Dure to the advancement of deep learning theory, especially the emergence of layer-by-layer learning and fine-tuning techniques, CNNs began to develop rapidly,

and the structure continued to deepen, and various learning and optimization theories were introduced after 2006. A. Krizhevsky et al. designed a famous CNNs named AlexNet and it became the champion in the competition of ImageNet Large Scale Visual Recognition Challenge (ILSVRC) in 2012 [55]. Then, several famous CNNs repeatedly became the champion in this competition, which were the ZFNet in 2013, GoogLeNet and VGGNet in 2014, ResNet in 2015 [56–58].

To sum up, the CNN is a kind of feedforward neural network with convolution calculation and deep structure. It constructs the visual perception mechanism of the creature, which can perform supervised learning and unsupervised learning. It is also called a shifting invariant ANN (SIANN) due to it can perform shifting invariant classification. The convolutional kernel parameter sharing and the sparseness of the inter-layer connection in the hidden layer enable the CNN to smaller computational computations for grid-like topology features such as pixel and audio, have a stable effect and have no additional feature engineering requirements for the data. In the late 20th century, with the introduction of deep learning theory and the improvement of numerical computing equipment, CNN has developed rapidly and is widely used in computer vision, pattern recognition, natural language processing and other fields.

1.6.2 Recurrent Neural Network

Although the CNN has very powerful picture information processing capabilities, when it is used to process pictures or signals with temporal characteristics, it shows certain congenital defects. Therefore, people have proposed an algorithm specifically used to process pictures with obvious timing characteristics, which is called Recurrent Neural Network (RNN) [59]. It is also a kind of ANN. Each node of it is strictly arranged in a directional array according to the time series. Therefore, RNN is very good at dealing with the nonlinear characteristics of time series. Its biggest feature is that it has a powerful parameters sharing ability and memory ability. RNN is mainly used to deal with various time series problems, such as stock forecasts, weather forecasts, typhoon forecasts, machine translation, speech recognition and other natural language processing (NLP) fields. Currently, the more famous RNNs are: Bidirectional RNN and Long Short-Term Memory networks (LSTM).

1.7 Motivation of This Study

Many previous papers confirmed that the HRV were affected by many factors, such as the sleep, diet, drug, exercise, stress et al. This study aims to explore the impact of water temperatures (WTs) on HRV during bathing.

In our previous study [60], we found that the WTs had an important impact on the personal identification using ECG during bathing. This study explores how to improve the personal identification performance using ECG during bathing. To accurately and fastly perform personal identification using ECG during bathing, choosing a suitable classifier is especially important. Therefore, we explore the impact of different classifiers such CNN and RNN on the personal identification rate using ECG during bathing.

In order to reduce the computational complexity and improve identification accuracy, the number of heart beats should be moderate. Therefore, this study also explores the impact of the number of heart beats on the personal identification rate using ECG during bathing.

1.8 Structure of This Dissertation

This study includes five chapters, chapter 1 is the introduction, which presents the relevant knowledge about HRV, HRV analysis, non-biometric and biometric personal identification methods, ECG-based personal identification history and methods, the development of ANN which including CNN and RNN, the main motivation of this study, the structure of this study. Chapter 2 elaborates the measurement of the ECG during bathing. Chapter 3 introduces the HRV analysis during bathing, twenty HRV features which including time domain, frequency domain, and non-linear domain are calculated in this study. Chapter 4 mainly elaborates the personal identification using ECG during bathing. Firstly, we explore how improve the personal identification performance using CNN. We transform the segmented QRS into the binary images and then perform personal identification using the CNN. Then, in order to quickly and accurately perform personal identification during bathing, the ECG data is collected at five mostly used WTs during bathing, which are 36.5 °C–37.5 °C, 37.5 °C–38.5 °C, 38.5 °C–39.5 °C, 39.5 °C–40.5 °C, 40.5 °C–41.5 °C, respectively. Finally, we explore the impact of different heart beats on the personal identification rate during bathing using ECG signal. We confirmed that when the number of test heart beats is more than 20, the variety of identification rate curve becomes stable. The structure of this dissertation is shown in Fig. 1.4.

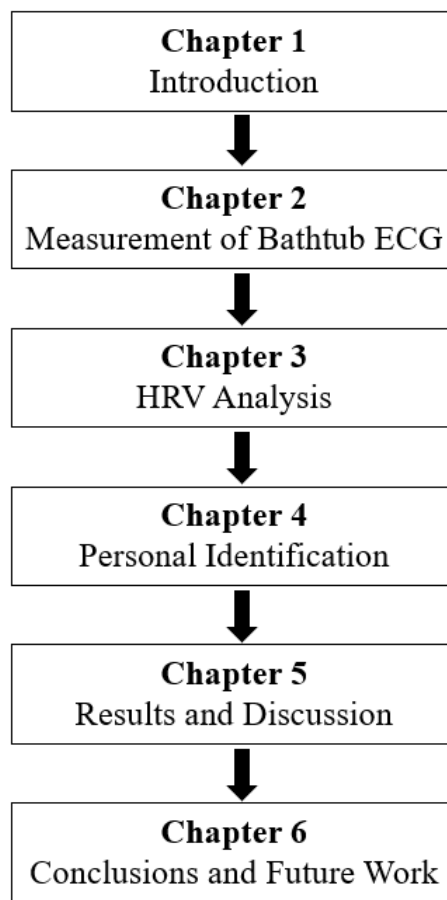


Figure 1.4: Structure of this dissertation.

Chapter 2

Measurement of Bathtub ECG

2.1 Historical Overview of Bathtub ECG

The research of bathtub ECG has a long history, many previous studies explore the collection and application of the bathtub ECG. In order to relieve the burden of the physicians and make early heart diseases detection and preventive diagnosis purpose, S. C. Kwatra et al. used a composite conductive medium formed by the patient's body and the external liquid medium such as tap water in a bathtub at a patient's home to collect ECG signal [61]. Then the suitably processed signals are transmitted to the physician's clinic by the telephone line. However, the disadvantage of this method is that the magnitude and phase of the ECG signal will distort in the low-frequency region in the process of transmission through the bathtub and recording electrodes.

T. Togawa et al. collected the bathtub ECG with three silver electrodes [62]. They add some salt into the water or let the water through an ion exchange resin column to change the electrical conductivity of the bathtub water. Then the ECG signal was collected by the battery-operated ECG unit with a high gain differential amplifier through a hum filter. They found that covering electrodes with porous materials can reduce the baseline wandering while the bathtub water was stirred, and increasing the conductivity of the water can reduce the amplitude of the ECG signal.

Y. K. Lim et al. proposed using insulated electrode to record the bathtub ECG [63]. The electrodes made by copper plate coated with Polyethylene Terephthalate (PET) film were placed on the bathtub. The designed high-input-impedance amplifier was used to amplify the sensed ECG signal by the high impedance insulated electrode. Although the amplitude of the R peaks was very big in the recording with this method, however, there were many common-mode noise and power line noise.

K. Motoi et al. developed a new sensor system installed in a bathtub, which allows simultaneous monitoring of the ECG together with the respiration and showed its usefulness for detecting the drowning in elderly care [64].

M. Ishijima proposes unobtrusive approaches to the health monitoring at home and assess their quality for the medical use [65]. The fundamental concept is that while the subject uses some household furniture or appliance fitted with sensors, the health monitoring is done automatically and unobtrusively without the subject's knowing about it.

Many elderly easily suffer from sudden death because of suddenly extend or shrink of blood vessels during daily bathing at home. Therefore, in order to prevent those accidents, S.-J. Jang et al. designed a bathtub-typed detector to collect the continuous ECG signal in the bathtub during a bath, which is able to acquire single channel ECG via 3 stainless electrodes attached in bathtub [66]. They use the band-pass filter which has very narrow bandwidth to prevent the motion artefact, consequently, QRS complex of ECG measured is able to be detected reliably. The experimental results showed that the collected ECG signal had a high quality although the subject's skin was out of contact with electrodes.

S. Tanaka et al. designed a bathtub system to monitor the ECG during bathing, their bathtub system is shown in Fig. 2.1 [1].

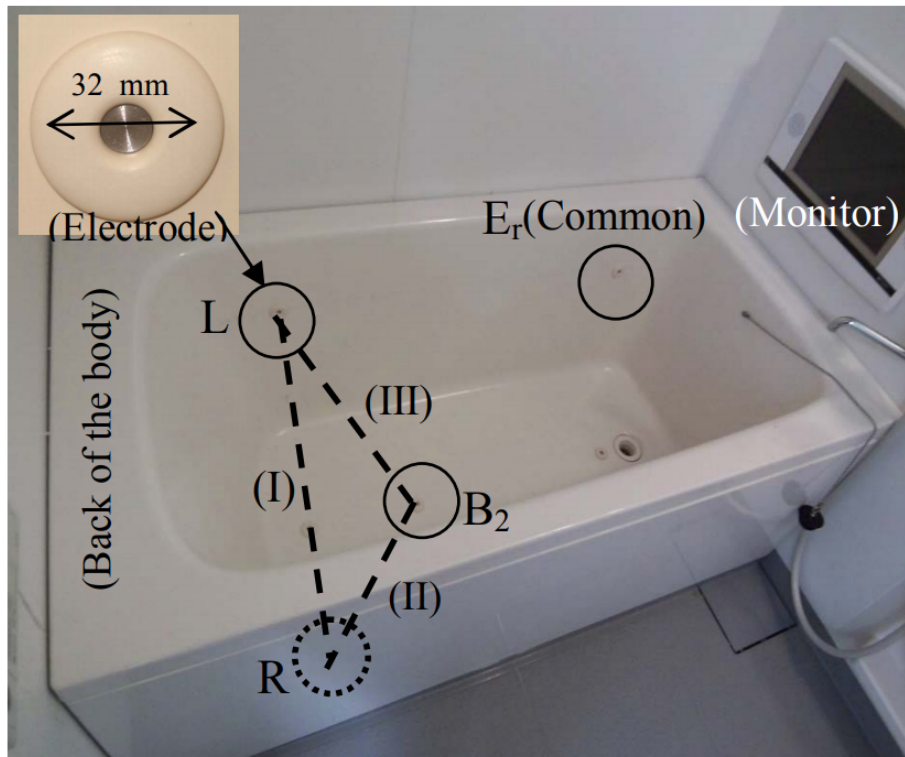


Figure 2.1: A bathtub system with electrodes for monitoring ECG [1].

There are four electrodes attached on the inner surface of the bathtub, the ECG signal is collected after the potential differences between two electrodes (I, II, III) are amplified and filtered. Fig. 2.2 shows the ECG signal waveform which is recorded by their bathtub system (red lines) using the lead I.

The blue lines represent the ECG is recorded using the general approach, which places the electrodes on the body surface. The red lines show the ECG is recorded by their designed bathtub. The ECG signal collected by these two methods are basically consistent.

Many previous studies proposed to collect the ECG signal during bathing with the electrodes attached on the inner surface of the bathtub. These electrodes inside the bathtub bring great inconvenience to the subjects. Therefore, K. Motoi et al. proposed a new attempt which is concerned with the initial development of a method to measure an ECG through tap water without conscious awareness of the presence of electrodes that are placed outside the bathtub wall [67]. Their ex-

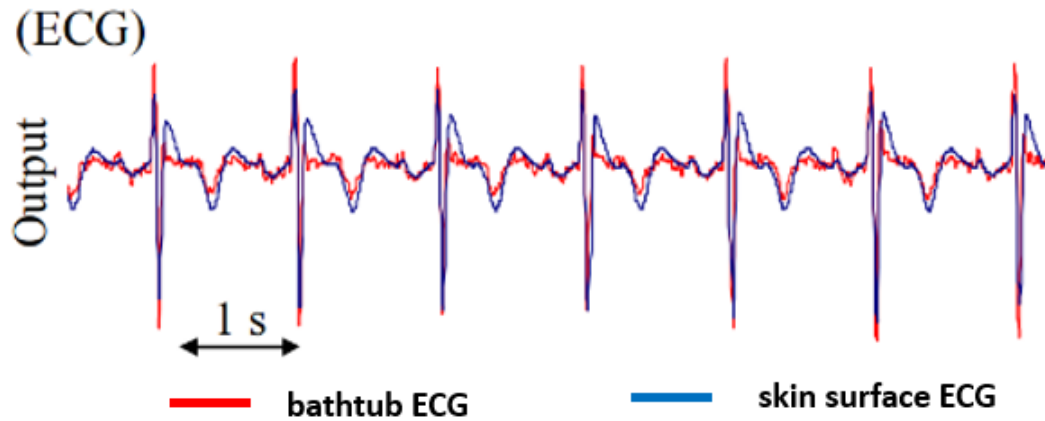


Figure 2.2: Typical recording of ECG signal obtained by the bathtub system (red lines) and by the conventional methods (blue lines) [1].

perimental result showed that the designed bathtub system was useful and precise for recording the ECG signal compared with the conventional direct methods.

The ECG signal, in particular QRS components, were successfully detected utilizing capacitive coupling electrodes placed outside the bathtub wall. Also, the RRI and respiration intervals were determined with reasonable accuracy as compared with the conventional direct methods.

2.2 Measurement System

The ECG collection system in this study includes four rectangular stainless steel electrodes, all of them are placed on the bathtub wall. When the subject is in the bathtub during bathing, the four electrodes are near the right foot, right arm, left foot, and left arm, respectively.

The electricity on the skin surface, which is produced by the electrical activity of the heart, arrives in the four electrodes through the water without contact with the subject, and three-lead ECG are recorded. The lead I ECG is the potential difference between the left arm (positive) and right arm (negative), the lead II ECG is the potential difference between the left foot (positive) and right arm (negative), and the lead III ECG is the potential difference between the left foot (positive) and left arm (negative). The detailed schematic diagram of four limb leads is shown in Fig. 2.3.

Four shielded wires are respectively welded onto the four electrodes. The three-lead ECG arrives in the ECG collection monitor (Open Brain Computer Interface Biosensing Ganglion Board-OpenBCI Ganglion; OpenBCI, USA) through the shielded wires, as is shown in Fig. 2.4, and the ECG monitor and the laptop (a MacBook Pro) are connected using a standard Bluetooth 4.0, and all the collected ECG recordings are stored on the laptop. The designed ECG collection system in this study is shown in Fig. 2.5 [68].

The ECG recording procedures were approved by the University of Aizu Research Ethics Committee. Written informed consent was obtained from each participant before the experiment.

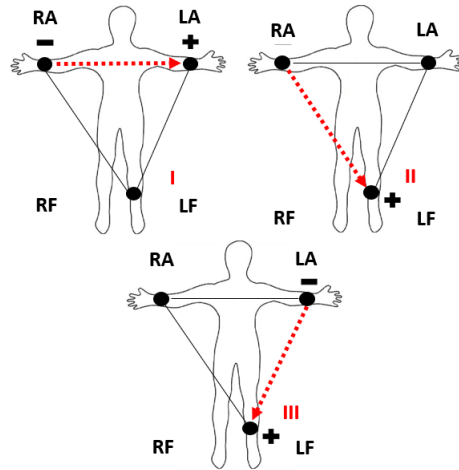


Figure 2.3: Connection of four limb leads.

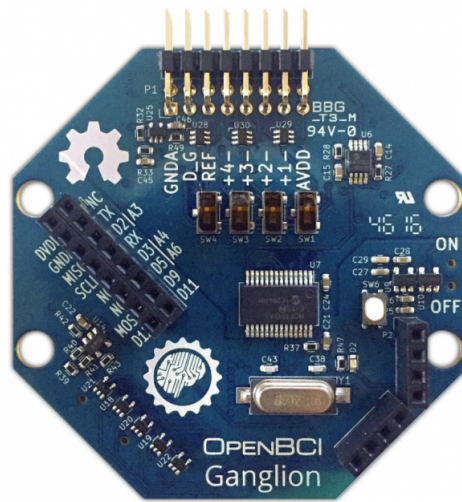


Figure 2.4: ECG monitor: OpenBCI Ganglion Biosensing Board.

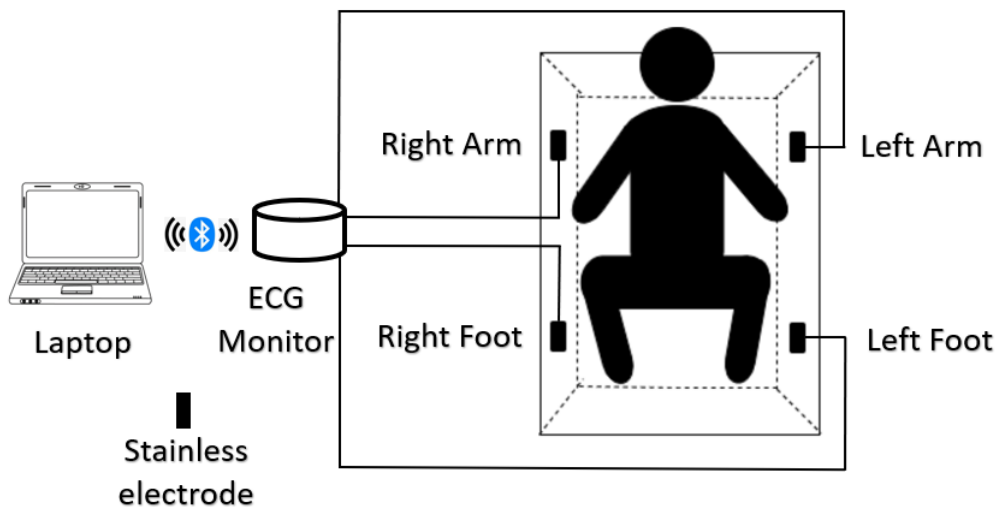


Figure 2.5: ECG collection system.

Ten subjects (five males and five females) aged 23 to 40 years old (mean±SD: 28.5±4.8 years) who were students from the University of Aizu participated in the data collection. The BP, body temperature, and body weight were recorded before and after the ECG collection, the water temperature and room temperature were recorded every second during the ECG collection using a temperature monitor (TR-71wb/nw; T&D Corporation, Japan), as shown in Fig. 2.6.



Figure 2.6: Bath water and bath room temperature monitor.

The ECG data was collected using the non-contact electrode at five different WTs during bathing, which were 36.5°C–37.5°C, 37.5°C–38.5°C, 38.5°C–39.5°C, 39.5°C–40.5°C, 40.5°C–41.5°C, respectively. Each subject collected 5 ECG recordings at each preset bathtub WT condition and each recording was 18 minutes long with a sampling rate of 200 Hz. In total, 150 ECG recordings and 150 temperature recordings were collected during bathing. The variety of water temperature from one subject is shown in Fig. 2.7.

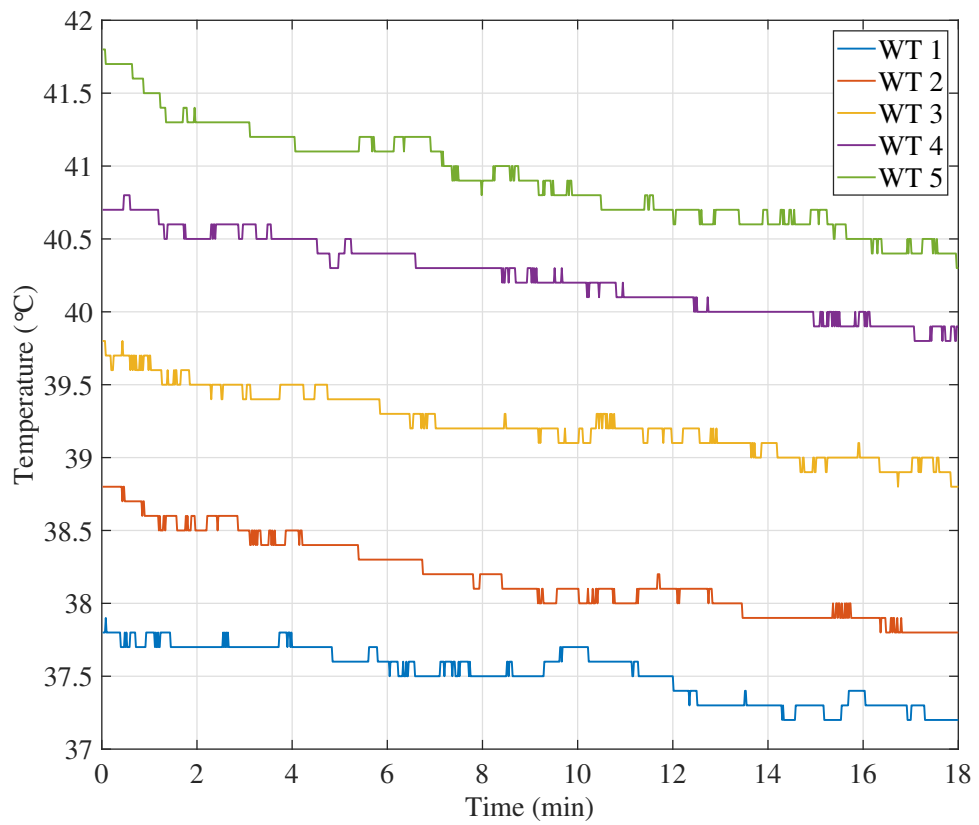


Figure 2.7: Profiles of bath water temperature from one subject during bathing under five conditions.

Chapter 3

HRV Analysis

3.1 Introduction

According to statistics from the World Health Organization (WHO), Japan's life expectancy has been among the best in the world's life expectancy rankings in recent years. This is not only due to Japan's excellent air and safe food, but also closely related to the unique healthcare habits of Japanese people in daily life. Survey data shows that almost every family has a bathtub, which shows that bathing is very popular in daily family life in Japan. When people enter the bathtub, especially in the cold winter, the stimulation from the water temperature (WT) and the water pressure will induce the sudden change of the heart rate (HR), which has been causing many drowning accidents during bathing every year, especially for elderly people with heart disease. As we all know, if a person's HR exceeds the safe range, life will be seriously threatened, especially for people with heart diseases. If the dependence of WT and HR is known, then, we can dynamically adjust the level of the WT and use the WT to affect the HR, so that the HR is within a safe range all the same during bathing. In addition, the sensitivity of different people to WT is dissimilar due to individual differences, it is necessary to establish a suitable WT control model for everyone. Therefore, the preliminary task of this study aims to explore the impact of WT on the HR, which is performed using the HR variability (HRV) analysis. The pulse rate and the heart rate (HR) are almost synchronized for the healthy person. However, they are not the same when a person is in a sick situation, especially for patients with cardiac diseases. Therefore, the HRV analysis is meaningful and helpful for the long-term healthcare. The variety of HR are closely related to the human nervous system. The sympathetic nervous system (SNS) and parasympathetic nervous system (PNS) branches of the autonomic nervous system (ANS) collectively control the balance of the various systems of the body [11]. For a healthy person, the level of the instantaneous HR is in a dynamic balance situation all the time. Therefore, the level of HR could be taken as a label of healthy or unhealthy. In the academic research and the clinical applications, the quantitative analysis of HRV could be used to diagnosis some diseases and mental stress. However, the HRV is easily affected by many internal and external factors. Now, only many a few factors have been revealed, which is insufficient for us to predict the physical and mental health conditions using the HRV analysis.

3.1.1 HRV and Age/Gender

It is well known that the heart size of a newborn baby and an adult are not the same. When a person gets older, his heart will be different from when he was young. In other words, the heart will change with age. Changes in the size and shape of the heart can also cause some changes in HR. Not only that, HR is also reflected in gender differences. For example, for the same newborn baby, the cry of male babies is often louder than that of female babies. The same adult men are more powerful and explosive than adult women. On the sports field, there are separate men's team matches and separate women's team matches. This is the best example.

All in all, the HR is always in a dynamic process in a short time. Ramaekers et al. and Schwartz et al. found that the levels of some HRV features would drop when a person was getting older, while Ramaekers et al. noticed that the people under 40 years old showed obvious HRV differences for different gender [69, 70]. Lochner et al. found that the HRV level of men was obvious higher than that of the women [71]. Nagy et al. confirmed that the girls showed significantly higher baseline of HR level, which was determined by the gender differences from at the beginning of the birth [72]. Bonnemeier et al. discovered that the differences of HRV level for different gender were significantly reduced with aging [73]. Yamasaki et al. found that the women's pLF was obvious lower than men's, and the aging highly determined the LF level [74].

3.1.2 HRV and Diseases

The diseases have an important impact on the HRV level, which the patients and the healthy people show obvious different HRV level, especially for the patients with cardiac diseases. Wilkowska et al. noticed that the depressed patients showed obvious lower HRV level than that of the nondepressed patients [75]. Lutfi and Sukkar confirmed that the higher BP values and the lower HRV levels appeared at the same time, people who had such a situation suffered a higher risk of developing hypertension [76]. T. Tombul et al. found that the HRV level of the multiple sclerosis patients was significantly lower than that of the healthy people [77]. D. Gurses et al. observed that the HRV levels of some time domain parameters (mean RRIs, SDNN, RMSSD, and PNN50) showed obvious lower trends for the thalassaemic patients than that of the healthy people [78]. M. Lan et al. confirmed that the patients with allergic rhinitis in the sitting position showed obvious lower LF% and LF/HF levels and higher mean RRIs levels than that of the healthy [79]. DelRosso et al. noticed that the sympathetic activation of the children with obstructive sleep apnea showed increased trends during sleep stage [80].

3.1.3 HRV and Stress

As the pace of life accelerates, people are facing increasing mental pressure. If the long-term mental stress is not relieved and released, it will lead to the emergence of various chronic diseases. Mental stress can also have a significant impact on HRV. The higher mental stress will lead to more activated SNS levels of the ANS branch [81]. Therefore, many previous studies explored the impact of different stressors on mental stress [82–91]. Some studies noticed that the level of HR

was obvious higher during stress states than that of non-stress states [84,86,92–99], while the mean R-R intervals (RRIs) [84,86–89,91,93–95,100] and the square root of the mean of the squares of the successive differences (RMSSD) between adjacent normal to normal intervals (NNs) [87,89,101–108] were obvious lower during stress states. Kofman et al. found that the percentage of high frequency power in total power (pHF) was obvious lower, while the percentage of low frequency power in total power (pLF) was obvious higher during an examination stress state [83]. Melillo et al. confirmed that the normal estimated glomerular filtration rate led to obvious higher HRV level of the LF/HF ratio [109], while Hjortskov et al. found that computer work stress states also led to obvious higher HRV level of the LF/HF ratio [82].

3.1.4 HRV and Sleep

Sleep quality greatly affects people's physical and mental health. During sleep, the various systems of the human body are recuperated, and the human basal metabolic rate is reduced, so that physical strength is restored and immunity is strengthened. The brain is also well rested during sleep, and various indicators of the body have changed. The HRV level is significantly changing during sleep, and different sleep stages have an important impact on the HRV. Herzig et al. found that the level of HR during slow wave sleep (deep sleep) was significantly lower than that of during REM sleep [110]. Padole and Ingale noticed that the normal, sleeping, and meditation states led to different HRV levels [111]. Arslan et al. revealed that the HRV levels of the HF, TP, standard deviation (SD) of NN intervals (SDNN), and pNN50 were obvious lower and the LF/HF ratio was obvious higher during the sleep deprivation stage [112]. ÁR. Sűdy et al. proved that the HRV levels of the young healthy men with social jetlag during sleep on workdays and free days were obvious different [113].

3.1.5 HRV and Other Factors

The HRV is not only affected by the above factors, but also affected by many other factors. Hynynen et al. confirmed that the marathon or moderate exercise sessions led to obvious higher HR level and lower HRV level for the healthy men at night [114]. James et al. noticed that the severe intensity exercise resulted in obvious HRV changed [115]. Davy et al. found that the physically active led to significantly increased HRV level and cardiac baroreflex sensitivity for the women than that of the women with sedentary state [116]. Zuanetti et al. proved that antiarrhythmic drugs resulted in obvious HRV variety for the patients [117]. Murgia et al. found that the HRV during the smoking cessation were obvious higher [118]. Young et al. noticed that the diet had an important impact on the link between mood and HRV [119]. Latha et al. confirmed that the stress levels of the medical students were significantly reduced when the students were listening the classical music [120]. Sollers et al. learned that the varying ambient temperature had an important impact on the HRV [121]. Shin investigated that the impact of the ambient temperature on the pulse rate variability and HRV was different, the higher of the ambient temperature, the greater of the difference [122].

3.2 Motivation

Although many previous studies explored the impact of some factors on the HRV, a few studies investigated the impact of WTs on the HRV. Mourot et al. and HC. Choo et al. learned that different WTs resulted in the HRV changing significantly when a person was immersing in the water [123,124]. Y. Kataoka et al. confirmed that the WTs of 38 °C and 41 °C had an important impact on the HRV, but only measured a few HRV features [125]. F Edelhäuser et al. found that the WTs of 33 °C, 36 °C, and 39 °C had an important impact on the HRV level when the whole-body was immersing in the water [126].

The main purpose of this study aims to explore the impact of different WTs on HRV during bathing. The experiment was carried out based on the most commonly used WTs in the daily family life, twenty HRV features (included time domain, frequency domain, and non-linear domain) were calculated.

3.3 Method

All the processes of this study are performed using the MATLAB (R2019a). The flowchart of ECG processing, HRV features calculation, and statistical analysis are shown in Fig. 3.1.

3.3.1 ECG Processing

There are many noises in the raw ECG. Firstly, in order to remove the baseline wandering which is produced by the respiration and motion artifacts of the subjects during bathing, the ECG is decomposed several important components which including the baseline wandering using the single-level 1-D discrete wavelet transform (DWT). The Daubechies wavelet at level 10 is used in this process because of its better capacity in decomposing the ECG signal. Then the ECG is reconstructed again at level 8 after the baseline wandering component is subtracted from the raw ECG signal. The equation of the DWT is shown in (3.1) and (3.2).

$$W_{\psi}(s, \tau) = \int_{-\infty}^{+\infty} x(t)\psi_{s,\tau}(t) dt \quad (3.1)$$

$$\psi_{s,\tau}(t) = \frac{1}{\sqrt{s}}\psi\left(\frac{t-\tau}{s}\right) \quad (3.2)$$

where $x[t]$ is relative to real-valued wavelet, $s = 2^j$ and $\tau = k*2^j$ are called scale and translation parameters, respectively, $(j, k) \in \mathbb{Z}^2$. $W_{\psi}(s, \tau)$ denotes the wavelet transform coefficients and ψ is the fundamental mother wavelet.

What's more, the hum noise is obvious with unknown frequency components although the baseline wandering is removed. Therefore, the fast Fourier transform (FFT) is used to reveal the spectrum distribution of the hum noise. The equation of the FFT is shown in (3.3).

$$X(f) = \sum_{n=-\infty}^{+\infty} x(n)w(n)e^{-j2\pi fn}, \quad (3.3)$$

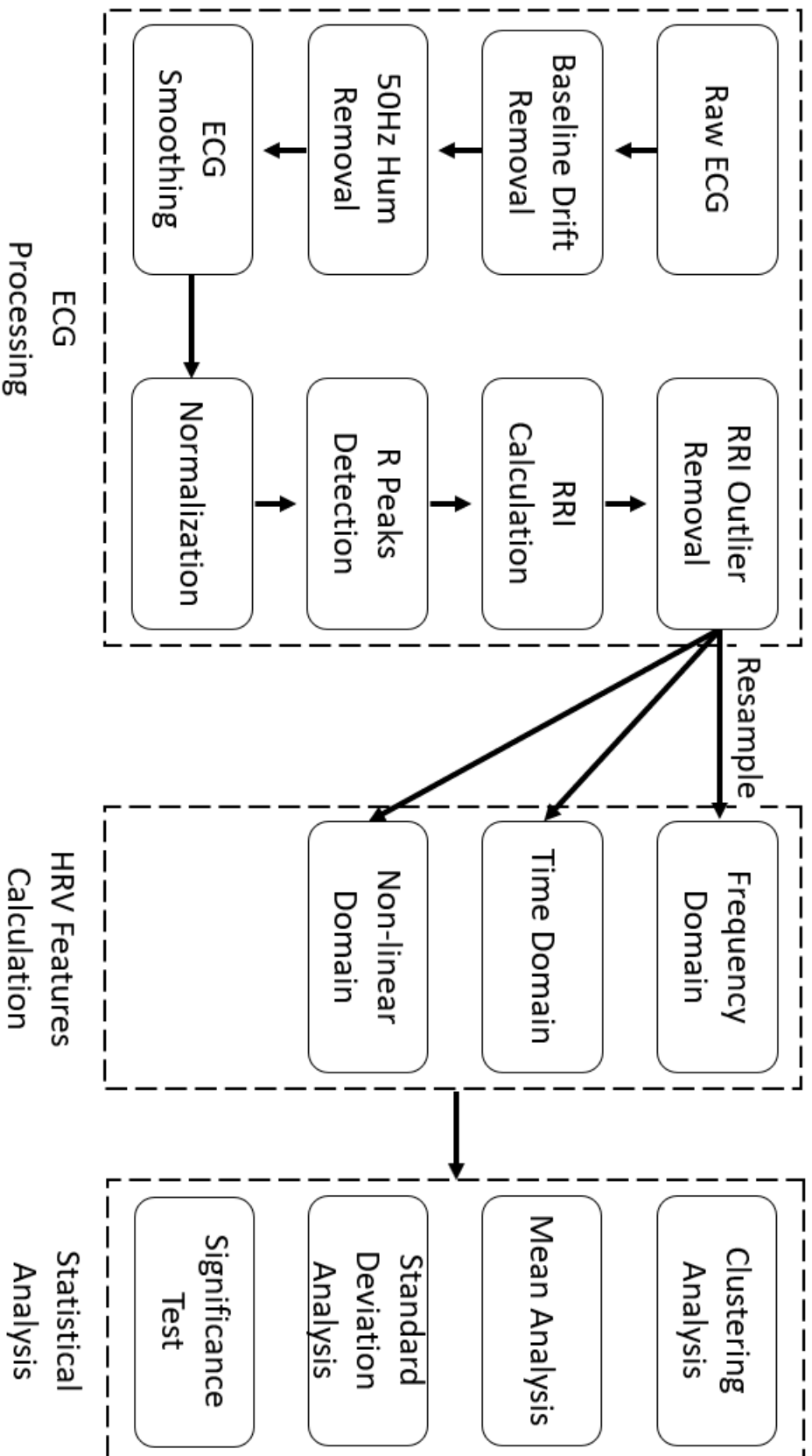


Figure 3.1: Flowchart for the ECG processing, HRV feature calculation, and statistical analysis.

where $x(n)$ is a sampled signal in time domain representation as is shown in equation (3.4),

$$x(n) = A \sin(2\pi \frac{f_0}{f_s} n + \theta), \quad (3.4)$$

f_0 is the fundamental frequency, f_s is the sampling frequency, A is the amplitude, θ is the initial phase angle, and $n = 0, 1, 2, \dots, N-1$. N is the number of sampling points. Therefore, the equation (3.3) can be replaced by equation (3.5).

$$X(f) = \frac{A}{2j} [e^{j\theta} W(\frac{2\pi(f-f_0)}{f_s}) - e^{-j\theta} W(\frac{2\pi(f+f_0)}{f_s})], \quad (3.5)$$

The spectrum analysis result is shown in Fig. 3.2. The main frequency spectrum of normal people's ECG is below 30 Hz [127]. The hum noise is from the obvious 50 Hz component, which is mainly produced by the electromagnetic interference between the power supply network and its equipment.

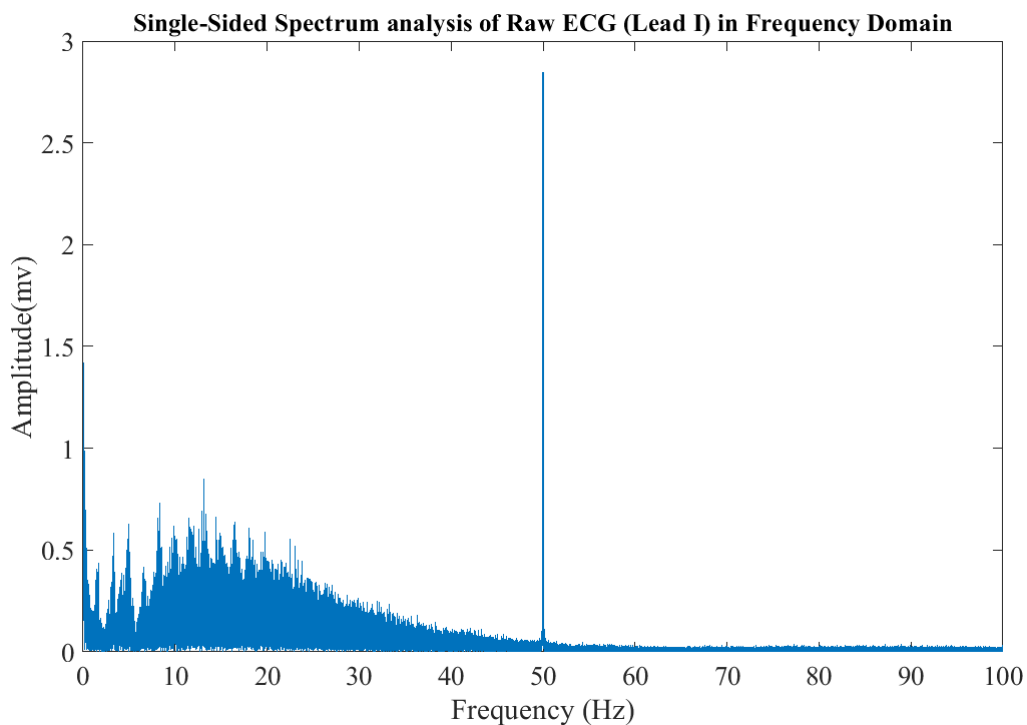


Figure 3.2: Spectrum analysis result.

To remove the component of the 50 Hz hum noise, a second-order infinite impulse response (IIR) digital notch filter is used. Before the numerator and denominator coefficients of the digital notch filter are calculated, the bandwidth is set at 0.0071 at the -3 dB level, and the ω must meet the condition of $0.0 < \omega < 1.0$. The difference equation of digital notch filter is defined in (3.6).

$$y[n] = \sum_{i=0}^N b_i x[n-i] - \sum_{i=1}^M a_i y[n-i], \quad n \geq 0 \quad (3.6)$$

where $x[n]$ is the filter input, $y[n]$ is the filter output, and a_i and b_i are the numerator and denominator coefficients of the digital notch filter, respectively.

Then, the ECG is smoothed using the 5-points moving average method. The 5-points moving average method is defined in (3.7):

$$y[n] = \frac{1}{M} \sum_{j=0}^{M-1} x[n-j] \quad (3.7)$$

where $x[n]$ is the input signal, $y[n]$ is the output signal, and M is 5.

Next, in order to reduce the computational complex, the 'mapminmax' function is used to normalize the ECG, as is shown in (3.8):

$$y = \frac{x - Xmin}{Xmax - Xmin} \quad (3.8)$$

where x is the input data, y is the output data, $Xmax$ is the biggest value of the input signal row vector, $Xmin$ is the smallest value of the input signal row vector.

At last, the function of 'findpeaks' is used to detect the R peaks of the ECG. When all the positions of R peaks are detected, the RRI is calculated. There are some outliers of the RRI, as is shown in Fig. 3.3. Because the median filter has an outstanding capability in suppressing the isolated outlier noise without blurring sharp changes in the original signal, it is used which is set at 1-D 11th order to remove the RRI outliers. The 1-D 11th order median filter is defined in (3.9):

$$y[i] = median\{x[i], i \in w\} \quad (3.9)$$

where $x[i]$ is the input signal, $y[i]$ is the output signal, and w is the moving window length.

The outputs of each process is shown in Fig. 3.4.

3.3.2 HRV Parameters

In this study, twenty HRV features are measured. Specifically, the time domain HRV features include the HR, mean RRI, SDNN, RMSSD between adjacent NNs, SD of the successive differences between adjacent NNs (SDSD), and area under RRI (AURRI). The frequency domain HRV features include very LF (VLF) power (0.003–0.04 Hz), LF power (0.04–0.15 Hz), HF power (0.15–0.4 Hz), total power (0–0.4 Hz), pLF, pHF, and the LF/HF ratio. The nonlinear domain HRV features include the correlation dimension (D_2), the SD of the Poincare plot perpendicular to the line of identity (SD1), the SD of the Poincare plot along to the line of identity (SD2), the SD1/SD2 ratio, and the sample (SE), fuzzy (FE), and approximate entropies (AE).

What needs special explanation is that the RRI data must be resampled before the frequency features are calculated. Nyquist's sampling theorem shows that the sample rate must be more than two times of the highest frequency of the signal. The highest frequency of the HRV is 0.4 Hz. Therefore, the new resampling rate of RRI in this study is set at 2 Hz. The cleaned RRI and the resampled RRI is shown in Fig. 3.5. To calculate the power spectral density (PSD) of the resampled RRI for a N points sequence, the discrete Fourier transform (DFT) is used, as is defined in (3.10):

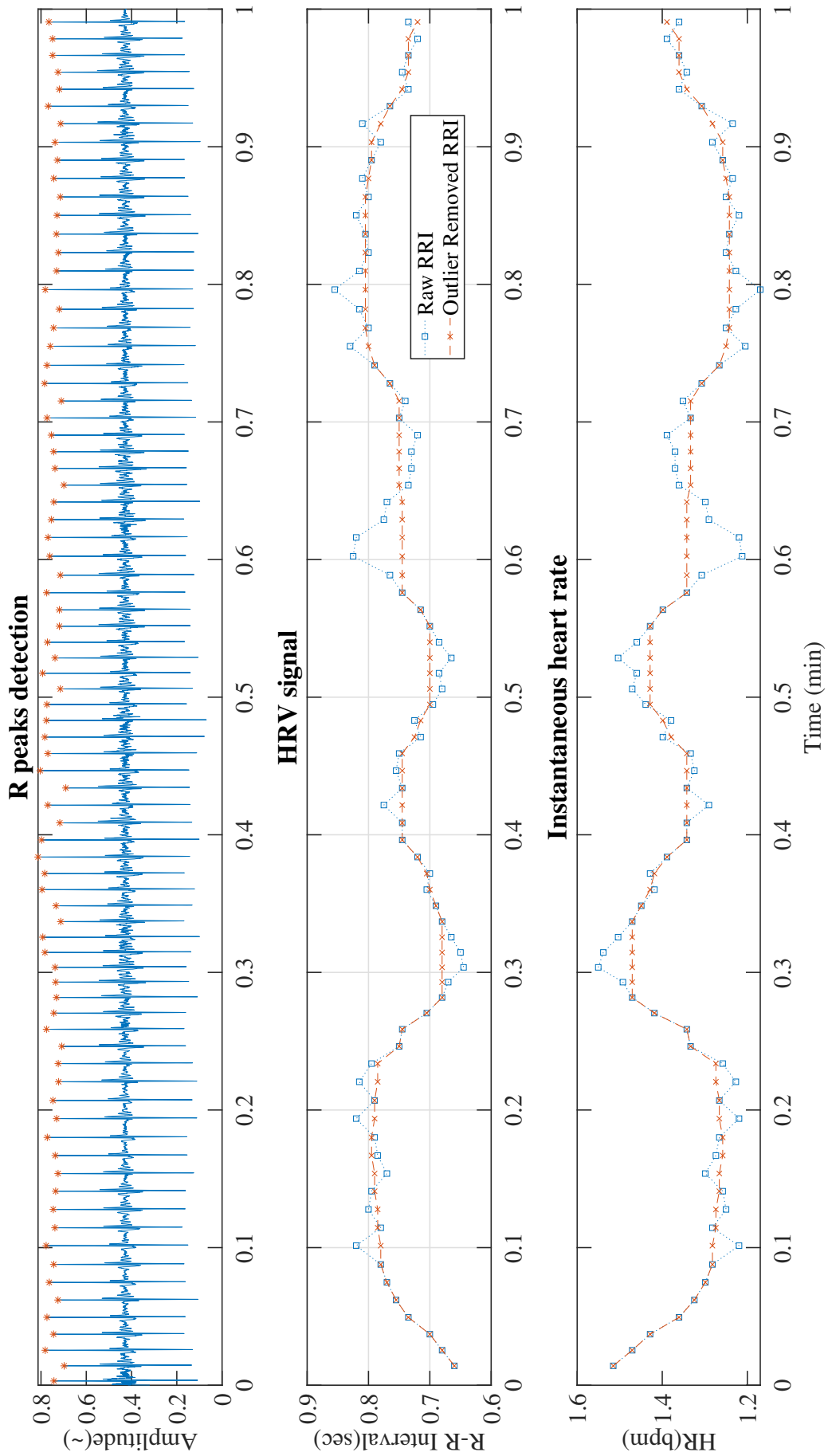


Figure 3.3: Noise removed HRV signal.

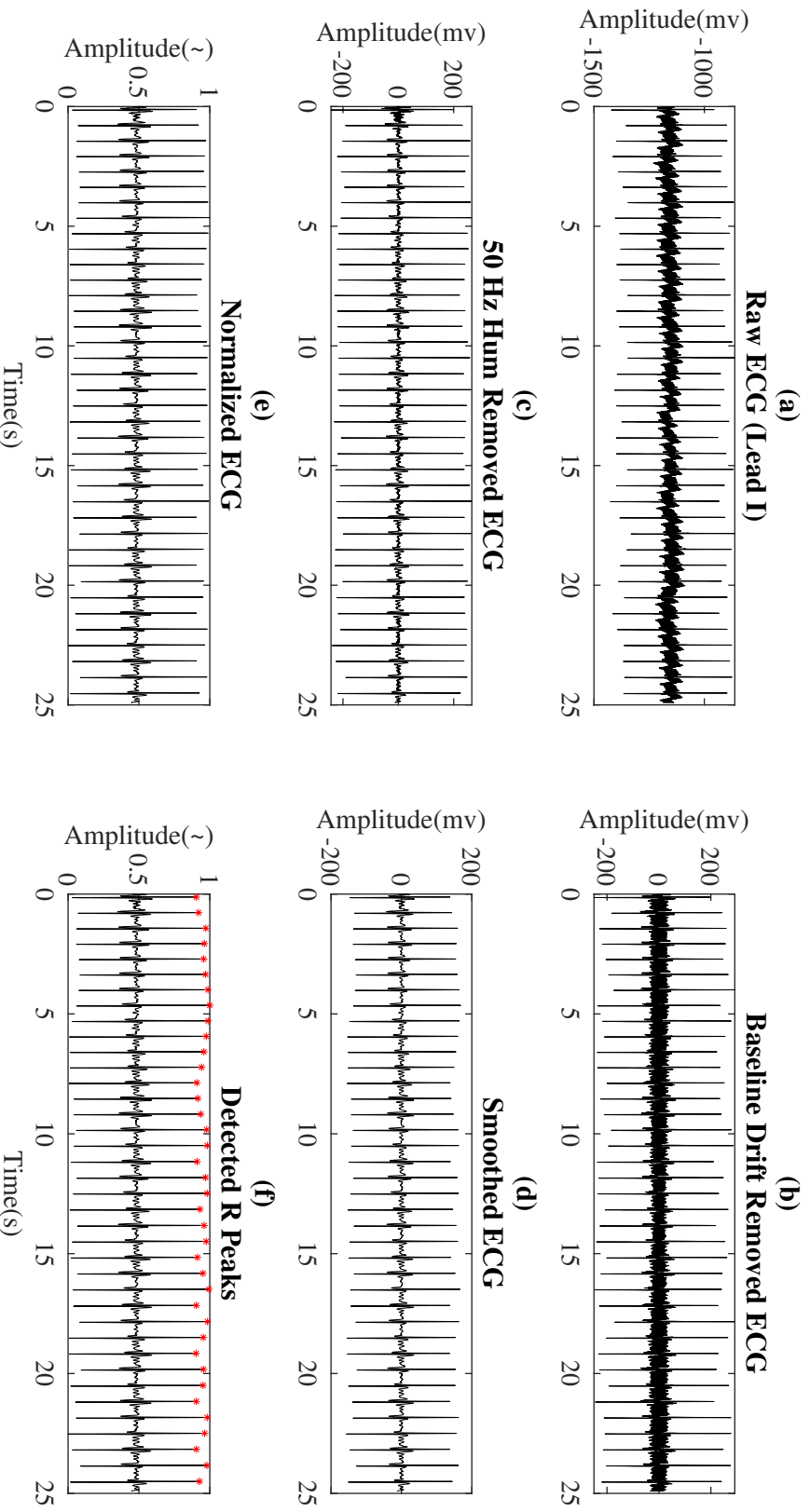


Figure 3.4: Output of ECG processing in each step.

$$X[k] = \sum_{n=0}^{N-1} x[n]e^{-i\frac{2\pi}{N}nk}. \quad (3.10)$$

where $k = 0, 1, 2, \dots, N-1$, and $i^2 = -1$.

3.3.3 Statistical Analysis

In this study, all the measured HRV features are calculated using the ultra-short-term (1-min) method. Each collected ECG recording is segmented into 18 equal parts, each segmentation is 1 min and is used to calculate the HRV features. All the measured HRV features are analyzed based on three WTs conditions, which are low WTs (36–38 °C), medium WTs (38–40 °C), and high WTs (40–42 °C), respectively. The clustering analysis method is used to visualize the variation trend of the measured HRV features based on different WTs conditions. In order to quantitatively analyze the changes of each measured HRV feature, the mean and the standard deviation (SD) are calculated. Then, the significant difference based on different WTs is analyzed using the t-test methods.

3.4 Results and Discussion

The clustering result is shown in Fig. 3.6, which clearly reflects the variation trend of each measured HRV features based on different WTs conditions. The bigger black dots are calculated using the K-means clustering analysis method based on each measured HRV feature. The measured HRV features are shown using the smaller dots with blue, yellow, and green colors, which are calculated using 1-min ECG. With increasing WT, the HRV features of pLF, LF/HF, HR, and SD1/SD2 are monotonously and significantly ($p < 0.05$) increased, and the D_2 , HF power, total power, pHF, mean RRI, SDNN, RMSSD, SDDSD, AURRI, SD1, and SD2 are monotonously and significantly ($p < 0.05$) decreased.

The SDs of the HR with blue, yellow, and green colours are 3.38, 4.65, and 4.17, respectively. The main reason is that when the WTs is lower (about 36 °C–38 °C), the simulation of the WTs on the subjects is smaller, the HR is almost same with the rest state. But when the WTs is higher (about 40 °C–42 °C), the simulation of the WTs on the subject is too high, and the HR of each subject is also too quick, so the SDs of HR for all the subjects is not high, which is 4.17. Each subject has different sensitivity to WTs due to the individual differences. The differences of the impact of WTs on the subjects are very large under 38 °C–40 °C condition. Although the value of instantaneous HR is lower at 38 °C–40 °C than that of the HR at 40 °C–42 °C, the SD of HR is 4.65 at 38 °C–40 °C, which is higher than that of the SD at 40 °C–42 °C.

We can also find that the distribution of the controlled WTs is uneven, as is shown in Fig. 3.6. In fact, the data collection conditions are not same for each subject. When the WTs is in the range of 40 °C–42 °C, some subjects can endure the high WTs, but some other subjects feel uncomfortable. Therefore, for personal safety, we have to turn on the cooling fan in this case. What's more, when the WT is about 42 °C, which is higher than the ambient temperature, it drops very quickly. The distribution of the HRV data near the 42 °C is rare.

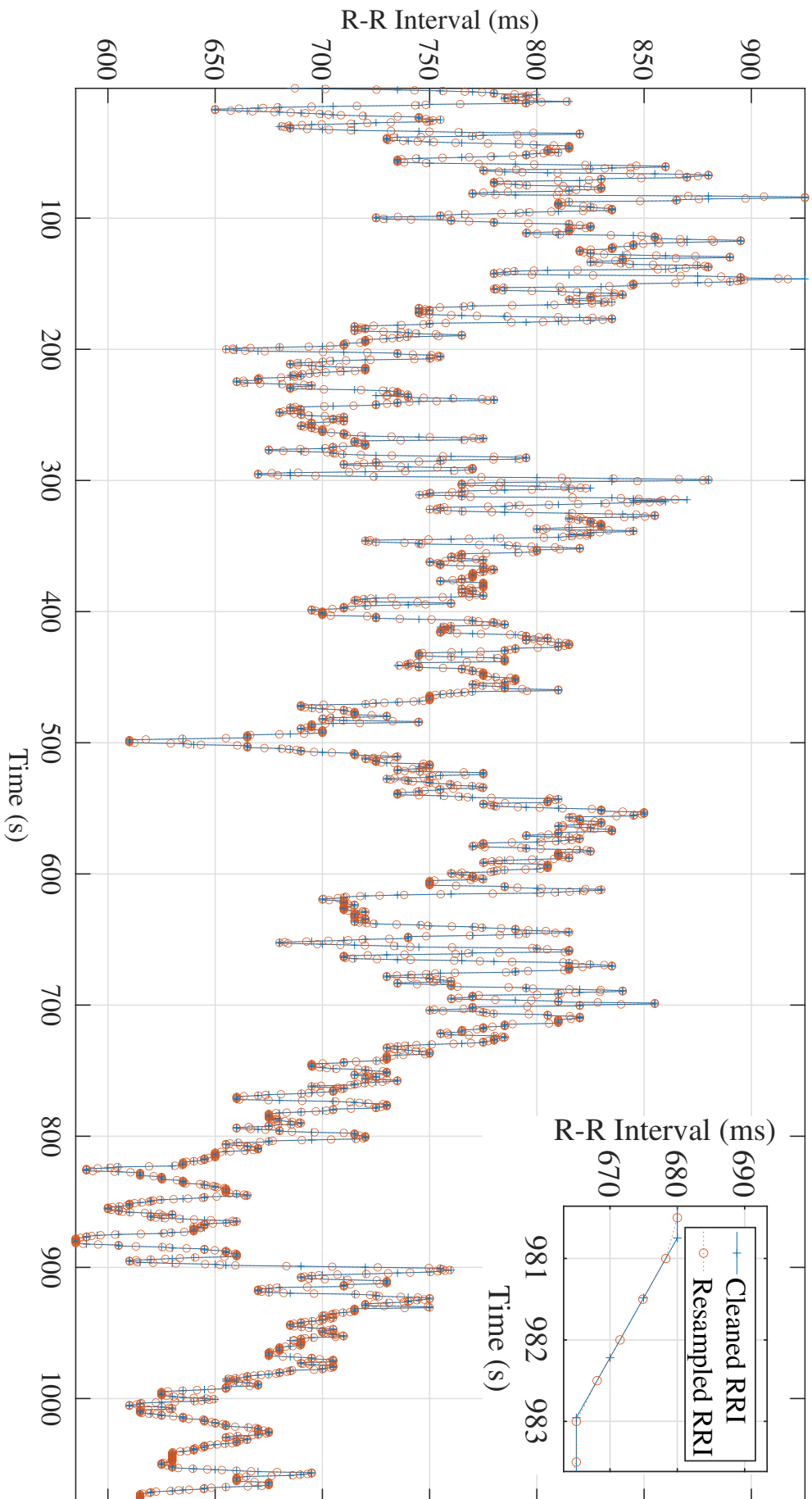


Figure 3.5: Comparison of the cleaned RRI and resampled RRI.

The significant difference of each measured HRV feature is visualized using the box plot, as is shown in Fig. 3.7. The distribution of each measured HRV feature at different levels based on each WT condition is very clear. Each measured HRV feature includes some outliers, which could also reflect that the sensitivity to the WT is different. The higher of the WTs, the bigger of the stimulation on the subjects, the more difficult for the subjects to adapt the data collection environment. With the WTs increasing, the outliers of the HR is increasing. The significant difference of the HR based on each two WTs conditions is existing and obvious. We can not find the obvious variations of the VLF, LF, SE, FE, and AE from the box plot, and the t-test results do not show significant differences for the five HRV features.

The mean and SD of the 20 measured HRV features which including time domain, frequency domain, and non-linear domain are shown in Tab. 3.1, and the pairwise significant differences of each two WT conditions are calculated. The multivariate analysis of *t*-test variance method is used to calculate the significant difference, where *p1* represents the significant difference between low and medium WT conditions, *p2* represents the significant difference between medium and high WT conditions, and *p3* represents the significant difference between low and high WT conditions. The experiment results show that with the increasing WT, the SD of the HR, mean RRI, AURRI, pLF, pHF, LF/HF ratio, and SD1/SD2 are first rising and then reduced, and the SD of LF, HF, TP are first reduced and then rising.

3.5 Conclusion

Some conclusions are revealed in this study. Individual differences lead to different sensitivity to WTs during bathing. When the WT is 40°C–42°C, the subjects 1, 6, and 9 can not tolerate the high WT because they are very sensitive to the high WT. Their foreheads quickly begin to sweat during the first 3 minutes, which is called the adaptation phase during bathing. The WT drops quickly during the first 3 minutes and they feel more comfortable during 4th-11th minutes. But the adaptation phases is the first minute for the other seven subjects. These seven subjects begin to sweat more after the first 10 minutes in the same high WT environment. The body weights of the subjects 1, 6, and 9 decreased more than the other seven subjects after the data collection, which shows that they are more sensitive to the high WT. Based on this finding, we speculate that people who are more sensitive to WT are less able to withstand water and WT pressure, and under higher WT conditions, they are more likely to experience higher mental and physical stress.

When the WT is 40°C–42°C, the subjects 2, 3, 5, and 10 feel a little uncomfortable at the beginning of data collection and then quickly adapt to the environment. When the WT is 36°C–38°C, all the ten subjects can adapt to the environment quickly. When the WT is 38°C–40°C, the subjects can relax themselves and feel more comfortable than that the other WT conditions.

Both of the experiment results and the questionnaire survey results show that the WTs have an important impact on the HRV during bathing. Although some discoveries are revealed in this study, there are also some limitations. First, the

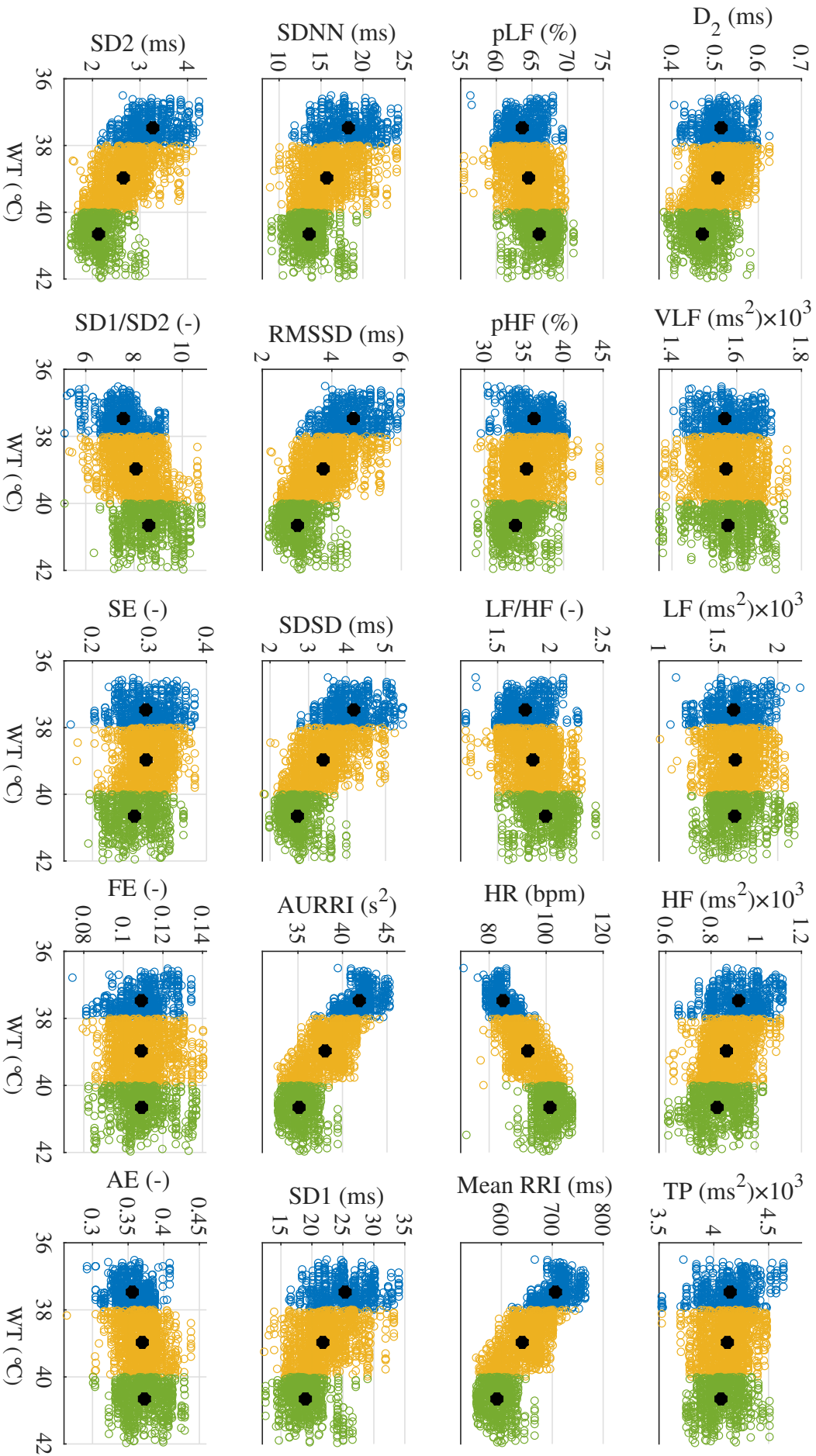


Figure 3.6: Feature trends for 20 HRV features in three analysis domains under three WT conditions.

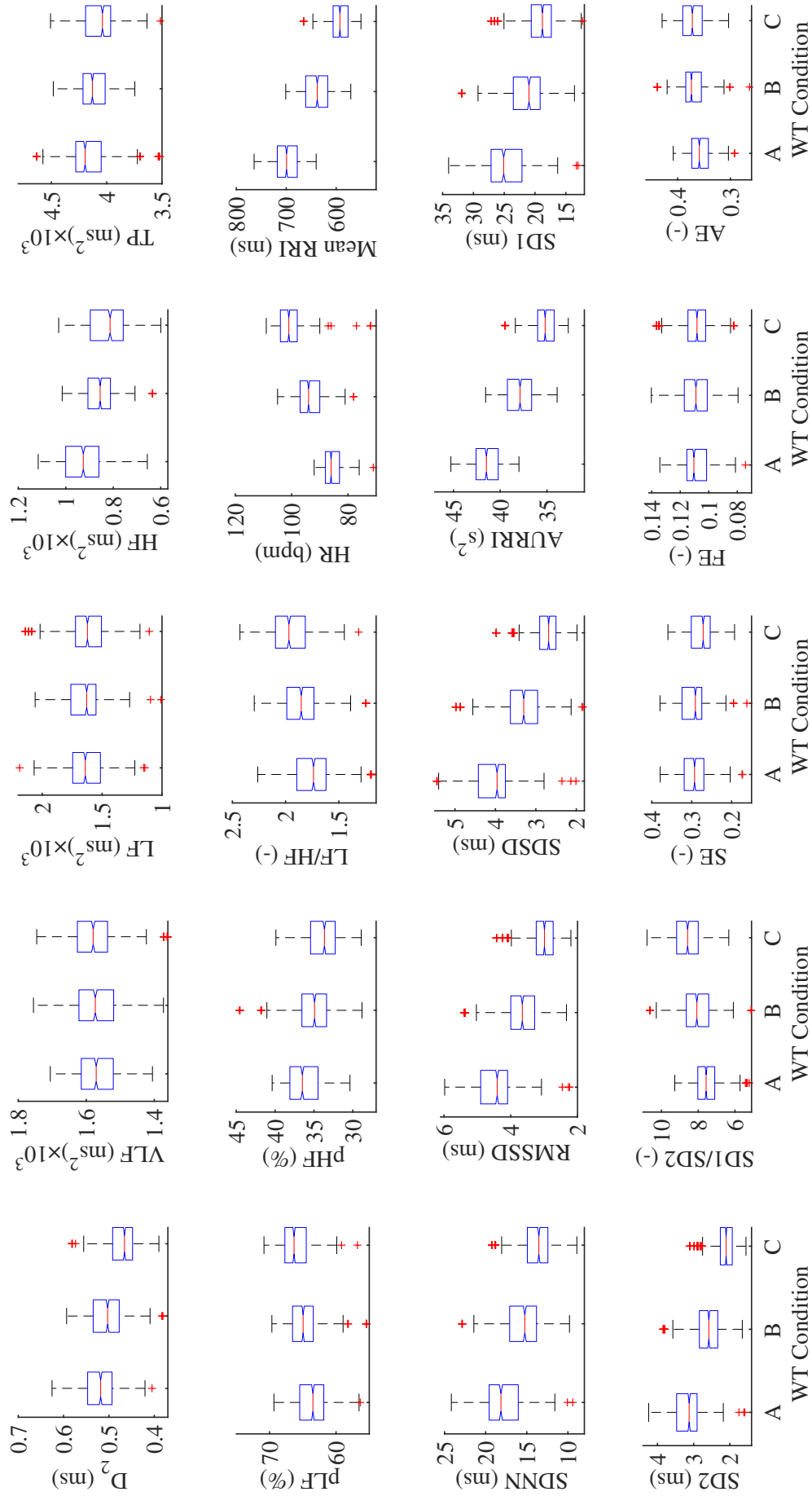


Figure 3.7: Analysis of significant differences for 20 HRV features in three analysis domains under three WT conditions: A = (36–38) °C, B = (38–40) °C, and C = (40–42) °C.

Table 3.1: The statistic results of the HRV features based on different bathtub WT.

HRV Features	Features trend	(36 38] $^{\circ}$ C		(38 40] $^{\circ}$ C		(40 42] $^{\circ}$ C		p value			
		Mean	SD	Mean	SD	Mean	SD	$p1$	$p2$	$p3$	
Time	HR (bpm)	$\uparrow\uparrow$	85.55	3.38	94.07	4.65	101.30	4.17	0	0	0
Domain	Mean RRI (ms)	$\downarrow\downarrow$	699.93	27.53	637.04	30.67	591.15	22.42	0	0	0
	SDNN (ms)	$\downarrow\downarrow$	17.99	2.94	15.48	2.48	13.70	1.87	0	0	0
	RMSSD (ms)	$\downarrow\downarrow$	4.54	0.74	3.69	0.57	3.03	0.42	0	0	0
	SDSD (ms)	$\downarrow\downarrow$	4.11	0.65	3.32	0.50	2.72	0.35	0	0	0
	AURRI (s^2)	$\downarrow\downarrow$	41.51	1.62	37.82	1.80	35.12	1.32	0	0	0
Frequency	VLF Power (ms^2)	\uparrow	1561.77	78.82	1567.90	87.13	1573.03	80.22	0.07	0.14	0
Domain	LF Power (ms^2)	\wedge	1631.05	182.50	1646.35	159.13	1633.92	175.79	0.04	0.11	0.74
	HF Power (ms^2)	$\downarrow\downarrow$	922.03	97.45	859.79	68.12	826.23	86.79	0	0	0
	Total Power (ms^2)	$\downarrow\downarrow$	4157.74	199.76	4114.04	158.49	4065.92	159.75	0	0	0
	PLF (%)	$\uparrow\uparrow$	63.53	2.37	64.75	2.58	65.91	2.29	0	0	0
	pHF (%)	$\downarrow\downarrow$	36.36	2.37	35.13	2.45	33.97	2.20	0	0	0
	LF/HF (-)	$\uparrow\uparrow$	1.75	0.18	1.85	0.20	1.95	0.19	0	0	0
Non-linear	D_2 (ms)	$\downarrow\downarrow$	0.52	0.04	0.51	0.04	0.47	0.04	0	0	0
Domain	SD1 (ms)	$\downarrow\downarrow$	24.94	4.10	21.51	3.48	19.11	2.62	0	0	0
	SD2 (ms)	$\downarrow\downarrow$	3.21	0.53	2.61	0.40	2.14	0.30	0	0	0
	SD1/SD2 (-)	$\uparrow\uparrow$	7.63	0.82	8.03	0.86	8.65	0.85	0	0	0
	SE (-)	\wedge	0.29	0.04	0.30	0.03	0.27	0.03	0.15	0	0
	FE (-)	\sim	0.11	0.01	0.11	0.01	0.11	0.01	0.21	0.04	0.43
	AE (-)	\sim	0.36	0.02	0.37	0.02	0.37	0.02	0	0.14	0

$\downarrow\downarrow$ ($\uparrow\uparrow$): Significantly reduced (increase) with increasing WT $p < 0.05$; \uparrow (\uparrow): Reduced (increase) with increasing WT $p > 0.05$; \wedge : Increased first and then reduced with increasing WT; \sim : Unobvious change; $p1$ = between (36–38) $^{\circ}$ C and (38–40) $^{\circ}$ C; $p2$ = between (38–40) $^{\circ}$ C and (40–42) $^{\circ}$ C; $p3$ = between (36–38) $^{\circ}$ C and (40–42) $^{\circ}$ C. (36–38) $^{\circ}$ C: $36 < WT \leq 38$ $^{\circ}$ C; (38–40) $^{\circ}$ C: $38 < WT \leq 40$ $^{\circ}$ C; (40–42) $^{\circ}$ C: $40 < WT \leq 42$ $^{\circ}$ C;

experiment only includes ten subjects, the number is too small. What's more, the experiment should include the healthy and unhealthy people from the young to older. Second, the variations of the WT is too big during the data collection process. Third, the controlled WTs condition is inconsistent for all the subjects. For example, when the WT is 40°C – 42°C , some subjects just feel a little uncomfortable and can continue to collect the data. But some other subjects can not endure the high WT environment. Therefore, in order to be safe, in this case, we must turn on the cooling fan for these wishers.

Some HRV features are significantly and monotonously increasing or decreasing when the WT is increasing, which is highly consistent with our initial hypothesis. However, further improvements are still needed. In future research works, we will compare the HRV levels between the bathing state and the rest state. We will quantitatively analyze the influence of WTs on mental stress level. Finally, we hope to accurately evaluate the mental stress during bathing via the HRV analysis in the daily life. The relationship between the HRV and causes of death from cardiac diseases during bathing is unknown now, which should be explored in the future work. In addition, we will explore how to control the WTs according to the HRV levels during bathing, so that the people feel more comfortable.

Chapter 4

Personal Identification

4.1 Introduction

There are many drowning accidents during bathing every year [128], especially among the elderly with heart diseases. The main reason may be that when the people enter the bathtub, the high WT and water pressure have an important impact on the people, which induces sudden change of the HR and cause sudden death during bathing. If we can monitor the health condition according to the level of dynamic changes of HR in real time during bathing, then some drowning accidents will be avoided in advance. And when the drowning accidents is happening, we can send the personal information which including the name, gender, address, medical history, medication history, and medication contraindications, etc. to the nearest hospital and quickly take some first aid measures. However, the preliminary task is how to accurately and quickly perform personal identification during bathing. There are many personal identification methods can be used, such as the fingerprint, iris, face, voice, etc. However, all of them have to rely on special equipments such as a scanner, camera, voice recorder, and so on. Moreover, the bathroom is a private and humid environment, it is not suitable to install these equipments in the bathroom. Therefore, this study proposes a new personal identification method using the ECG signal at different WTs during bathing. In our previous study, we confirmed that it was feasible to perform personal identification using ECG during bathing. And we also noticed that the different water temperatures (WTs) had an important impact on the personal rate during bathing. To be specific, when we use the ECG which is collected at low WT ($38\pm 0.5^{\circ}\text{C}$) to train and test the classification model, the best and robust identification rate is 82.67%. But when we use the ECG at high WT ($42\pm 0.5^{\circ}\text{C}$) to test the trained model, the identification rate is only 13.33%. In the same way, when we use the ECG which is collected at high WT ($42\pm 0.5^{\circ}\text{C}$) to train and test the classification model, the best and robust identification rate is 85.50%. But when we use the ECG at low WT ($38\pm 0.5^{\circ}\text{C}$) to test the trained model, the identification rate is only 12.17%.

This chapter mainly introduces the personal identification using the ECG signal during bathing. In the above chapter, we notice that the WTs have an important impact on the HRV, which results in the significant varieties in the level of some HRV characteristics. The main reasons may be the irritation of the water temperature and water pressure on the people during bathing. What's more, our

previous study confirmed that different WTs have an important impact on the identification rate. Therefore, we will first explore how to improve the identification performance of using ECG during bathing. Because ECG has a strong time dependence, in order to improve the identification accuracy and reduce computational complexity, a RNN-based identification system is designed. Finally, in order to quickly and accurately perform personal identification during bathing, we explore the impact of the number of heart beats on the identification rate.

4.2 Improvement of Personal Identification Rate

In each cardiac cycle, as the pacing point, the atrium, and the ventricle are successively excited, there will be changes in bioelectricity. The repeated mechanical beating of the heart generates static electricity on the surface of human skin. We collect this static electricity through special equipment, which could be drew out by the electrocardiograph. Then we can get a series of digital signals, which is called the electrocardiogram (ECG). The ECG exists in all the living creatures and has its unique characteristics. The first characteristic is that it has strong randomness. It is a quasi-periodic signal and has strong non-linearity and non-stationarity, which cannot be described mathematically with accurate mathematical functions. The second characteristic is that it is extremely weak. ECG is a very weak signal, the amplitude is about millivolt (mv) level. Its frequency range is about [0.05Hz, 100Hz], where the signal energy is mainly concentrated in [0.5Hz, 45Hz]. The third characteristic is that it is easily affected by the poor interference resistance. Because of the distinctions in anatomy, size, and position of the heart, the ECG differs in all people. And it also shows individual difference because different sex, age, body weight, chest configuration, health conditions, and so on. Because the ECG is very weak, it is extremely susceptible to the influence of human internal and external environments during the acquisition process, such as the movement of human limbs, breathing, electromagnetic interference in the surrounding environment, etc. Therefore, the directly collected ECG signal includes a lot of noise. Common noises include baseline wandering, power frequency interference, electromyogram(EMG) interference, and motion artifacts. There are some important features in ECG signal, all of the features are unique and distinguishable for each person. The most important components of the ECG in a healthy person include the P wave, QRS complex, and T wave, as are shown in Fig. 4.1. The depolarization of the atria produces the P wave, the depolarization of the ventricles produces the QRS complex wave, and the repolarization of the ventricles produces the T wave [129]. According to the collection method using different leads, the ECG can be distinguished into three types, which are 3-lead ECG, 5-lead ECG and 12-lead ECG. The most common ECG in the clinical application is named 12-lead ECG, which can record the potential changes of 12 sets of leads on the body surface at the same time, and draw 12 sets of lead signals. The 3-lead and 5-lead ECG are mostly used in situations where the electrical activity of the heart needs to be continuously monitored in real time, such as during surgery or on the way of an ambulance is transferring a patient. Now, the ECG has been taken as a useful and standard tool for the cardiac diseases detection both in the clinical application and academic research work because of its noninvasive and

convenient collection method.

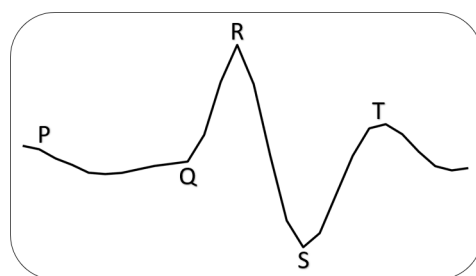


Figure 4.1: Main components of the normal ECG waveform.

Many previous studies took the ECG as an identification tool and achieved well performance. Since L. Biel et al. explored the feasibility of the ECG as an identification tool in 1999 [130], then more and more studies took the ECG as an emerging and useful biomedical identification tool in recent years [15, 131–144]. However, there are a few studies used the bathtub ECG to perform personal identification. In our previous study, we have proven the feasibility of bathtub ECG in identity validation [145] and achieved good result. We also explored the impact of bathtub water temperature on identity validation with ECG signal during bathing and we found that it had an important impact on the identity validation rate [60]. This study aims to explore how to improve the identification performance using ECG at low and high WT during bathing.

4.2.1 Methods and Materials

4.2.1.1 Subjects and ECG Recordings

The data collection system is shown in Fig. 2.5. In this study, the sampling rate is 100 Hz, and the ECG monitor is not the OpenBCI Ganglion Biosensing Board, we use another monitor to collect the ECG signal. The data collection procedures which involving the human subjects described in this study were approved by the Public University Corporation, the University of Aizu Research Ethics Committee. Written informed consent was obtained from each participant before the experiments. Ten participants which were the subjects in the university of Aizu attended the data collection. There were five males and five females, who were approximately between 20 and 25 years old. The data collection process was detailed as follows: firstly, the WTs was controled at 38 ± 0.5 °C. After 220 s, we increased the WTs, which was controled at 42 ± 0.5 °C. After 220 s, the data collection was finished.

4.2.1.2 Data Processing and Analysis

The collected data includes many noises. In order to remove the baseline wandering noise, the Wavelet decomposition and reconstruction method is used. First, the raw ECG is decomposed into several components using the 'db6' mother wavelet at level 4. Then the approximation coefficients is subtracted from the raw ECG. Next, the ECG is reconstructed. The decomposition and reconstruction result is shown in Fig. 4.2.

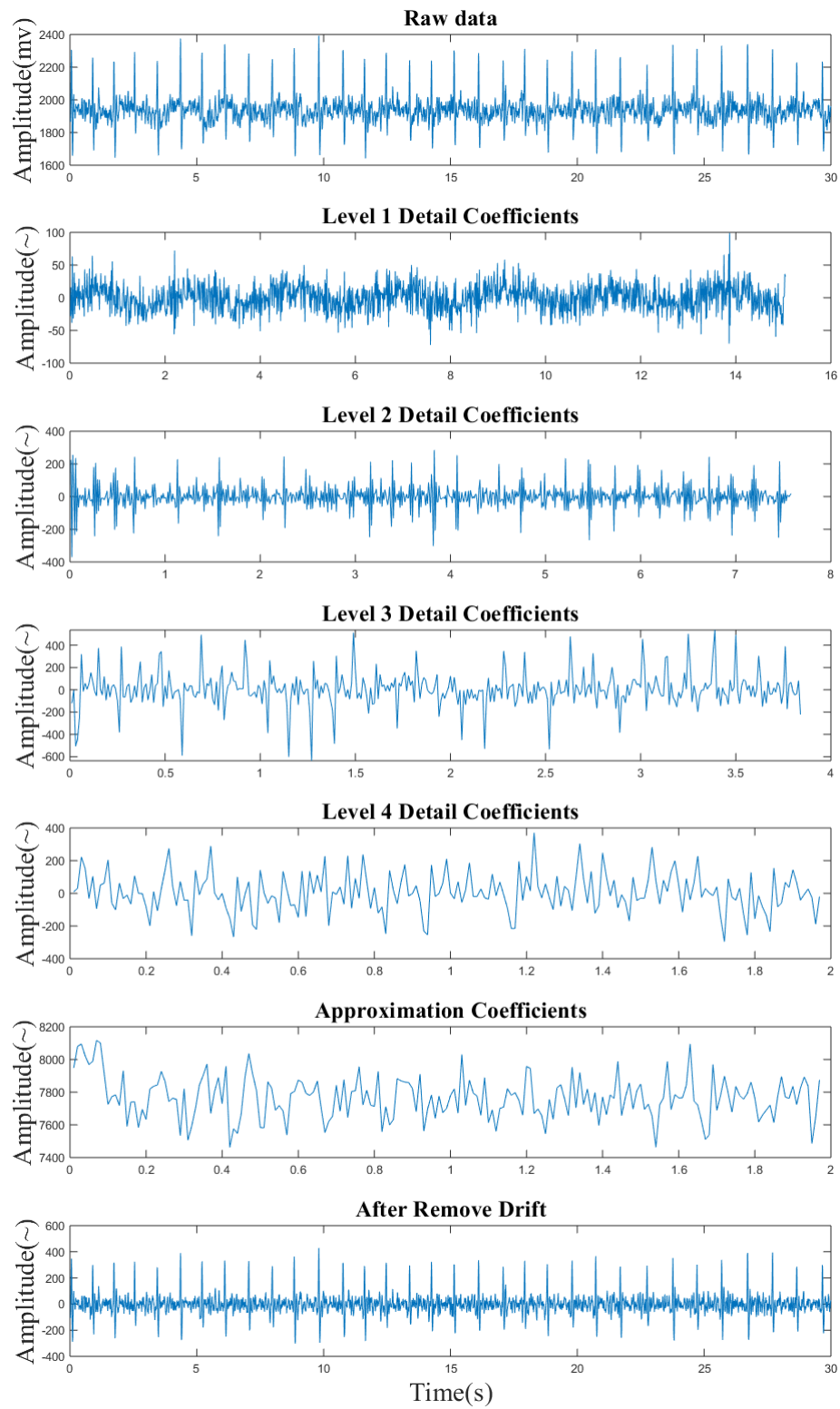


Figure 4.2: Process of the ECG decomposition and reconstruction.

In order to reduce the computational complex, the ECG is normalized into the range of 0 to 1 using the 'mapminmax' function, the equation is shown in (4.1):

$$y = \frac{x - Xmin}{Xmax - Xmin} \quad (4.1)$$

where x is the input data, y is the output data, $Xmax$ is the biggest value of the input signal row vector, $Xmin$ is the smallest value of the input signal row vector.

Next, the R peaks are detected using the function of 'findpeaks', where the 'MinPeakProminence' is 0.42. Then all the RRI and amplitude of R peaks are calculated, the details are shown in Fig. 4.3 and Fig. 4.4. A to J represents every subject respectively, L represents 38 ± 0.5 °C bathtub water temperature and H represents 42 ± 0.5 °C bathtub water temperature.

We can find that the RRI level of each subject in low WT condition (38 ± 0.5 °C) is higher than that in high WT condition (42 ± 0.5 °C), as is shown in Fig. 4.3. However, compare with the R peaks amplitude in low WT, there are three situations of the R peaks amplitude in high WT: the R peaks amplitudes of the subject A, F, G, and J are significantly increasing, the R peaks amplitudes of the subject B, D and H are almost unchanged, and the R peaks amplitudes of the subject C, E and I are significantly decreasing. The details are shown in Fig. 4.4

4.2.1.3 Data Structure and CNN Model Design

In this study, the convolutional neural network (CNN) is used to perform personal identification. Before the classification, the training data and test are prepared. The QRS complex is the most important component of the ECG. Therefore, the QRS complex is used to perform classification. The duration of a complete QRS complex is about 60 ms to 100 ms for a healthy person. In order to segment a complete QRS complex, the segmentation includes 28 points, which is 280 ms. Specifically, when all the R peaks are detected, centering on the position of each detected R peak, 13 sampling points forward and 14 sampling points backward are segmented, which is represented using a 1×28 one-dimensional array. Finally, 470 QRS complex are segmented for each subject, where the first 235 QRS complex are segmented at 38 ± 0.5 °C, and the other 235 QRS complex are segmented at 42 ± 0.5 °C.

Based on each WT condition, the 1st to 28th QRS complex are taken as the first image, the 2nd to 29th QRS complex are taken as the second image, and so on. Finally, 208 images are prepared, the first 167 (about 80%) images are taken as the training data and the other 41 images (about 20%) are taken as the testing data. One of the images is shown in Fig. 4.5. For all the subjects, the number of training images is 3340, where first 1670 images are from the low WT and the other 1670 images are from the high WT. And the number of test images is 820, where first 410 images are from the low WT and the other 410 images are from the high WT.

The designed CNN model includes five layers, the details are shown in Fig. 4.6. The input data is a 28×28 grayscale image. The convolution layer includes 20 3×3 filters. After one convolution operation, its output includes 20 $26 \times 26 \times$ subsampling images. The downsampling result of the pooling layer can be represented using $13 \times 13 \times 20$ 3D array. The fully connected method is used in the

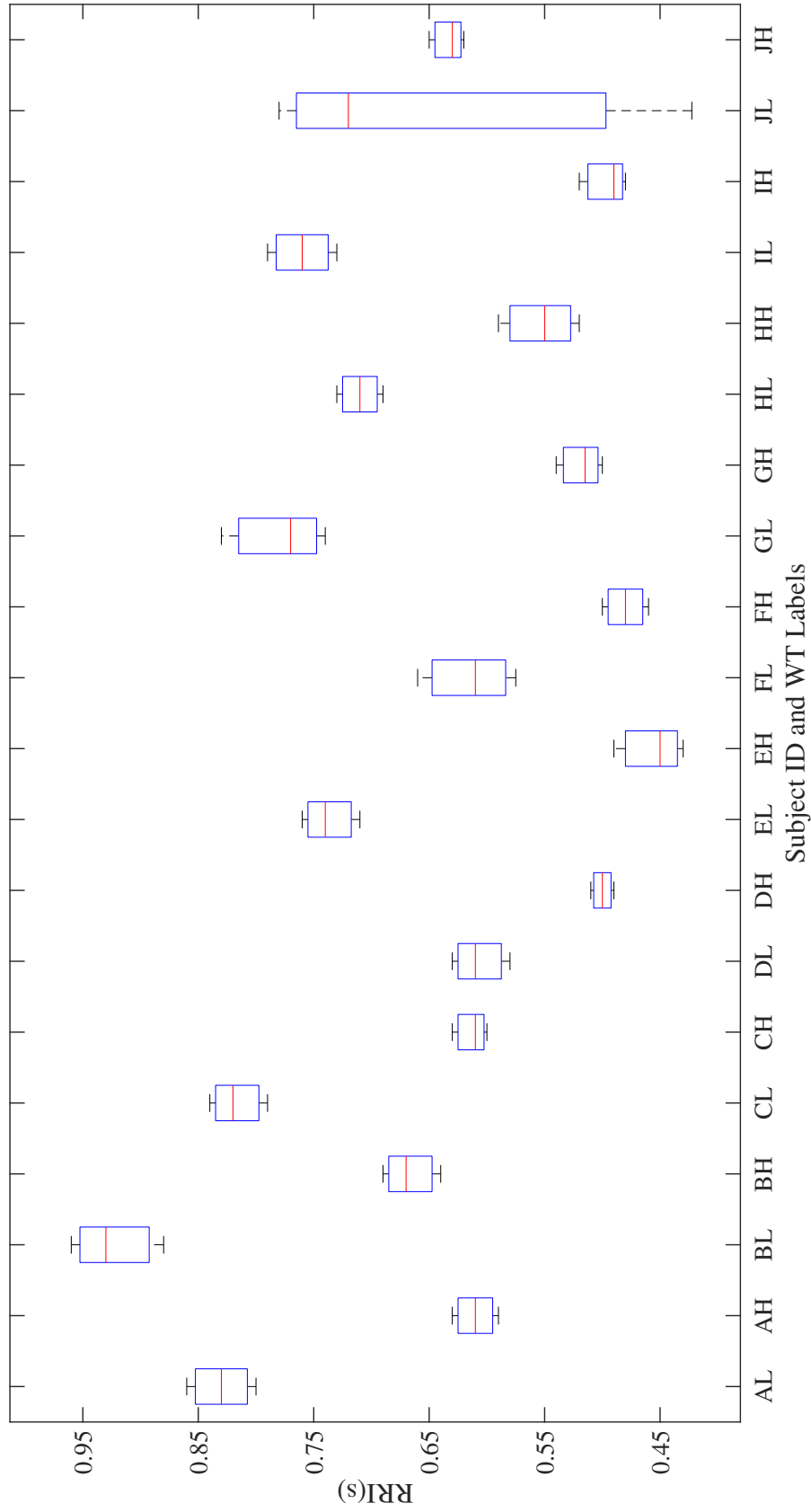


Figure 4.3: Comparison of RRI in different WTs (A to J represents each subject, L represents low water temperature, H represents high water temperature).

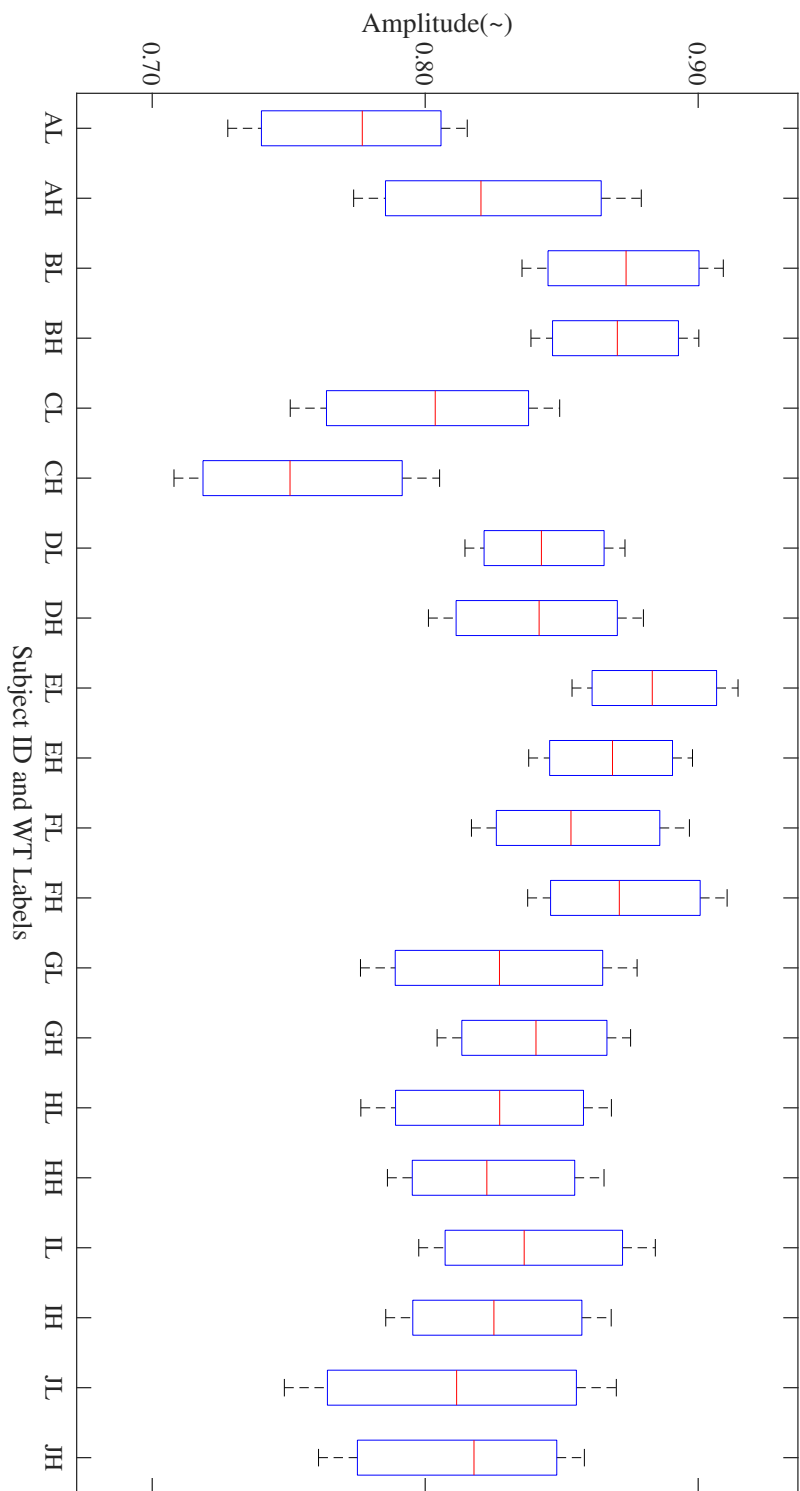


Figure 4.4: Comparison of R peaks amplitude in different WTs (A to J represents each subject, L represents low water temperature, H represents high water temperature).

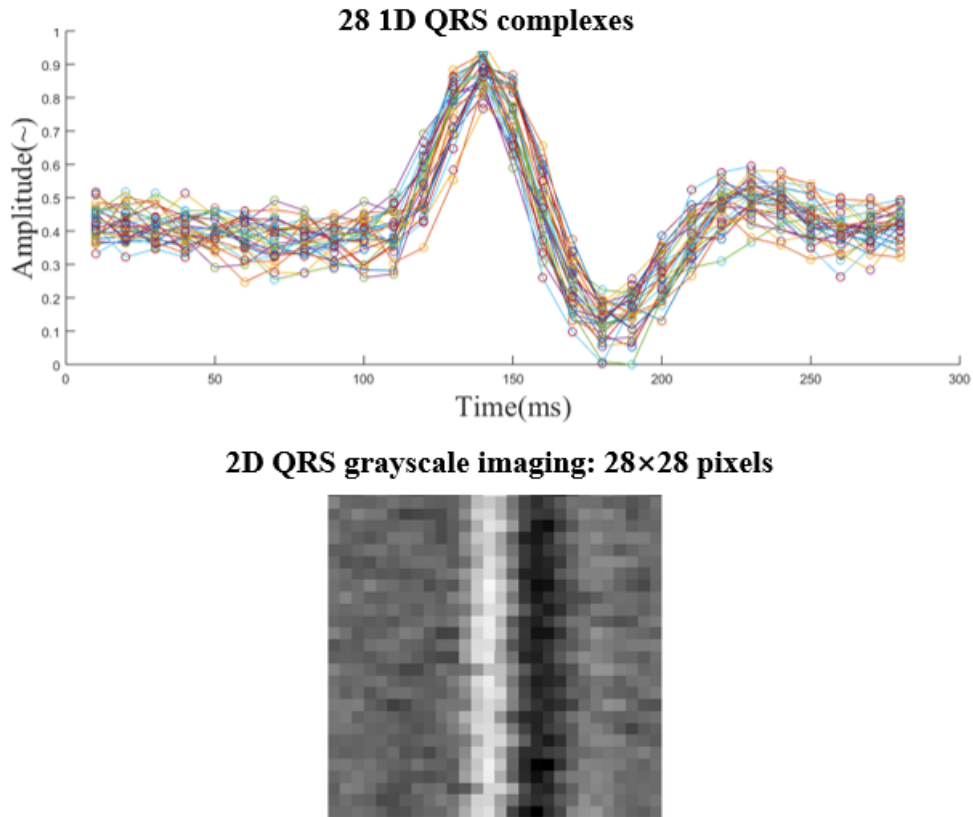


Figure 4.5: 28 1D QRS complexes to 2D QRS imaging.

hidden layer. In the output layer, the 'softmax' function is used to calculate the identification rate. The output of the 'softmax' function is a 10×1 vector, each value indicates the possibility of each subject. When the label of the input data is same with the row of the maximum of this vector, then accept; otherwise, reject.

4.2.2 Results and Discussion

In this study, we do not use the transfer learning method. All the parameters of the CNN model are firstly initialized. If the training epoch is too short, the model will not converge quickly and its classification performance will be very poor. But if the training epoch is too long, then the model will be overfitting and its generalization ability will not be strong. Therefore, the training epoch should be moderate. During the training process, all the training images are randomly rearranged with a new order. During the test process, the varieties of accuracy which includes the low WT and high WT are shown in Fig. 4.7. We can find that the identification rates of the low and high WT data are no more than 91%, and the variation curves of low and high WT are not stable.

To reveal the reasons, some evaluation parameters are defined, such as the true positive (TP), false positive (FP), true negative (TN), false negative (FN), Precision, Recall, F-score, TP rate (TPR), FP rate (FPR), where,

$$precision = \frac{TP}{TP + FP} \quad (4.2)$$

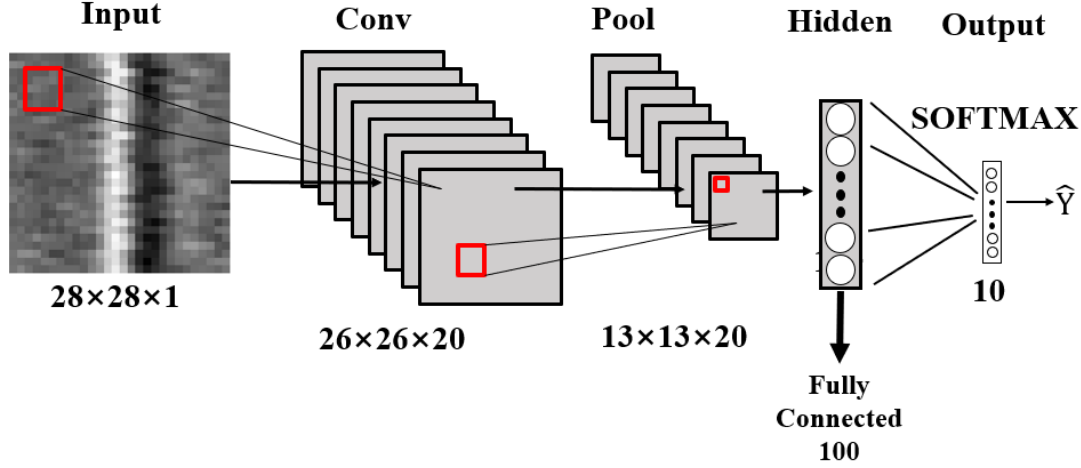


Figure 4.6: CNN model.

$$Recall (TPR) = \frac{TP}{TP + FN} \quad (4.3)$$

$$F\text{-score} = \frac{2 * precision * Recall}{precision + Recall} \quad (4.4)$$

$$FPR = \frac{FP}{FP + TN} \quad (4.5)$$

What's more, the confusion matrix of the multi-classification problem is used, as is shown in Fig. 4.8 and 4.9. When the test data is from the low WT, the trained model easily took the subject 1 as subject 9, and took the subject 10 as the subject 4. When the test data is from the high WT, the trained model easily took the subject 1 as subject 3 and 4, and took the subject 3 as the subject 10, and also easily took the subject 9 as subject 2. The detailed accuracy of each subject on the low and high WT is shown in Tab. 4.1 and 4.2.

In order to choose a moderate and better training epoch, the receiver operating characteristic (ROC) curve is used, which are shown in Fig. 4.10 and 4.11. The area under curve (AUC) is shown in Tab. 4.3. It shows that when the training epoch is in the range of 400 to 500, the classification model becomes stable. When the training epoch is more than 500, the model will be overfitting.

The training data must be randomly rearranged with a new order before the training process, or the training model will not converge, and the final accuracy is only 10%. When design the classification model, the number and size of the filter on the convolutional layer is most important. What's more, the learning rate and the batch size also affect the convergence curve and identification rate. Only when all parameters are in a reasonable range can the constructed model achieve the best classification performance. In this study, the learning rate is test from the range of 0.01 to 0.6, and the batch size is test from 10 to 100. Finally, the learning rate is set at 0.01 and the batch size is set at 50. The training data is constructed using the ECG which is collected at low and high WT, then the accuracy of low WT is increasing from 12.17% to 90.49%, and the accuracy of high WT is increasing from 13.33% to 90.00%. It can be seen that increasing

Table 4.1: Test result based on low WT.

Subject	TP	FP	FN	TN	Precision (%)	F-score (%)	TPR (%)	FPR (%)
1	36	2	5	367	94.74	91.14	87.80	0.54
2	41	0	0	369	100.00	100.00	100.00	0.00
3	41	0	0	369	100.00	100.00	100.00	0.00
4	41	32	0	337	56.16	71.93	100.00	8.67
5	41	0	0	369	100.00	100.00	100.00	0.00
6	41	0	0	369	100.00	100.00	100.00	0.00
7	41	0	0	369	100.00	100.00	100.00	0.00
8	41	0	0	369	100.00	100.00	100.00	0.00
9	41	5	0	364	89.13	94.25	100.00	1.36
10	7	0	34	369	100.00	29.17	17.07	0.00
Total	371	39	39	3651	90.49	90.49	90.49	1.06

Table 4.2: Test result based on high WT.

Subject	TP	FP	FN	TN	Precision (%)	F-score (%)	TPR (%)	FPR (%)
1	18	0	23	369	100.00	61.02	43.90	0.00
2	41	8	0	361	83.67	91.11	100.00	2.17
3	34	11	7	358	75.56	79.07	82.93	2.98
4	41	14	0	355	74.55	85.42	100.00	3.79
5	41	0	0	369	100.00	100.00	100.00	0.00
6	41	0	0	369	100.00	100.00	100.00	0.00
7	41	0	0	369	100.00	100.00	100.00	0.00
8	38	0	3	369	100.00	96.20	92.68	0.00
9	33	3	8	366	91.67	85.71	80.49	0.81
10	41	5	0	364	89.13	94.25	100.00	1.36
Total	369	41	41	3649	90.00	90.00	90.00	1.11

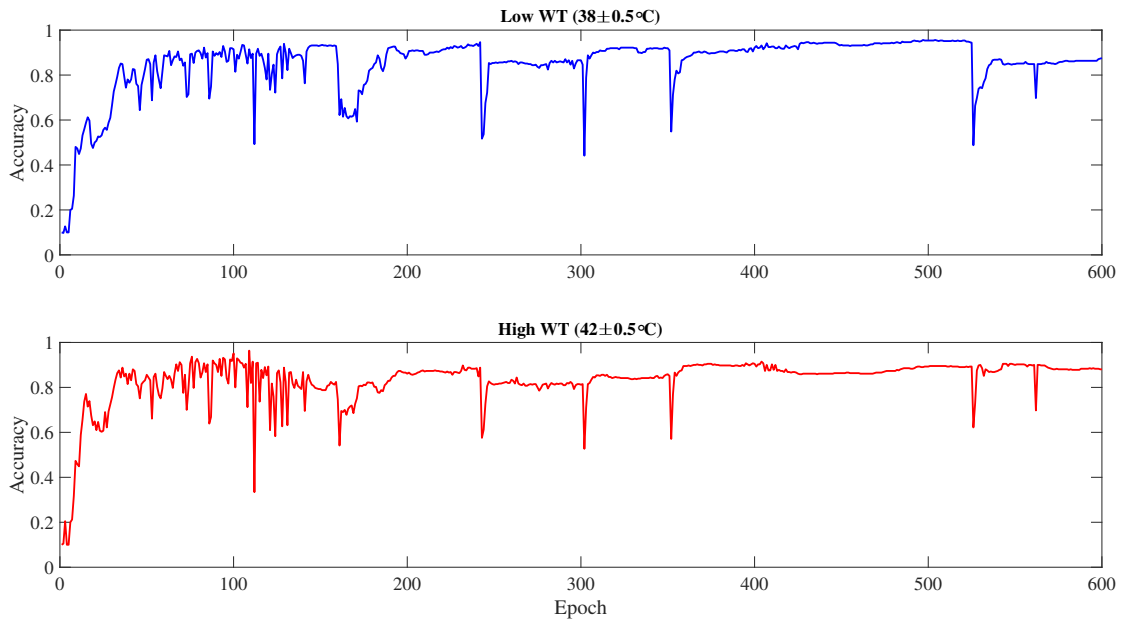


Figure 4.7: Varieties of accuracy based on different training epoch.

Table 4.3: Varieties of AUC based on different training epoch.

Epoch	100	200	300	400	500	600
AUC on Low WT	0.59	0.60	0.84	0.97	0.97	0.43
AUC on High WT	0.75	0.83	0.75	0.94	0.96	0.72

the diversity of samples can greatly improve the identification rate. When the training epoch is increasing from 100 to 600, the AUC of the low WT is increasing first and then suddenly decreasing. However, the AUC of the high WT is slowly increasing and then slowing decreasing. When the training epoch is smaller than 400, the trained model has a strong ability to classify the images from the high WT. When the training epoch is in the range of 400 to 500, the trained model has the strongest ability to classify both of the images from low WT and high WT. But when the training epoch is bigger than 500, the classification ability of the trained model drops rapidly, especially it has a poorest classification ability for the low WT, which once again illustrates the importance of the training epoch to the model classification ability.

4.2.3 Conclusions and Future Work

This study explores how to improve the identification performance using the ECG during bathing. The experiment result shows that increasing the diversity of training samples can greatly improve the identification rate of the model. The identification rate of this study increased by about 6 times compare to the previous study. What's more, appropriate model parameters have an important influence on the convergence speed and identification ability of the model. The most important is that the training epoch should not be too short or too long.

The final identification rate is not more than 91% for both of low and high WT. There are two possible reasons. The first is that there are too much noises in the collected ECG and the signal processing is not very good. The second reason

		Predicted subject ID										
		1	2	3	4	5	6	7	8	9	10	
True subject ID	1	87.8% 36	0.0% 0	0.0% 0	4.9% 2							
	2	0.0% 0	100.0% 41	0.0% 0	0.0% 0	0.0% 0						
	3	0.0% 0	0.0% 0	100.0% 41	0.0% 0	0.0% 0	0.0% 0	0.0% 0	0.0% 0	0.0% 0	0.0% 0	0.0% 0
	4	0.0% 0	0.0% 0	0.0% 0	100.0% 41	0.0% 0	0.0% 0	0.0% 0	0.0% 0	0.0% 0	0.0% 0	78.0% 32
	5	0.0% 0	0.0% 0	0.0% 0	0.0% 0	100.0% 41	0.0% 0	0.0% 0	0.0% 0	0.0% 0	0.0% 0	0.0% 0
	6	0.0% 0	0.0% 0	0.0% 0	0.0% 0	0.0% 0	100.0% 41	0.0% 0	0.0% 0	0.0% 0	0.0% 0	0.0% 0
	7	0.0% 0	0.0% 0	0.0% 0	0.0% 0	0.0% 0	0.0% 0	100.0% 41	0.0% 0	0.0% 0	0.0% 0	0.0% 0
	8	0.0% 0	0.0% 0	0.0% 0	0.0% 0	0.0% 0	0.0% 0	0.0% 0	100.0% 41	0.0% 0	0.0% 0	0.0% 0
	9	12.2% 5	0.0% 0	100.0% 41	0.0% 0	0.0% 0						
	10	0.0% 0	0.0% 0	0.0% 0	0.0% 0	0.0% 0	0.0% 0	0.0% 0	0.0% 0	0.0% 0	0.0% 0	17.1% 7

Figure 4.8: Confusion matrix of test result based on low WT.

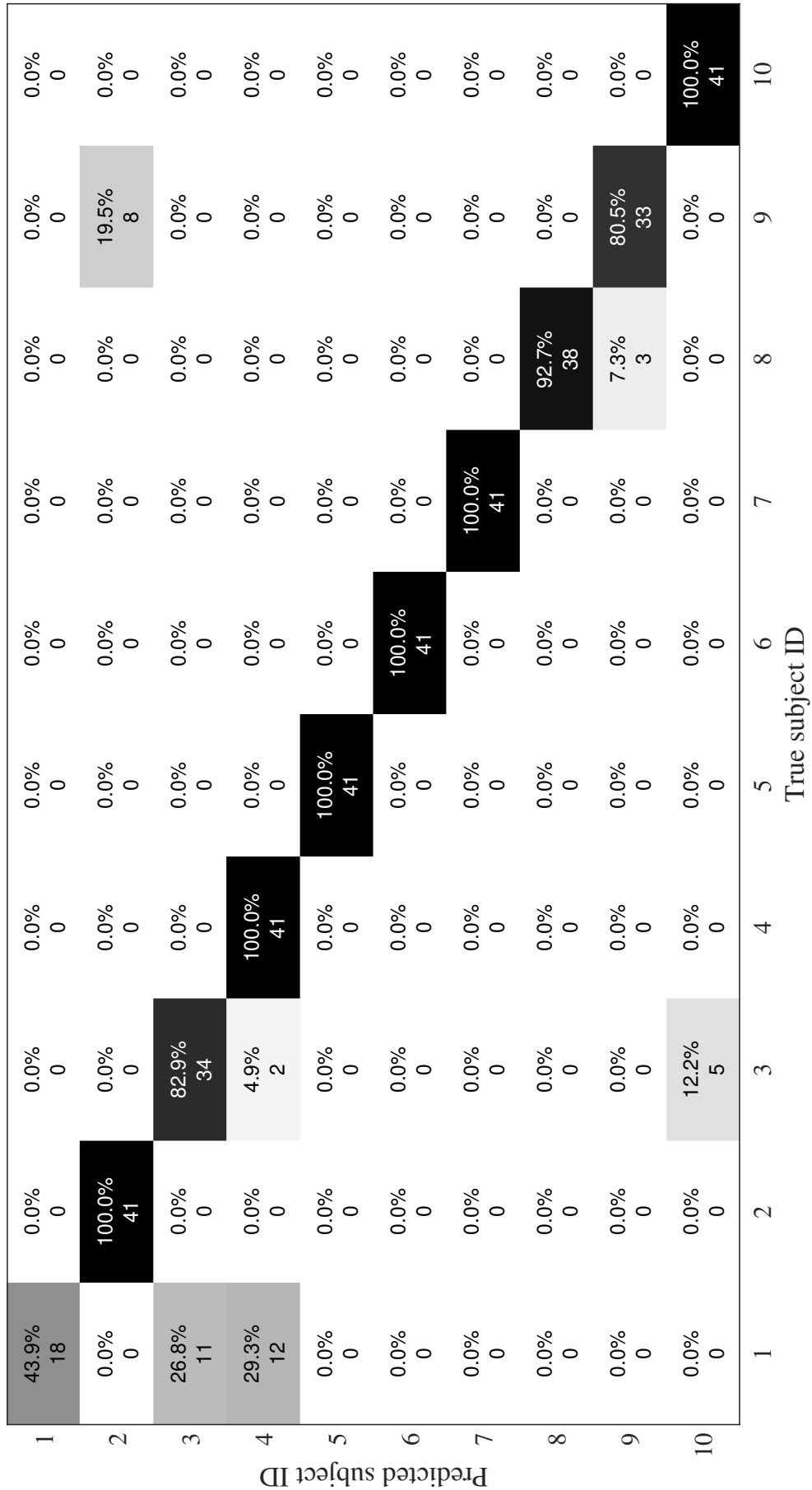


Figure 4.9: Confusion matrix of test result based on high WT.

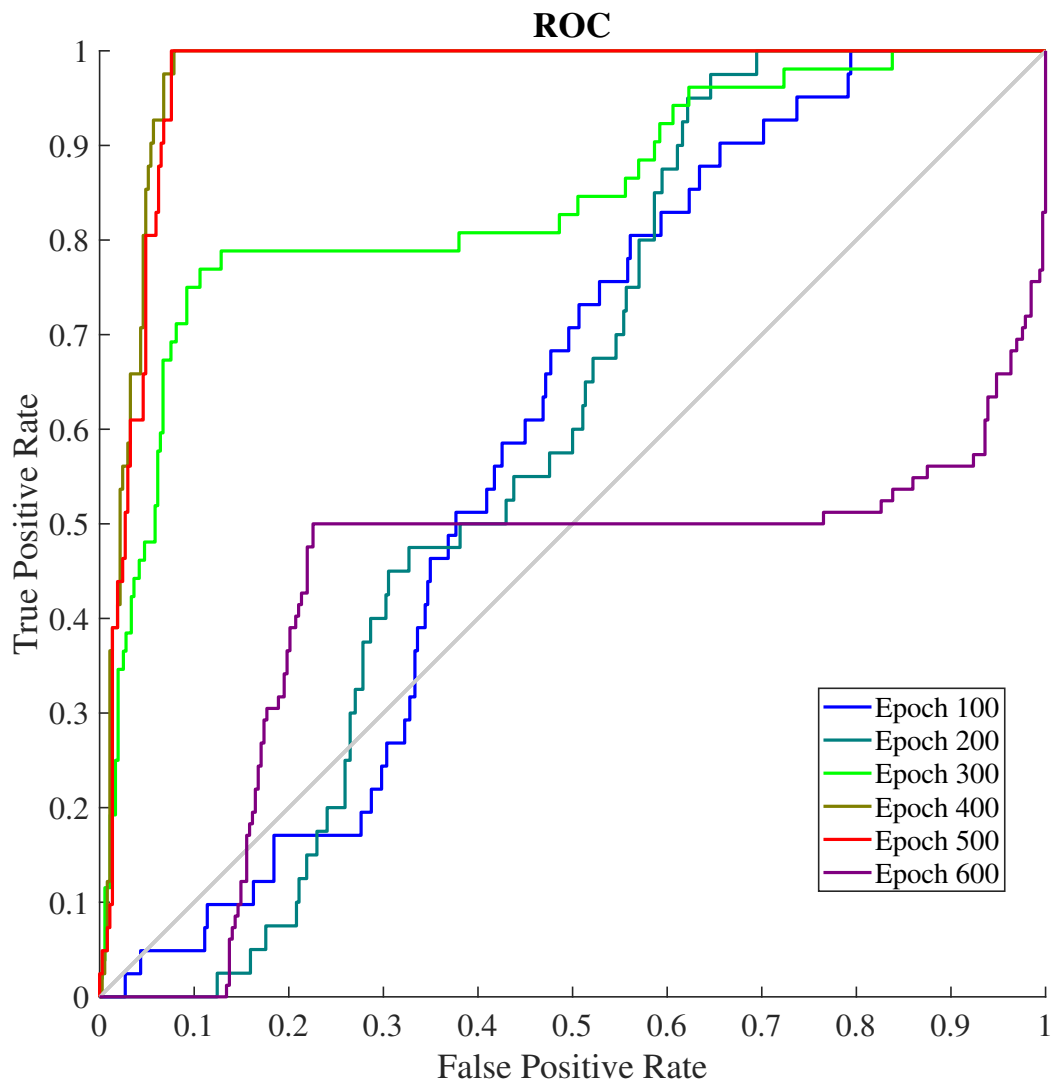


Figure 4.10: ROC curve of low WT based on different training epoch.

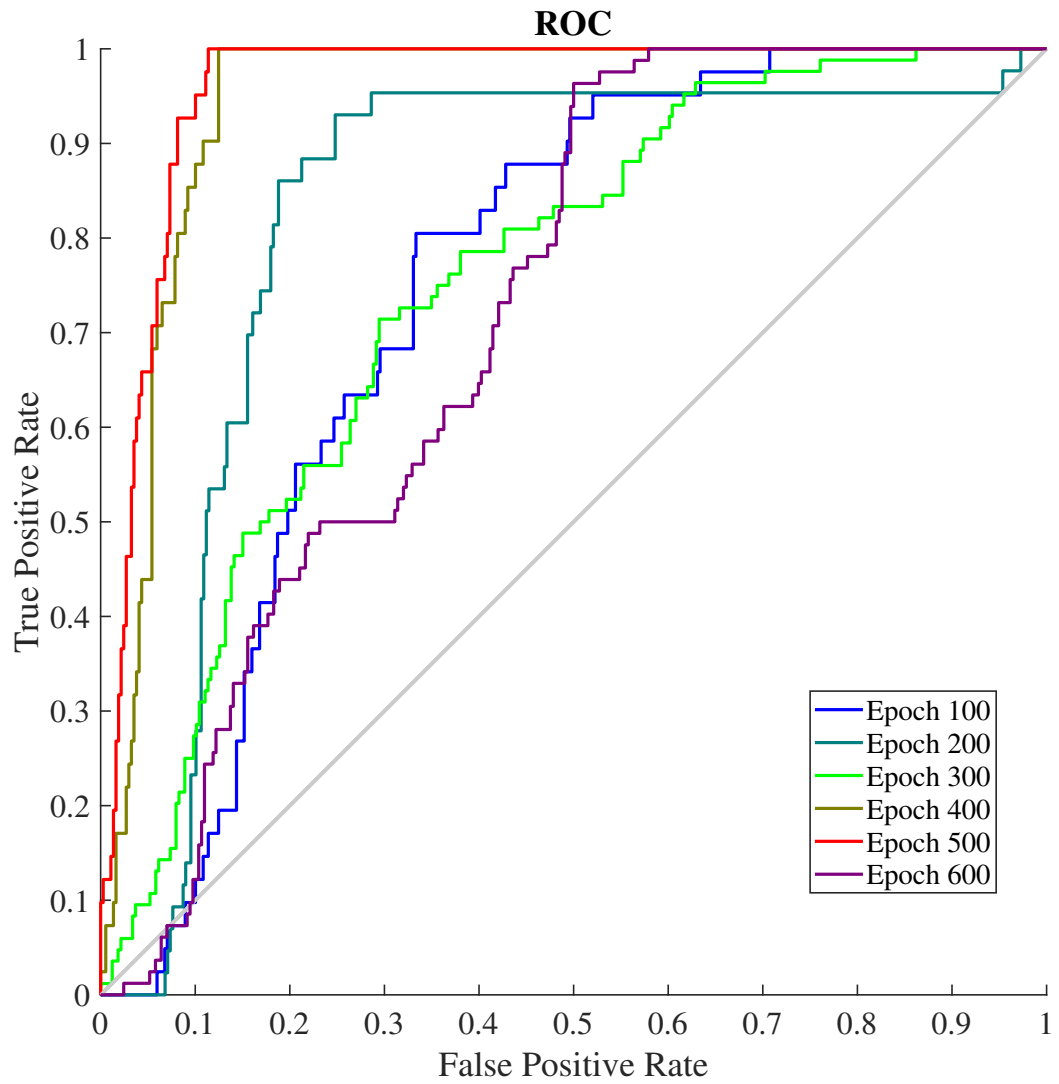


Figure 4.11: ROC curve of high WT based on different training epoch.

is that the ECG is a time-dependence signal, maybe the CNN has a poor ability to classify such a signal. In the future work, we will select a better ECG collection monitor and collect the ECG data with less noise. We will also choose a better way to remove the noise. Because the ECG has a time-dependent characteristic, in order to improve the identification performance, we will try and choose a better classification method.

4.3 RNN-based Personal Identification

In the above section, we explore how to improve the identification rate using ECG during bathing. We find that increasing the diversity of the training data can greatly improve the identification rate. However, the final identification rate is not more than 91% for the low and high WT, which can not meet the practical application. We think there are two reasons, which are that the raw ECG includes more noise and the denoise method is not appropriate, and the CNN is not good at classifying the time-dependent signal. Therefore, this study proposes the RNN-based personal identification using the ECG at different WTs during bathing, aims to design an accurate and fast identification system.

The recurrent neural network (RNN) is a kind of artificial neural network (ANN). It has a strong ability to deal with the time-dependent problems. In this study, we use the long short-term memory (LSTM) network to perform personal identification using the ECG at different water temperatures (WTs) during bathing. The LSTM network is particularly good at dealing with classification problems that are time-dependent. It has been used in the field of deep learning since it was proposed in 1997, which is suitable for processing and predicting important events with relatively long intervals and delays in time series.

LSTM is a special recurrent neural network which is proposed to solve the problem of 'gradient disappearance' in the structure of recurrent neural networks. The reason why LSTM can remember long-term information lies in the designed 'gates' structure. The 'gates' structure is a method for information to pass selectively, including a 'sigmoid' neural network layer and a pointwise multiplication operation. The 'sigmoid' function is shown in equation (4.6):

$$\delta(x) = \frac{1}{1 + e^{-x}} \quad (4.6)$$

where the output of 'sigmoid' function is an array in the range of 0 and 1, it is generally used for binary classification problems. The output value close to 0 means 'not allowed', and the output value close to 1 means 'allowed'.

There are three important gates in the LSTM, as is shown in Fig. 4.12. The first stage is the 'forget gate', which determines what information needs to be forgotten from the previous node, which will 'forget the unimportant, remember the important'. The next stage is the 'input gate', which determines what new information can be stored in the cell state. The final stage is the 'output gate', which determines the output values.

The output f_t in forget gate is shown in equation (4.7): it represents the forgotten probability of the previous cell state.

$$f_t = \delta(W_f \cdot [h_{t-1}, x_t] + b_f) \quad (4.7)$$

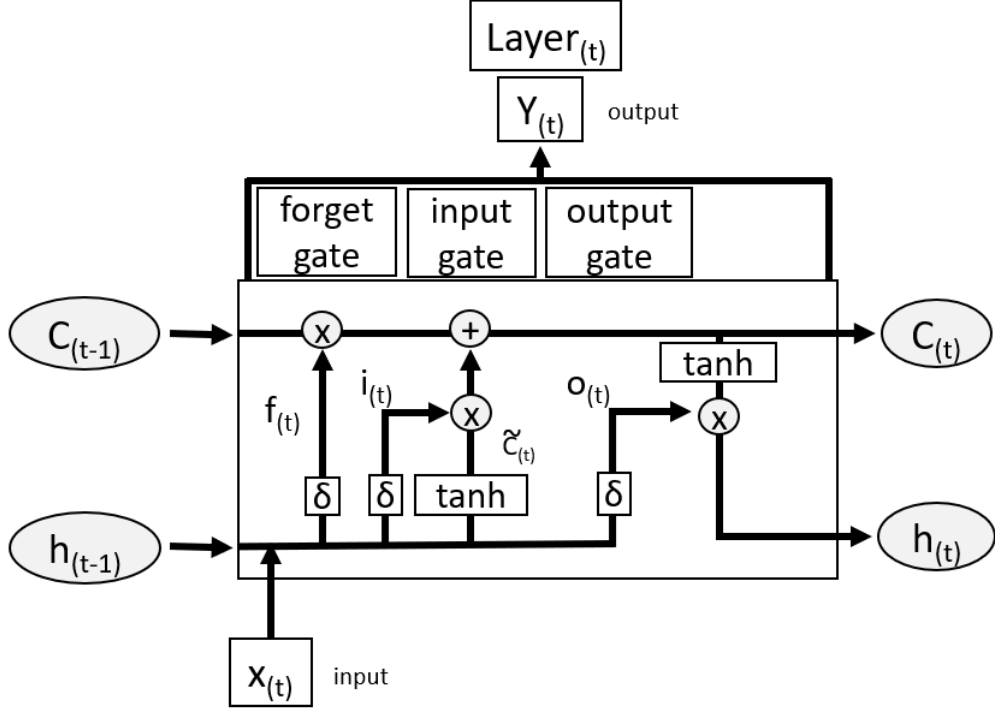


Figure 4.12: Components of one layer in the whole RNN architecture.

where h_{t-1} is the output of last layer, x_t is the input of current layer, δ is the activation function of 'sigmoid' in equation (1). f_t is in the range of $[0,1]$, 0 means 'reject', 1 means 'accept'.

The output C_t in input gate is shown in equation (4.8):

$$C_t = f_t * C_{t-1} + i_t * \tilde{C}_t \quad (4.8)$$

C_t represents the new cell state, $i_t * \tilde{C}_t$ represents the quantity of new information which is retained, i_t and \tilde{C}_t are shown in equation (4.9) and (4.10) respectively:

$$i_t = \delta(W_i \cdot [h_{t-1}, x_t] + b_i) \quad (4.9)$$

$$\tilde{C}_t = \tanh(W_C \cdot [h_{t-1}, x_t] + b_C) \quad (4.10)$$

The output gate is used to control how much of the layer's cell state should be filtered, the output h_t in this layer is shown in equation (4.11):

$$h_t = o_t * \tanh(C_t) \quad (4.11)$$

where o_t is shown in equation (4.12):

$$o_t = \delta(W_o \cdot [h_{t-1}, x_t] + b_o) \quad (4.12)$$

4.3.1 Methods and Materials

4.3.1.1 Data Processing and Analysis

The data collection system is shown in Fig. 2.5, and the ECG monitor is shown in Fig. 2.4, it is the Open Brain Computer Interface Biosensing Ganglion Board. In this study, we collect the ECG signal at five different WT conditions, which include the most commonly used bathtub water temperature environments in daily life. During the data processing stage, we perform baseline removal, spectrum analysis, 50 Hz noise removal, signal smoothing, R peaks detection and QRS complex segmentation. The flowchart of data processing and personal identification is shown in Fig. 4.13.

In order to remove the noise in the raw data, we perform the spectrum analysis. The spectrum analysis result shows that the raw data includes obvious 50 Hz hum noise, which is produced by the electromagnetic interference of the power supply network and its equipment. And the movement and respiration of the subjects during bathing produces obvious baseline wandering. First, we use the 1-D Wavelet decomposition and reconstruction method to remove the baseline wandering. The mother wavelet of 'db6' at level 10 is used to decompose the raw ECG. Then the approximation coefficient is subtracted from the raw ECG data. Next, the ECG is reconstructed using the Wavelet reconstruction at level 8. According to the characteristics of the raw ECG, we notice that the decomposition at level 10 and reconstruction at level 8 can not only effectively separate the baseline wandering component from raw ECG data, but also could keep the useful information of the ECG data as much as possible. To remove the 50 Hz electromagnetic interference hum noise, we choose the the second-order infinite impulse response (IIR) notch digital filter and 1-D digital filter. When calculate the numerator coefficient and denominator coefficient of the digital notching filter, we set the notch located at 0.5 Hz and the bandwidth at 0.0071 at the -3 dB level. The magnitude response is shown in Fig. 4.14, and the difference equation of the 1-D digital filter is shown in equation (4.13).

$$y[n] = \sum_{i=0}^N b_i x[n-i] - \sum_{i=1}^M a_i y[n-i], \quad n \geq 0 \quad (4.13)$$

where $x[n]$ is input to the filter, $y[n]$ is output to the filter, a_i and b_i are the numerator coefficient and the denominator coefficient of the digital notching filter.

Finally, the ECG is smoothed using the 5-point moving average method. The definition of the moving average is shown in equation (4.14):

$$y[n] = \frac{1}{M} \sum_{j=0}^{M-1} x[n-j] \quad (4.14)$$

where $x[n]$ is input signal, $y[n]$ is output signal, M is 5.

The outputs of each step in the data processing are shown in Fig. 4.15. Then we use the 'findpeaks' function to detect the R peaks. And the QRS complex is segmented based on the detected positions of the R peaks, which is a 1×30 array (centering on the position of the R peak, 14 sampling points before and 15 sampling points after are segmented).

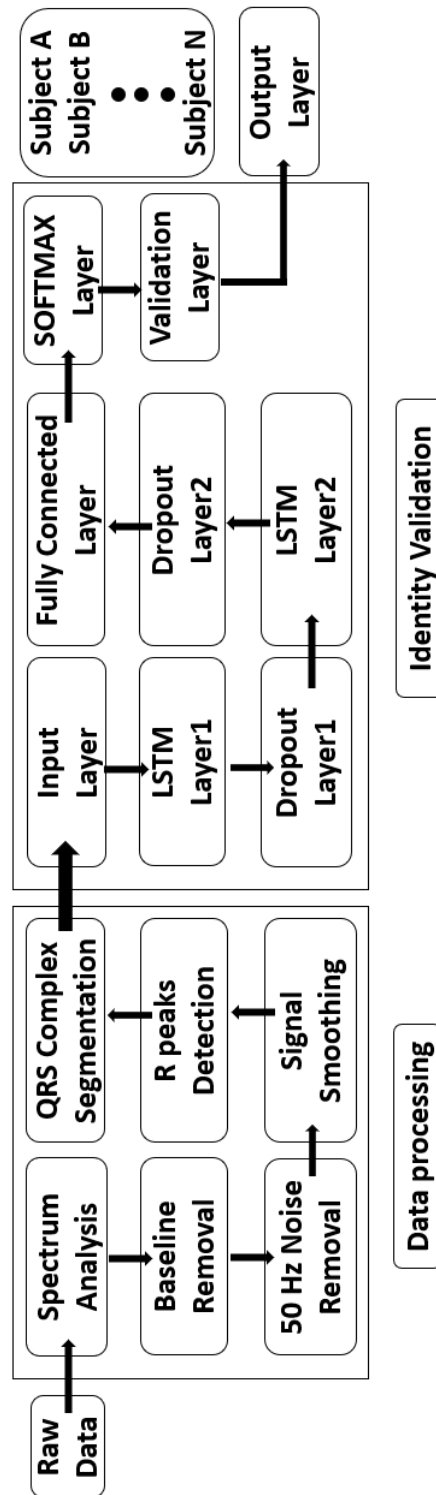


Figure 4.13: Flowchart of data processing and personal identification.

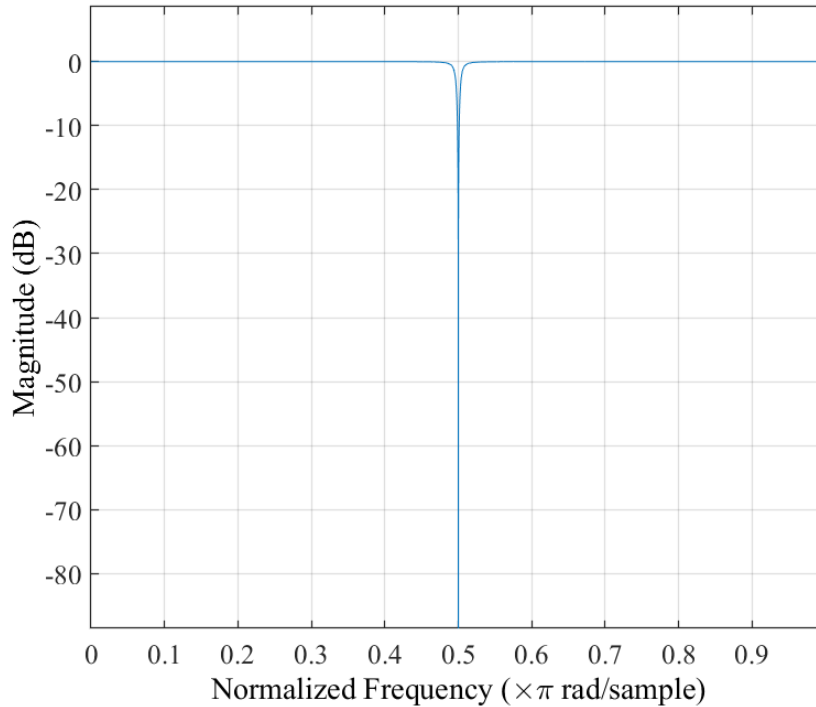


Figure 4.14: Magnitude response.

4.3.1.2 Data Structure and Classification Model Design

In this study, one of artificial recurrent neural networks (RNNs) named long short-term memory (LSTM) network is used to perform personal identification because of its strong ability to deal with time series problems that appears strictly in chronological order. There are eight layers in the designed LSTM networks. The first layer is the input layer, the input is a one-dimensional vector with the size of 1×30 . The second layer is the LSTM layer with 125 hidden units. The third layer is the dropout layer with a 20% drop rate. The fourth layer is the LSTM layer with 100 hidden units. The fifth layer is the dropout layer with a 20% drop rate. The sixth layer is the fully connected layer. The seventh layer is the softmax layer. The eighth layer is the output layer. The information of the LSTM networks is shown in Tab. 4.4.

Table 4.4: Detailed parameters of LSTM networks.

	Layers	Parameters
1	Input	sequence input with 1×30 array
2	LSTM	125 hidden units
3	Dropout	20%
4	LSTM	100 hidden units
5	Dropout	20%
6	FullyConnected	10 layers
7	Softmax	softmax
8	Output	crossentropyex

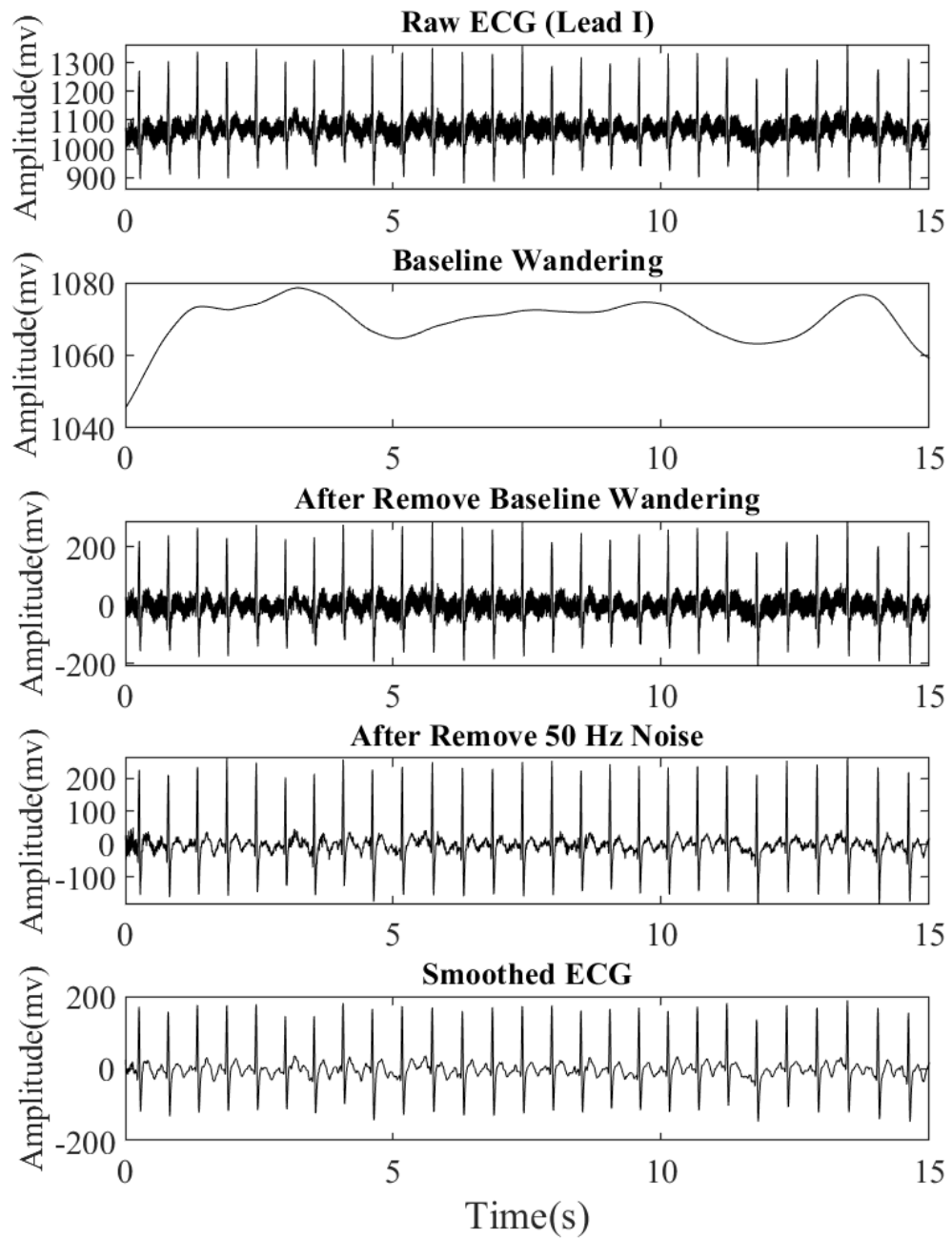


Figure 4.15: Noise removal and signal smoothing process.

4.3.2 Results and Discussion

During the training progress, the learning rate is set at 0.001 and the schedule of the learning rate is constant. The min batch size is 10 and the training epoch is 10. The hardware resource is single GPU. First, five single classification models (model 1-5) are trained based on each WT condition and the cross-validation method is used. The experiment result shows that the identification rate is highest when the training and test data is from the same WT for each trained single model. And the number of heart rate is increasing with the WT increasing. Then a mixed classification model is trained which the training data includes the ECG from the five different WT conditions. When we use the ECG of each WT condition to test the mixed model, each of the accuracy is more than the accuracy that using the single model. This result once again proves that increasing the diversity of samples can greatly improve the identification rate. The information of the dataset and the identification accuracy are shown in Tab. 4.5.

The ECG is stable with a short-term immutability characteristic under a normal circumstances for a healthy person. But some internal reasons such as disease outbreaks or external reasons such as external stimuli will affect the ECG. The stimulation of the water pressure and hot water temperature has an important impact on the ECG, which is also reflected in the impact on the identification rate. For each single and mixed model, the training data and test data are from different sessions, which is collected at different days. This is more reasonable for the application purpose. And the generalization ability of the trained model is stronger than that the training data and test are from the same sessions. The identification rate of the mixed model is more than 96.31% based on the most common used WTs (36-42 °C) in the daily life. It shows that it can meet the practical application. The average accuracy of the mixed classification model is 97.68%, the highest accuracy is 98.43%, which is based on the 38 ± 0.5 °C WT condition. The questionnaire survey results show that when the WT condition is 38 ± 0.5 °C and 39 ± 0.5 °C, all the subjects feel very comfortable during the data collection. The variations of the ECG is smaller at the two WT conditions. The identification rate are higher at these two WT conditions than that the other WT conditions. Therefore, we notice that the more comfortable of the subject, the smaller variations of the ECG during bathing, and the higher identification rate using ECG during such a WT condition. When the WT is 37 ± 0.5 °C, only a few subjects feel a little cold at the beginning of the data collection. When the WT is 40 ± 0.5 °C, the subjects feel a little uncomfortable but can endure the hot temperature. But when the WT is 40 ± 0.5 °C, all the subjects feel uncomfortable and several subjects can not endure the hot temperature. And the identification rates are lowest at these two higher WT conditions than that the other WT conditions. When the WT is higher than 38 ± 0.5 °C, the identification rate and the WT have a negative correlation, that with the WT increasing, the identification rate is decreasing.

4.3.3 Conclusion and Future Work

This study proposes a RNN-based personal identification system using the ECG at different water temperatures (WTs) during bathing. The long short-term memory (LSTM) network is used to perform classification. The experiment result

Table 4.5: Dataset and validation accuracy.

Model	WT for Training Data	No. of Training Data	WT for Test Data	Accuracy (%)
1	37 ± 0.5	15219	37 ± 0.5	97.79
			38 ± 0.5	87.03
			39 ± 0.5	77.28
			40 ± 0.5	80.47
			41 ± 0.5	80.69
2	38 ± 0.5	16047	37 ± 0.5	80.98
			38 ± 0.5	97.97
			39 ± 0.5	85.99
			40 ± 0.5	91.32
			41 ± 0.5	85.16
3	39 ± 0.5	17323	37 ± 0.5	84.61
			38 ± 0.5	79.41
			39 ± 0.5	96.26
			40 ± 0.5	77.42
			41 ± 0.5	79.66
4	40 ± 0.5	17329	37 ± 0.5	82.29
			38 ± 0.5	94.07
			39 ± 0.5	83.07
			40 ± 0.5	96.16
			41 ± 0.5	85.39
5	41 ± 0.5	18095	37 ± 0.5	92.54
			38 ± 0.5	93.92
			39 ± 0.5	87.77
			40 ± 0.5	89.93
			41 ± 0.5	94.85
Mixed	[36.5, 41.5]	84013	37 ± 0.5	98.14
			38 ± 0.5	98.43
			39 ± 0.5	98.16
			40 ± 0.5	97.34
			41 ± 0.5	96.31

shows that increasing the diversity of the training data could greatly improve the identification rate. When the training and test data are from the same WT condition, each trained single model could achieve the highest accuracy. When the WT is higher than 38 ± 0.5 °C, the identification rate of the mixed model is decreasing with the WT increasing. They have a negative correlation. The training data of the mixed model includes the most common used WT conditions, and the identification rate of the mixed model is more than 96.31% based on each WT condition, which could meet the practical applications. All the length of the training and test data are 18 minutes. Therefore, in the future work, we will explore the number of heart beats on the identification rate.

4.4 Number of Heartbeats and Personal Identification Rate

4.4.1 Motivation

Bathing is an effective and cheap way to release the mental stress and keep the body cleaning, which has been very popular in the daily life. However, one statistical results display that there are about 5,398 drowning accidents during bathing in Japan in 2018 [128]. And the trend of the drowning accidents has been increasing these years. The reason for so many drowning accidents is that people cannot be rescued in time when a drowning accident occurs. In addition, some survivors will suffer long-term psychological effects after being physically traumatized because they have not received timely and appropriate treatment. When the drowning accident is happening, if the information of the people could be immediately sent to the nearest emergency services, then the possibility of the mortality will reduce. Therefore, how to accurately and quickly perform personal identification during bathing is the preliminary task. In the above section, we propose a RNN-based personal identification system using the ECG at different WT condition during bathing. Although the identification rate of the mixed model is higher than 96.31%, each of training and test data is 18 minutes, it cost a long time recognize a person. This study aims to explore the impact of the number of heartbeat on the identification rate.

Many previous studies explored the ECG in the field of personal identification. Since L. Biel et al. firstly proposed the ECG in the application of personal identification in 2001 [40], then more and more studies use the ECG to perform identification and achieve good result in the academic development and the practical application. Compare with the traditional identification methods such as the gait, voice, signature, fingerprint, face, ear, iris, retina and hand geometry, now the ECG-based identification method has been taken as an emerging biometric. In recent twenty years, with the development of the artificial neural networks (ANNs) and digital signal processing technologies, the ECG-based identification method has also achieved rapid improvement and prosperity. TH. Yen et al. proposed an ECG-based identification system with a portable, real-time, smartphone-based characteristics [146]. It can identify seven types heartbeat with only 78 milliseconds and achieved 98.34% accuracy. MG. Kim et al. designed a non-fiducial-based identification system using the ECG [138]. They used a 1-D ensemble network in

the classification and achieved 99.6% accuracy based on only 1-sec ECG for each subjects. JS. Arteaga-Falconi et al. designed an ECG authentication algorithm in the application of mobile devices [147]. This algorithm achieved a 1.41% false acceptance rate and a 81.82% true acceptance rate using only 4 second ECG. AF. Hussein et al. proposed a fiducial points-based identification system using the ECG [148]. They used the discrete cosine transform to extract the ECG features and achieved 97.78% accuracy with only 1.21 seconds ECG. DP. Coutinho et al. designed an ECG identification system and achieved 99.5% accuracy only using 5 heartbeats for the test patterns [149]. SZ. Fatemian et al. introduced an identification system using ECG and achieved 99.61% identification rate using only 2 heart beats [131]. M. Li et al. designed an ECG-based identification system and achieved 0.5% equal error rate (EER) and 98.3% identification rate in the test stage with only ten seconds ECG [150]. A. Lourenço et al. proposed an identification system using the finger ECG [151]. They used 30 heartbeats to register the enrolment template and the other 30 heartbeats to construct the test templates. Finally, the designed system achieved 94.3% identification rate and 13.0% EER based on a group of 16 subjects. I. Odinaka et al. proposed an identification system using the ECG signal based on a comparatively large sample of 269 subjects [152]. And they explored the impact of long-term variability, health status, data fusion, number of training and testing heartbeats, and database size on the identification rate. The experiment result confirmed that with increasing of training and test heartbeats, the EER reduced and identification rate increased. When the training and testing heartbeats were from different days, the designed system could achieve 5.58% EER in verification, 76.9% accuracy in rank-1 recognition, and 93.5% accuracy in rank-15 recognition. B. H. Kim et al. introduced an ECG-based identification system using the long short-term memory network and obtained an overall identification rate of 99.73% with only 3 test heartbeats [153]. H. M. Lynn et al. proposed a recurrent neural network-based identification system using the ECG signal [154]. They performed classification using a deep bidirectional GPU network model and achieved 97.60% identification rate using only 3 test heartbeats.

Although the above studies explored the relationship between ECG length and the identification rate, no studies were based on ECG during bathing. The collection of the ECG is noninvasive, it must need to attach several electrodes on the skin surface, which cause uncomfortable and inconvenience to the people during the collection process. Therefore, in order to reduce the uncomfortable and inconvenience, S. C. Kwatra et al. firstly designed an ECG collection system using the non-contact electrodes during bathing in 1986 [61]. Then, more and more studies investigated the ECG during bathing [62–67]. The sensitivity to WTs for different people is different because of the individual difference. The WTs have an important impact on the ECG because of the the water pressure on the chest and thermal stimulus on hemodynamics during bathing, which will cause additional physical and mental stress on the people. In our previous studies, we noticed that the WT has an important impact on the identification rate and designed a RNN-based identification system using the ECG at different WTs during bathing. This study aims to explore the impact of ECG length on the identification rate using the convolutional neural network (CNN).

4.4.2 Methods and Materials

4.4.2.1 Features Extraction

The data collection system is shown in Fig. 2.5, and the ECG monitor is shown in Fig. 2.4. The data processing process is shown in Fig. 4.13. In this study, we propose a fiducial points-based identification system using the QRS complex of the ECG. Therefore, how to accurately segment the QRS complex has an important impact on the identification rate. During the data collection, the sampling rate is 200 Hz and the sampling interval is 5 milliseconds. The duration of the complete QRS complex wave for a healthy person is about 80–120 milliseconds. In order to segment a complete QRS complex wave, we segment 30 sampling points centering on the position of the detected R peak, which is 150 milliseconds. Then we transform the one-dimensional (1-D) segmented QRS complex wave into a one-dimensional (2-D) binary image, as is shown in Fig. 4.16.

4.4.2.2 Identification

For each subject, all the training, validation, and test data are the transformed binary images, which are from the first, second, and third ECG recordings based on each WT condition. The size of the binary image is a 30×30 2-D matrix, with the values of zero or one. The numbers of training and validation images are 84297 and 81867. There are two stages in the whole classification process. In the first stage, we use a simple 2-D CNN to perform classification, as is shown in Fig. 4.17. It includes input layer, convolution layer, ReLU layer, pool layer, fully connected layer and the output layer. In the input layer, we feed into a binary image with the size of 30×30 , which represents a QRS complex wave. In the convolution layer, twenty filters with a size of 9×9 are used to perform the convolution computation, the result of the convolution computation could be represents by a $22 \times 22 \times 20$ 3-D matrix. The main purpose of the convolution computation aims to extract the characteristics of the input data. The Relu layer is also named the increasing activation function: it often uses to increase the nonlinear segmentation ability of the network. After the 'ReLU' computation, the input and output are same. In the pooling layer, the output is represented using an $11 \times 11 \times 20$ 3-D matrix. There are two main functions of the pooling layer. The first is to compress the space size of the input data volume and reduce the number of parameters in the network, and also reduce the complexity of network calculations, thereby avoiding excessive consumption of computing resources. The second is to compress unnecessary features, extract main features, prevent overfitting, and improve the generalization ability of the model. Then, we perform 'reshape' operation and two times of fully connected operations. In the output layer, we calculate the identification rate using the 'Softmax' function. The output of the 'Softmax' function is a 10×1 vector. Each value represents the possibility of each subject. If the label of the input image is same with the row of the maximum of the vector, then accept; otherwise, reject.

In the second stage, the majority vote method is used to perform the secondary classification. In order to investigate the impact of ECG length on the identification rate, we randomly select N (1 to 60) consecutive QRS complex waves from the third recording for each subject to test the trained model. When the number

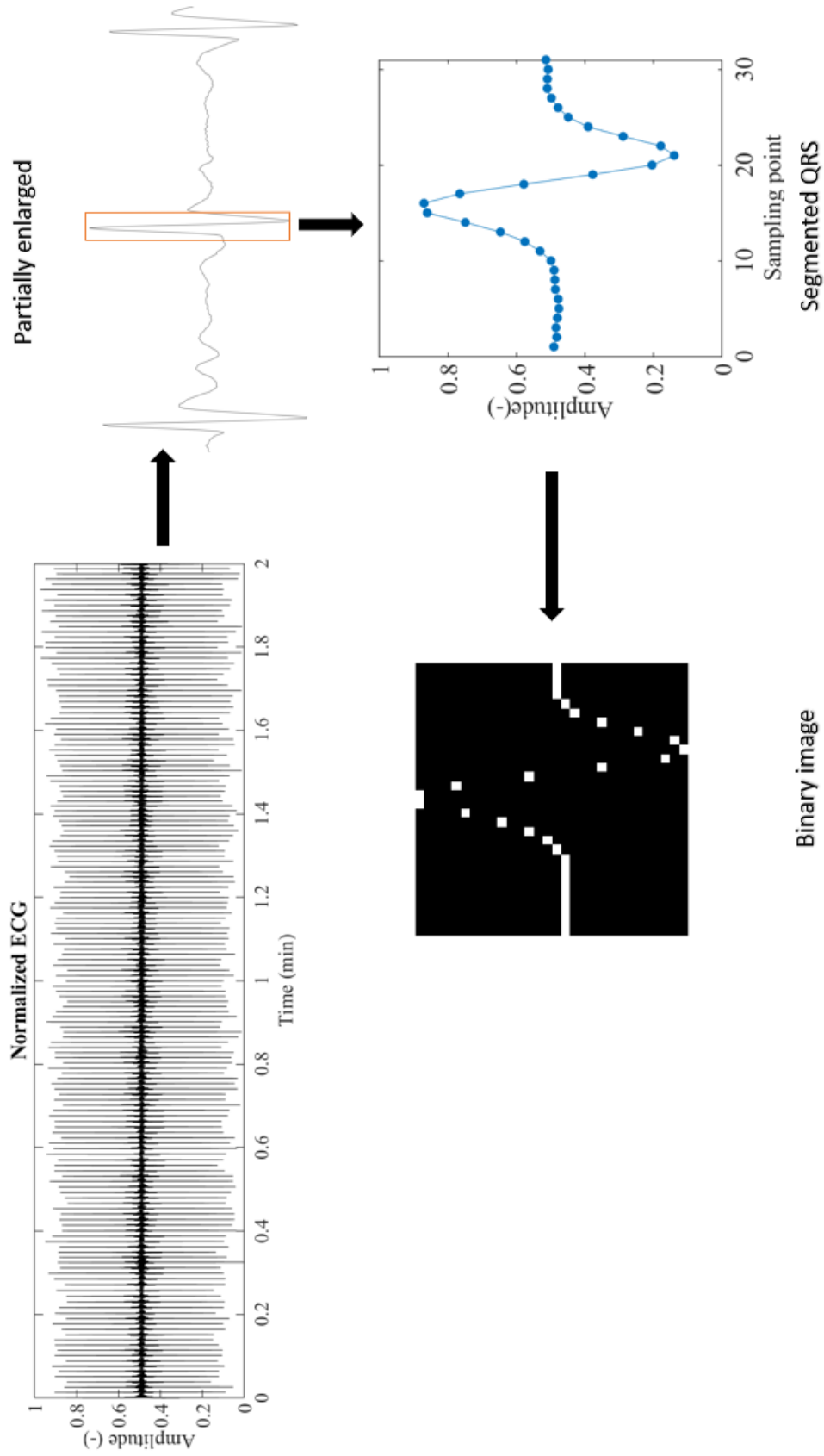


Figure 4.16: 1-D QRS complex to 2-D binary image.

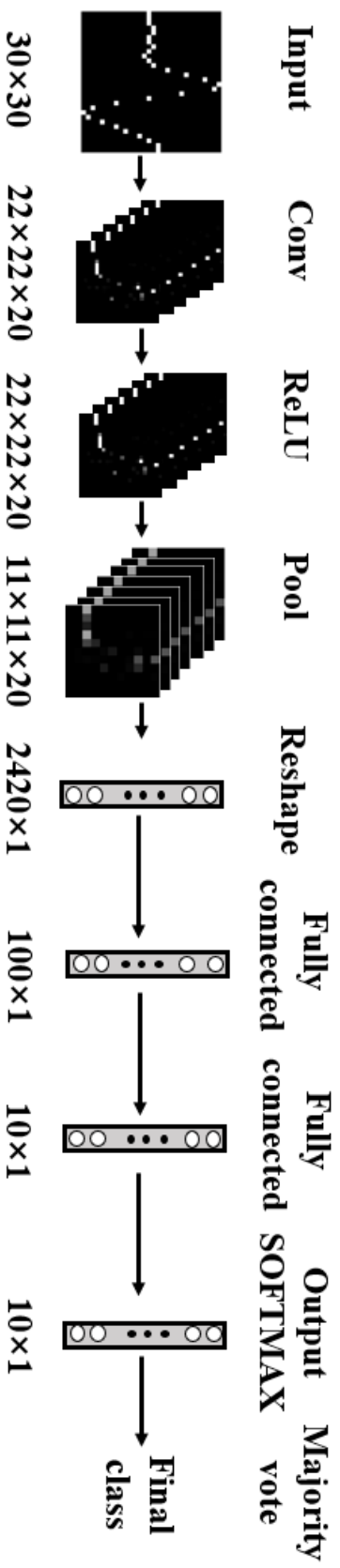


Figure 4.17: CNN model.

of correctly identified heartbeats is greater than or equal to half of N , then it is accepted; otherwise, it is rejected.

4.4.3 Results and Discussion

During the test stage, in order to effectively evaluate the performance of the trained model, some performance evaluation parameters are defined, such as the true positive (TP): true positive samples which is predicted to be positive samples by the model, true negative (TN): true negative samples which is predicted to be negative samples by the model, false positive (FP): true negative samples which is predicted to be positive samples by the model, false negative (FN): true positive samples which is predicted to be negative samples by the model, precision, recall, F-score, TP rate (TPR), FP rate (FPR). Specifically,

$$Precision = \frac{TP}{TP + FP} \quad (4.15)$$

$$Recall (TPR) = \frac{TP}{TP + FN} \quad (4.16)$$

$$F\text{-score} = \frac{2 * precision * Recall}{precision + Recall} \quad (4.17)$$

$$FPR = \frac{FP}{FP + TN} \quad (4.18)$$

During the training stage, in order to achieve a high accuracy with a low computational complex, different combinations of important training parameters are tested. At last, the learning rate is set at 0.01, the batch size is set at 256, and the epoch is set at 40. The validation result is shown in Fig. 4.18 and Tab. 4.6. The experiment result of subject 6 shows the highest FPR (0.57%). From the confusion matrix we can find that the trained model easily takes the subject 6 to subject 8, and takes the subject 2 as the subject 6, 8, and 9. The FPR of the subject 3 is 0 and the precision of the subject 3 is 99.98%, which shows that the trained model achieves a strongest discrimination ability for subject 3. The average FPR is 0.14%, the average precision is 98.71%. Therefore, this trained model could be applied in the next stage.

When we investigate the impact of heartbeats on the identification rate, in order to reduce the random errors and increase the robustness of the trained model, the identification process is performed 1000 times. The final identification rate of each heartbeat is the average of 1000 times identification rate. First, the trained model is directly used to explore the impact of heartbeats on the identification rate. The best and robust identification rate is about 90% when the number of heartbeats is three or greater. Next, the majority vote method is used based on the preliminary classification result. When the number of heartbeats is 17 or greater, the average and robust identification rate is more than 98%. The relationship between the number of heartbeats and the identification rate based on 1000 times experiments before and after majority vote is shown in Fig. 4.19. When the number of heartbeats is 17 or greater, the identification rate is more than 98% based on the majority vote method, which is higher than the identification rate of

		Predicted Subject ID									
		1	2	3	4	5	6	7	8	9	10
True Subject ID	1	99.9% 8934	0.0%	0.0%	0.0%	0.0%	0.0%	0.0%	0.0%	0.0%	0.0%
	2	0.0%	95.4% 7440	0.0%	0.0%	0.0%	0.1%	0.1%	0.0%	0.1%	0.0%
	3	0.0%	0.0%	100.0% 8589	0.4%	0.0%	0.0%	0.0%	0.0%	0.0%	0.6%
	4	0.0%	0.0%	0.0%	99.1% 6918	0.0%	0.0%	0.0%	0.0%	0.4%	0.0%
	5	0.0%	0.1%	0.0%	0.0%	99.9% 8519	0.0%	0.0%	0.0%	0.0%	0.0%
	6	0.0%	2.0% 157	0.0%	0.0%	0.0%	94.8% 7817	0.2%	0.4%	0.0%	0.0%
	7	0.0%	0.3% 23	0.0%	0.0%	0.0%	0.0%	99.4% 8175	0.0%	0.0%	0.0%
	8	0.0%	1.0% 77	0.0%	0.0%	0.0%	5.2% 425	0.1% 11	99.6% 8142	0.0%	0.0%
	9	0.0%	1.1% 87	0.0%	0.4%	0.0%	0.0%	0.1% 5	0.0%	98.9% 9255	0.0%
	10	0.0%	0.0%	0.0%	0.0%	0.0%	0.0%	0.0%	0.0%	0.0%	99.7% 8868

Figure 4.18: Confusion matrix of the validation result based on first recognition stage.

Table 4.6: Validation result.

Subject	TP	FP	FN	TN	Precision (%)	F-score (%)	TPR (%)	FPR (%)
1	8934	6	7	74787	99.93	99.93	99.92	0.01
2	7440	359	25	75910	95.40	97.48	99.67	0.47
3	8589	2	107	75036	99.98	99.37	98.77	0.00
4	6918	65	44	76707	99.07	99.22	99.37	0.08
5	8519	5	16	75194	99.94	99.88	99.81	0.01
6	7817	432	205	75280	94.76	96.09	97.44	0.57
7	8175	47	23	75489	99.43	99.57	99.72	0.06
8	8142	29	513	75050	99.65	96.78	94.07	0.04
9	9255	102	130	74247	98.91	98.76	98.61	0.14
10	8868	30	7	74829	99.66	99.79	99.92	0.04
Total	82657	1077	1077	752529	98.71	98.71	98.71	0.14

90% without the majority vote method. It increases about 8.89%. The curve of the identification rate based on the majority vote is very stable when the number of heartbeats is 20 and later. The relationship of the number of heartbeats and the identification rate for each subject is shown in Fig. 4.20. When the number of heartbeats is 20 or greater, the identification rate of each subject is more than 95%. Both of Fig. 4.19 and Fig.4.20 show that the trained model is accurate and robust.

The QRS complex wave is the most discriminative feature of the ECG. Therefore, it is taken as the identification marker in this study, which is transformed into a 2-D binary image with a size of 30×30 . The matrix of the binary image only includes the values of 0 and 1. Compare with the RGB and grayscale images, the binary image can greatly reduce the computational complexity. The ability of the image classification is strong and powerful for the CNN. So the identification problem is taken as an image classification problem, which aims to apply the characteristic of the CNN. There are five layers of the designed CNN, which are the input layer, convolutional layer, ReLU layer, pooling layer, and fully connected layer. It has a low computational complexity. The classification curve could quickly converge with a high identification rate based on a low training epoch.

In order to ensure the experimental results are robust and practical, the training, validation, and test data are from different sessions. The validation rate is 98.71% in the preliminary classification stage, as is shown in Tab. 4.6. The number of correctly recognized binary images is 82657, and The number of incorrectly recognized binary images is 1077. The confusion matrix of the preliminary classification result is shown in Fig. 4.18. It shows that the trained model easily takes the subject 2 as subject 6 and takes the subject 6 as subject 8, which greatly reduces the overall identification rate. In the test stage, N (1 to 60) adjacent and consecutive binary images are randomly selected for each subject from the third recording and then fed into the trained CNN model. The relationship of the number of heartbeats and the identification rate is shown in Fig. 4.19. It shows that the trained model is fluctuating and not robust. The average identification rate is about 90%, the SD of the identification rate for ten subject is large. In order to increase the identification rate, a majority vote algorithm is applied in the secondary classification stage. According to the majority vote mechanism, if the number of binary images which is correctly identified is greater than or equal to half of N, then it is accepted; otherwise, it is rejected. The average identification rate is about 98.00% when the number of heartbeats is greater than twenty after the majority vote is used, with an increase of about 8.89 percentage points. The variation of the average identification rate is shown in Fig. 4.19. The curve with red is convergent and stable. Fig. 4.20 shows that the identification rate of each subject is robust when the number of heartbeats is 20 or greater.

During the data collection process, we can divide it into three stages, which are the adaptation period, stable period, and pressure rise period. The first two minutes is called the adaptation period. In this stage, when the subject enter the bathtub, the heart rate will increase and the ECG has a strong fluctuation. The subject must adapt to the water pressure on the chest and thermal stimulus on hemodynamics. The third to twelfth minutes is called the stable period. In this stage, the ECG is stable, the subject has adapted to the WT environment and

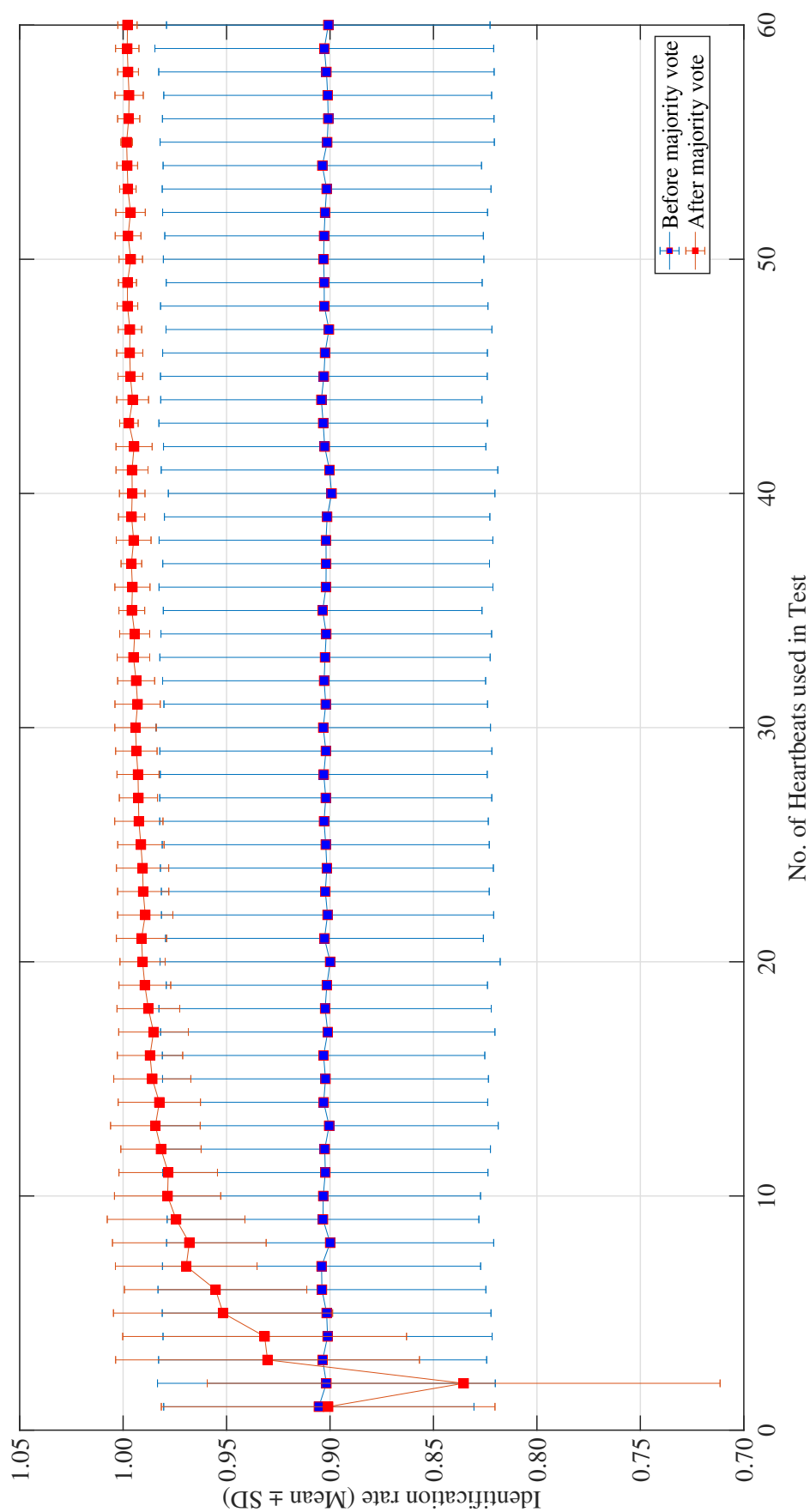


Figure 4.19: Variety of mean recognition rate based on different testing ECG length.

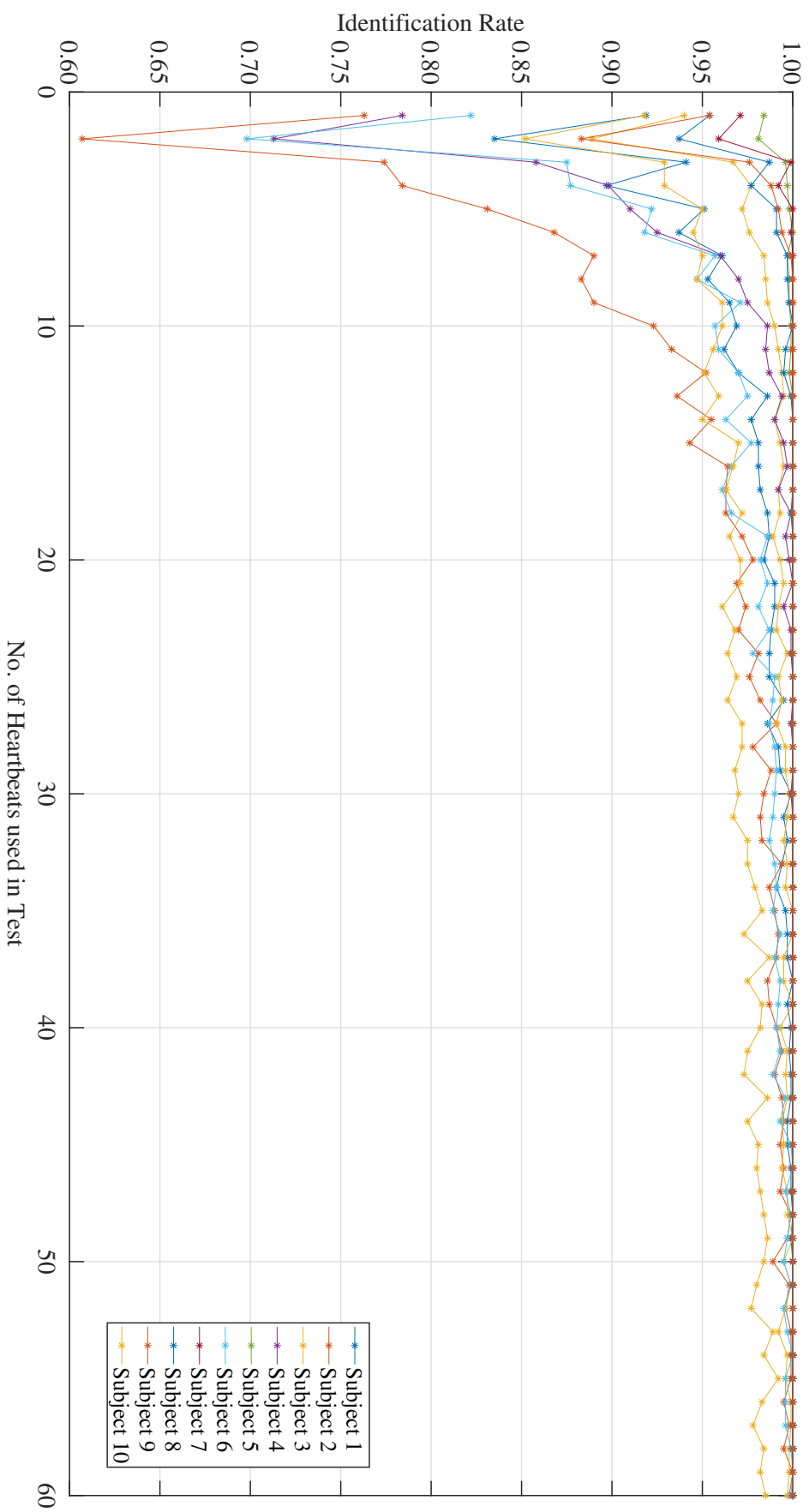


Figure 4.20: Variation in recognition rate for each subject.

feel more comfortable. The thirteenth to eighteenth minutes is called the pressure rise period. In this stage, the physical and mental stress of the subject will greatly increase because the subject has been in the bathtub about twelve minutes. And the subject will feel uncomfortable due to a long time of water pressure on the chest and thermal stimulus on hemodynamics. The different periods have an important impact on the ECG, and different WT has a stronger impact on the ECG. In addition, the ECG differs among different people due to the individual differences and different sensitivity to water pressure and WT. Therefore, how to accurately detect the positions of the R peaks at different WT conditions is the biggest challenge of this study. The ECG has a stronger fluctuation during bathing than that during resting state. It is difficult for an algorithm to detect the R peaks at different periods, and it is more difficult to correctly detect all the R peaks at different WT conditions. There are many outliers of the R peaks detection results.

During the feature extraction stage, we transform the segmented QRS complex wave into a binary image. This transformation will change the relative positions of the sampling points. The shape of the QRS complex is not all the same in the binary image with a 1-D QRS complex shape. This transformation contributes to reducing the computational complexity during the training stage, but it can not retain all the inherent features of the ECG. Some important information of the ECG will be lost. What's more, there are thirty sampling points (150 ms) in the segmented QRS complex. For a healthy person, the duration of a complete QRS complex is about 80 ms to 120 ms. Although the segmented data includes a complete QRS complex wave, thirty sampling points is insufficient when it is transformed into a binary image. Intuitively, the more of the sampling points, the more the converted image can retain the inherent characteristics of the original signal. However, further experiments are needed to verify whether the sampling points have an important impact on the identification rate.

4.4.4 Conclusion and Future Work

This study investigates the number of heartbeats on the identification rate at different WTs during bathing. There are three major contributions in this study. The first contribution is that the identification problem is formulated as the image classification problem, which could be fully utilized the powerful image classification capabilities of CNN. Specifically, we transform the 1-D QRS complex wave into the binary image and take the binary image as the input data. The second contribution is that we use a combination of preliminary classification and secondary classification method to perform personal identification. In the preliminary classification stage, a CNN is used. In the secondary classification stage, a majority vote algorithm is designed to perform the personal identification based on the preliminary classification result. The identification rate increases by about 10%. The third contribution is that the designed identification system has a strong robustness and identification performance. In order to increase the generalization ability and ensure high enough robustness of the system, the training data, validation data, and test data are taken from different sessions (days), which is collected in the commonly used WT (36.5 °C–41.5 °C) conditions. In the test stage, N (1 to 60) adjacent and consecutive QRS complex waves are randomly selected for each subject from the third recording, which could meet the practical

application. And the final identification rate is the average of 1000 experiment results, which could fully ensure the robustness of the system.

To the best of our knowledge, this is the first study to explore the impact of heartbeats on the identification rate at different WTs during bathing. The average identification rate is more than 98% when the number of heartbeats is 20 or greater. The identification system achieves high performance. It has a strong robustness, which could meet the practical application in daily life. Although some discoveries are revealed in this study, there are also some limitations. First, in order to reduce the noise, the subject is told to keep as still as possible during the data collection process, which will cause inconvenience to the subject. Of course, it contributes to reducing the noise and achieving higher identification rate. However, this approach is a bit out of the reality, because a person cannot always keep still while in a bathtub. Actually, the amplitude of the ECG is very weak, which is in the order of millivolts. In this study, we use the non-contact electrodes to collect the ECG. The weak electricity on the skin surface is conducted to the electrode through the water medium. The collected data will includes obvious baseline wandering and other noise when the subject do not keep still during the data collection process. Second, the controlled WT conditions are not unified for all subjects. When the WT is more than 41 °C, some subjects can not bear the hot environment and feel very uncomfortable. Therefore, for the personal safety of subjects, we turned on the cooling fan. Third, the water pressure on the chest and thermal stimulus on hemodynamics will cause additional stress to the subjects during the ECG collection process, which may create some bias regarding the results.

In the future research works, we will explore the relationship of sampling rate and identification rate. In order to further reduce the computational complexity and outliers of the R peaks detection, we will explore how to perform personal identification using the non-fiducial points method. Besides, we will investigate the impact of frequency domain ECG features on the identification rate.

Chapter 5

Results and Discussion

In this study, we perform HRV analysis and personal identification using ECG signal at different WT during bathing. With the increased WT, 11 HRV features (i.e., mean RRI, SDNN, RMSSD, SDSD, AURRI, HF power, total power, pHF, D₂, SD1, and SD2) were significantly ($p < 0.05$) and monotonously reduced and four of the HRV features (i.e., HR, pLF, LF/HF ratio, and SD1/SD2) were significantly ($p < 0.05$) and monotonously rising, which shows that the WT has an important impact on the HRV during bathing. Before the identification system is designed using the RNN, we explore how to improve the identification rate. The experiment result shows that increasing the diversity of training samples can greatly improve the accuracy of identification. The main reason of using the RNN to design the identification system is that the ECG is a kind of time dependent signal and the RNN is good at dealing with time series problems. The results of the five trained models show that when the trained data and test data are from the same WTs condition, the identification rate is highest. The training data of the final mixed model are from five different WTs and each test result is more than 96%. Then, we explore the number of test heart beats on the identification rate. The result shows that when the number of test heart beat is 20 or greater, the identification rate is more than 98% and then becomes stable.

To accurately and quickly perform personal identification at different WTs during bathing, a novel identity validation method using the 1-D ECG signal during bathing based on different bathtub water temperature ranges has been proposed. For each subject, both of the training ECG recording and test ECG recording are 18 mins, one recording is used to train and another recording is used to test, and each dataset represents a QRS complex. Under normal circumstances, a person's ECG is stable in the short term. However, the ECG will also change due to internal reasons such as disease outbreaks or external reasons such as external stimuli. During the data collection stage, the body below the neck of the subject is in the water, the stimulation from the water pressure and hot water temperature will cause some changes to the ECG.

Tab. 4.5 shows the details of the training dataset, test dataset, and accuracy. When the bathtub water temperature increases, the number of total heartbeats is also increasing, the RRI and amplitude of the ECG also change at different bathtub water temperature. For classification model 1, the 10 training ECG recordings are collected at 37 ± 0.5 °C water temperature range, total training heartbeats are 15219, the test ECG recordings are collected at 5 different bathtub water

temperature ranges, respectively. Tab. 4.5 shows that only the test dataset is collected at the same bathtub water temperature range with the training dataset, the classification accuracy is highest, which directly proves that the ECG changes greatly at different bathtub water temperature.

For the final classification model, the average accuracy is 97.68%, the highest accuracy is 98.43%, which is based on the 38 ± 0.5 °C water temperature range. Our questionnaires show that most of the subjects feel more comfortable when the bathtub water temperature ranges are 38 ± 0.5 °C and 39 ± 0.5 °C, and they feel a little cold when the bathtub water temperature is 37 ± 0.5 °C, but they feel too hot when the bathtub water temperature ranges are 40 ± 0.5 °C and 41 ± 0.5 °C. Therefore, we can conclude that the ECG is more stable when the subject feels comfortable and the classification accuracy is also higher at a comfortable state.

In the future research work, we will find more subjects, which should include the child and the older, the healthy and unhealthy, as well as the people from different skin colors and races. We will also explore how to collect the ECG during bathing and how to perform identity validation using ECG if there are 2 or more people in the bathtub.

During the data-processing stage, the median filter was used three times to remove the outliers of the RRI signal. The skin surface electricity is very weak, in the millivolts. The gentle movement of the four limbs will induce relatively large fluctuations in the ECG amplitude. Therefore, the raw ECG signal includes some noise and there are some outliers in the R peaks detection and RRI signal results. If the median filter is only used once to remove the RRI outliers, then either only the outliers with big amplitude can be removed or there is a gross distortion in the RRI signal after the outliers are removed. Therefore, the median filter was used to remove the outliers with big, median, and small amplitudes, respectively.

Different changes in WT during bathing have very different impacts on HRV. For example, if the WT drops from 40°C to 38°C during the data collection process, the subject will feel very uncomfortable in the first minute and need a longer time to adapt to the WT environment. But, if the WT increases from 38°C to 40°C during the data collection process, the subject will adapt to the WT environment easily. Even if the WT reaches 40°C, the subjects will not feel very uncomfortable because they have adapted to this WT environment. A WT of 40°C appeared during two different processes, but had very different instantaneous effects on the HRV and their physiological meanings were also different in these processes. Therefore, some outliers appear in the box plot as shown in Fig. 2.8.

With the increasing WT, some change trends in the HRV features were consistent with previous research (e.g., from rest to stress states). The change trend in HR was consistent with [84, 86, 92–99], while the change trend in mean RRI was consistent with [84, 86–89, 91, 93–95, 100], the change trend in RMSSD was consistent with [87, 89, 101–108], the change trend in the LF/HF ratio was consistent with [82, 107, 109], the change trend in pLF is consistent with [83], and the change trend in SD2 was consistent with [155]. What's more, the HRV feature of AURRI was newly defined in this study and its unit is s^2 . The AURRI reflects the fluctuation of HRV signal over time: i.e., with the increasing WT, the mean RRI and AURRI are reduced.

With the increasing WT, the HR in medium and high WT increased by 6.53% and 15.78%, respectively, compared with the low WT, which reflects a decreased

vagal modulation. The significantly and monotonously reduced SDNN with increasing WT shows a significantly reduced whole HRV fluctuation, which is highly consistent with the significantly and monotonously reduced total spectral power (0–0.4 Hz). The LF power (0.04–0.15 Hz) in the PSD reflects both SNS and PNS activities, while the HF power (0.15–0.4 Hz) in the PSD reflects the PNS activity and the LF/HF ratio represents the balance between the SNS and PNS activities. With the increasing WT, the LF and HF are significantly and monotonously reduced, which reflects the finding that SNS and PNS activities are enhanced significantly. The increased LF/HF ratio shows that the ratio of the cardiac sympathetic to parasympathetic tones (i.e., the sympathovagal balance) was enhanced significantly, which shows that the stimulation of high WT on the subject was also enhanced significantly. The stimulation on the subject under high WT increased by 6.43% and 5.20% over the low and medium WT, as shown in Tab. 2.1.

Chapter 6

Conclusions and Future Work

6.1 Conclusions

This study mainly explores the HRV analysis and personal identification at different bathtub WT during bathing. The main contributions of this study are shown as follows:

Firstly, in chapter 3, we find that different WT has an important impact on the HRV during bathing. The statistics show that with increasing WT, 11 HRV features are significantly ($p < 0.05$) and monotonously reduced, four HRV features are significantly ($p < 0.05$) and monotonously rising, two HRV features are rising first and then reduced, two HRV features (fuzzy and approximate entropy) are almost unchanged, and vLF power is rising.

Secondly, in chapter 4, our research reveals that the WT has an important impact on the personal identification rate using ECG during bathing. Different water temperature will affect the amplitude and interval of ECG, especially the interval between normal R-R peaks, which leads to great differences in ECG under different water temperatures, which will have a great impact on the recognition rate. Therefore, the training sample must contain data at various water temperatures, so that the generalization ability and robustness of the obtained model will be stronger.

Thirdly, a fast and robust identification system is designed. The RNN can achieve better performance than the CNN when dealing with and classification the time series signal. The trained model can quickly and accurately identify a person's identity in the most commonly used water temperature environment (36 °C-42 °C). This model can meet the practical application in daily family life, general small nursing homes and other scenarios.

Finally, our study confirms that the number of test heart beats has an important impact on the identification rate using ECG during bathing. When the number of test heart beats is 20 or greater, the identification rate is more than 98% and then the identification rate curve becomes stable.

6.2 Future Work

With the urgent need for medical and health care in the daily life, many topics should be proposed in the future works.

Firstly, we will continue to explore how to perform personal identification in real time using the ECG during bathing at different WTs. And then perform HRV analysis during bathing and the resting state at the same time.

Secondly, the quantitative analysis of ECG amplitude and interval as well as the geometric characteristic and spectral differences based on different water temperature during bathing should be performed.

Thirdly, real-time mental and physical stress monitoring and evaluation model using ECG are needed.

Lastly, how to perform precise and fast cardiac disease prediction using ECG in daily life is an important problem to be addressed.

References

- [1] S. Tanaka, K. Motoi, A. Ikarashi, N. Masamichi, Y. Higashi, H. Asanoi, and K.-i. Yamakoshi, “Development of non-invasive and ambulatory physiological monitoring systems for ubiquitous health care,” in *SICE, 2007 Annual Conference*. IEEE, 2007, pp. 311–315.
- [2] G. Ernst, “History of heart rate variability,” *Springer*, pp. 3–8, 2014.
- [3] D. E. Bedford, “The ancient art of feeling the pulse,” *British heart journal*, vol. 13, no. 4, pp. 1–15, 1951.
- [4] D. D. Gibbs, “The physician’s pulse watch,” *Medical history*, vol. 15, no. 2, pp. 187–190, 1971.
- [5] S. Hales, “Statistical essays: concerning haemastaticks; or, an account of some hydraulick and hydrostatical experiments made on the blood and blood-vessels of animals,” *London: W. Innys and R. Manby*, vol. 1, pp. 1–438, 1733.
- [6] C. Ludwig, “Beitrage zur kenntniss des einflusses der respirationsbewegungen auf den blutlauf im aortensysteme,” *Arch Anat Physiol Leipzig*, vol. 13, pp. 242–302, 1847.
- [7] W. Einthoven, “Uber die from des menschlichen elektrokardiogramms.” *Pflugers Arch fd ges des Physiol*, vol. 60, p. 101, 1895.

- [8] N. J. Holter, “New method for heart studies: continuous electrocardiography of active subjects over long periods is now practical,” *Science*, vol. 134, no. 3486, pp. 1214–1220, 1961.
- [9] B. Hyndman and J. Gregory, “Spectral analysis of sinus arrhythmia during mental loading,” *Ergonomics*, vol. 18, no. 3, pp. 255–270, 1975.
- [10] A. L. Goldberger and B. J. West, “Applications of nonlinear dynamics to clinical cardiology a,” *Annals of the New York Academy of Sciences*, vol. 504, no. 1, pp. 195–213, 1987.
- [11] J. P. Saul, “Beat-to-beat variations of heart rate reflect modulation of cardiac autonomic outflow,” *Physiology*, vol. 5, no. 1, pp. 32–37, 1990.
- [12] D. T. Akomolafe, B. O. Afeni *et al.*, “Using database management system to generate, manage and secure personal identification numbers (pin),” *Journal of Software Engineering and Applications*, vol. 7, no. 05, pp. 1–10, 2014.
- [13] S. A. Israel and J. M. Irvine, “Heartbeat biometrics: a sensing system perspective,” *International Journal of Cognitive Biometrics*, vol. 1, no. 1, pp. 39–65, 2012.
- [14] B. Nasri, M. Guennoun, and K. El-Khatib, “Using ECG as a measure in biometric identification systems,” in *Science and technology for humanity (TIC-STH), 2009 IEEE Toronto international conference*. IEEE, 2009, pp. 28–33.
- [15] I. Odinaka, P.-H. Lai, A. D. Kaplan, J. A. O’Sullivan, E. J. Sirevaag, and J. W. Rohrbaugh, “ECG biometric recognition: A comparative analysis,” *IEEE Transactions on Information Forensics and Security*, vol. 7, no. 6, pp. 1812–1824, 2012.
- [16] M. D. Bugdol and A. W. Mitas, “Multimodal biometric system combining ECG and sound signals,” *Pattern Recognition Letters*, vol. 38, pp. 107–112, 2014.

-
- [17] M. Abo-Zahhad, S. M. Ahmed, and S. N. Abbas, “Biometric authentication based on PCG and ECG signals: present status and future directions,” *Signal, Image and Video Processing*, vol. 8, no. 4, pp. 739–751, 2014.
- [18] I. Odinaka, J. A. O’ Sullivan, E. J. Sirevaag, and J. W. Rohrbaugh, “Cardiovascular biometrics: combining mechanical and electrical signals,” *IEEE Transactions on Information Forensics and Security*, vol. 10, no. 1, pp. 16–27, 2015.
- [19] E. Marasco and A. Ross, “A survey on antispoofing schemes for fingerprint recognition systems,” *ACM Computing Surveys (CSUR)*, vol. 47, no. 2, pp. 1–36, 2015.
- [20] S. Yoon and A. K. Jain, “Longitudinal study of fingerprint recognition,” *Proceedings of the National Academy of Sciences*, vol. 112, no. 28, pp. 8555–8560, 2015.
- [21] R. D. Labati, A. Genovese, V. Piuri, F. Scotti *et al.*, “Toward unconstrained fingerprint recognition: A fully touchless 3-d system based on two views on the move.” *IEEE Trans. Systems, Man, and Cybernetics: Systems*, vol. 46, no. 2, pp. 202–219, 2016.
- [22] R. Vera-Rodriguez, R. Tolosana, J. Ortega-Garcia, and J. Fierrez, “E-biosign: stylus-and finger-input multi-device database for dynamic signature recognition.” in *3rd International Workshop on Biometrics and Forensics*, 2015, pp. 1–6.
- [23] F. Schroff, D. Kalenichenko, and J. Philbin, “Facenet: A unified embedding for face recognition and clustering,” in *Proceedings of the IEEE conference on computer vision and pattern recognition*, 2015, pp. 815–823.
- [24] R. Asnawi and M. Said, “Testing of other languages usage in addition to the default languages for the easy voice recognition module,” in *2018 Inter-*

- national Conference on Electronics Technology (ICET)*. IEEE, 2018, pp. 321–324.
- [25] A. Aloudat, K. Michael, and R. Abbas, “The implications of iris-recognition technologies: Will our eyes be our keys?” *IEEE Consumer Electronics Magazine*, vol. 5, no. 3, pp. 95–102, 2016.
- [26] S. K. Dewangan, “Human authentication using biometric recognition,” *International Journal of Computer Science & Engineering Technology (IJCS-SET)*, vol. 6, no. 04, pp. 240–245, 2015.
- [27] A. Sharma, P. Chaturvedi, and S. Arya, “Human recognition methods based on biometric technologies,” *International Journal of Computer Applications*, vol. 120, no. 17, pp. 1–7, 2015.
- [28] N. Karimian, Z. Guo, M. Tehranipoor, and D. Forte, “Highly reliable key generation from electrocardiogram (ECG),” *IEEE Transactions on Biomedical Engineering*, vol. 64, no. 6, pp. 1400–1411, 2017.
- [29] V. Chutchavong, K. Nualon, O. Sangaroon, and K. Janchitrapongvej, “A mathematical model for ECG waveform using rational bézier curves and bernstein polynomials,” in *Electrical Engineering/Electronics, Computer, Telecommunications and Information Technology (ECTI-CON), 2014 11th International Conference on*. IEEE, 2014, pp. 1–5.
- [30] C. He, W. Li, and D. Chik, “Waveform compensation of ECG data using segment fitting functions for individual identification,” in *Computational Intelligence and Security (CIS), 2017 13th International Conference on*. IEEE, 2017, pp. 475–479.
- [31] T. Olmez, Z. Dokur, and E. Yazgan, “Classification of ECG waveforms using a novel neural network,” in *Engineering in Medicine and Biology Society, 1998. Proceedings of the 20th Annual International Conference of the IEEE*, vol. 3. IEEE, 1998, pp. 1616–1619.

-
- [32] A. Walinjkar and J. Woods, "Personalized wearable systems for real-time ECG classification and healthcare interoperability: Real-time ECG classification and FHIR interoperability," in *Internet Technologies and Applications (ITA), 2017*. IEEE, 2017, pp. 9–14.
- [33] G. Da Poian, R. Bernardini, and R. Rinaldo, "Separation and analysis of fetal-ECG signals from compressed sensed abdominal ECG recordings," *IEEE Transactions on Biomedical Engineering*, vol. 63, no. 6, pp. 1269–1279, 2016.
- [34] S. Szilagyi, Z. Benyo, L. Szilagyi, and L. David, "Adaptive wavelet-transform-based ECG waveforms detection," in *Engineering in Medicine and Biology Society, 2003. Proceedings of the 25th Annual International Conference of the IEEE*, vol. 3. IEEE, 2003, pp. 2412–2415.
- [35] I. Saini, D. Singh, and A. Khosla, "Delineation of ECG wave components using k-nearest neighbor (KNN) algorithm: ECG wave delineation using KNN," in *Information Technology: New Generations (ITNG), 2013 Tenth International Conference on*. IEEE, 2013, pp. 712–717.
- [36] Z. Zhang and D. Wei, "A new ECG identification method using bayes' theorem," in *TENCON 2006-2006 IEEE Region 10 Conference*. IEEE, 2006, pp. 1–4.
- [37] Y. N. Singh and P. Gupta, "Biometrics method for human identification using electrocardiogram," in *International Conference on Biometrics*. Springer, 2009, pp. 1270–1279.
- [38] Y. Wang, F. Agrafioti, D. Hatzinakos, and K. N. Plataniotis, "Analysis of human electrocardiogram for biometric recognition," *EURASIP journal on Advances in Signal Processing*, vol. 2008, no. 1, p. 148658, 2007.

- [39] Y. N. Singh and P. Gupta, "ECG to individual identification," in *2008 IEEE Second International Conference on Biometrics: Theory, Applications and Systems*. IEEE, 2008, pp. 1–8.
- [40] L. Biel, O. Pettersson, L. Philipson, and P. Wide, "ECG analysis: a new approach in human identification," *IEEE Transactions on Instrumentation and Measurement*, vol. 50, no. 3, pp. 808–812, 2001.
- [41] M. Kyoso and A. Uchiyama, "Development of an ECG identification system," in *Engineering in medicine and biology society, 2001. Proceedings of the 23rd annual international conference of the IEEE*, vol. 4. IEEE, 2001, pp. 3721–3723.
- [42] A. D. Chan, M. M. Hamdy, A. Badre, and V. Badee, "Wavelet distance measure for person identification using electrocardiograms," *IEEE transactions on instrumentation and measurement*, vol. 57, no. 2, pp. 248–253, 2008.
- [43] T.-W. D. Shen, W. J. Tompkins, and Y. H. Hu, "Implementation of a one-lead ECG human identification system on a normal population," *Journal of Engineering and Computer Innovations*, vol. 2, no. 1, pp. 12–21, 2010.
- [44] Z. Zhao and L. Yang, "ECG identification based on matching pursuit," in *Biomedical Engineering and Informatics (BMEI), 2011 4th International Conference on*, vol. 2. IEEE, 2011, pp. 721–724.
- [45] F. Zeng, K.-K. Tseng, H.-N. Huang, S.-Y. Tu, and J.-S. Pan, "A new statistical-based algorithm for ECG identification," in *Intelligent Information Hiding and Multimedia Signal Processing (IIH-MSP), 2012 Eighth International Conference on*. IEEE, 2012, pp. 301–304.
- [46] Z. Zhao, L. Yang, D. Chen, and Y. Luo, "A human ECG identification system based on ensemble empirical mode decomposition," *Sensors*, vol. 13, no. 5, pp. 6832–6864, 2013.

-
- [47] W. S. McCulloch and W. Pitts, “A logical calculus of the ideas immanent in nervous activity,” *The bulletin of mathematical biophysics*, vol. 5, no. 4, pp. 115–133, 1943.
- [48] A. Waibel, T. Hanazawa, G. Hinton, K. Shikano, and K. J. Lang, “Phoneme recognition using time-delay neural networks,” *IEEE transactions on acoustics, speech, and signal processing*, vol. 37, no. 3, pp. 328–339, 1989.
- [49] W. Zhang, K. Doi, M. L. Giger, Y. Wu, R. M. Nishikawa, and R. A. Schmidt, “Computerized detection of clustered microcalcifications in digital mammograms using a shift-invariant artificial neural network,” *Medical physics*, vol. 21, no. 4, pp. 517–524, 1994.
- [50] Y. LeCun *et al.*, “Generalization and network design strategies,” *Connectionism in perspective*, vol. 19, pp. 143–155, 1989.
- [51] Y. LeCun, B. Boser, J. Denker, D. Henderson, R. Howard, W. Hubbard, and L. Jackel, “Handwritten digit recognition with a back-propagation network,” *Advances in neural information processing systems*, vol. 2, 1989.
- [52] P. Y. Simard, D. Steinkraus, J. C. Platt *et al.*, “Best practices for convolutional neural networks applied to visual document analysis.” in *Icdar*, vol. 3, no. 1, 2003, pp. 1–6.
- [53] Z. Xu and G. Wang, “The construction of portrait identification tracking system based on mask r-cnn,” in *2019 2nd International Conference on Information Systems and Computer Aided Education (ICISCAE)*. IEEE, 2019, pp. 371–374.
- [54] W. Cheng, Y. Sun, G. Li, G. Jiang, and H. Liu, “Jointly network: a network based on cnn and rbm for gesture recognition,” *Neural Computing and Applications*, vol. 31, no. 1, pp. 309–323, 2019.

- [55] A. Krizhevsky, I. Sutskever, and G. E. Hinton, “Imagenet classification with deep convolutional neural networks,” *Advances in neural information processing systems*, vol. 25, 2012.
- [56] M. D. Zeiler and R. Fergus, “Visualizing and understanding convolutional networks,” in *European conference on computer vision*. Springer, 2014, pp. 818–833.
- [57] K. Simonyan and A. Zisserman, “Very deep convolutional networks for large-scale image recognition,” *arXiv preprint arXiv:1409.1556*, pp. 1–14, 2014.
- [58] K. He, X. Zhang, S. Ren, and J. Sun, “Deep residual learning for image recognition,” in *Proceedings of the IEEE conference on computer vision and pattern recognition*, 2016, pp. 770–778.
- [59] P. Rodriguez, J. Wiles, and J. L. Elman, “A recurrent neural network that learns to count,” *Connection Science*, vol. 11, no. 1, pp. 5–40, 1999.
- [60] J. Xu, T. Li, Y. Chen, and W. Chen, “The impact of bathtub water temperature on personal identification with ecg signal based on convolutional neural network,” in *2018 IEEE 4th International Conference on Computer and Communications (ICCC)*. IEEE, 2018, pp. 1341–1345.
- [61] S. C. Kwatra and V. K. Jain, “A new technique for monitoring heart signals—part I: instrumentation design,” *IEEE Transactions on Biomedical Engineering*, no. 1, pp. 35–41, 1986.
- [62] T. Togawa, T. Tamura, J. Zhou, H. Mizukami, and M. Ishijima, “Physiological monitoring systems attached to the bed and sanitary equipments,” in *Images of the Twenty-First Century. Proceedings of the Annual International Engineering in Medicine and Biology Society*. IEEE, 1989, pp. 1461–1463.
- [63] Y. K. Lim, K. K. Kim, and K. S. Park, “The ECG measurement in the bathtub using the insulated electrodes,” in *The 26th Annual International*

-
- Conference of the IEEE Engineering in Medicine and Biology Society*, vol. 1. IEEE, 2004, pp. 2383–2385.
- [64] K. Motoi, S. Kubota, A. Ikarashi, M. Nogawa, and Tanaka, “Development of a fully automated network system for long-term health-care monitoring at home,” in *Engineering in Medicine and Biology Society, 2007. EMBS 2007. 29th Annual International Conference of the IEEE*. IEEE, 2007, pp. 1826–1829.
- [65] M. Ishijima, “Unobtrusive approaches to monitoring vital signs at home,” *Medical & biological engineering & computing*, vol. 45, no. 11, pp. 1137–1141, 2007.
- [66] S.-J. Jang, J.-H. Lee, J.-H. Lee, S.-B. Park, S.-O. Hwang, H.-R. Yoon, and Y.-R. Yoon, “Upiqitous home healthcare management system with early warning reporting,” in *Convergence Information Technology, 2007. International Conference on*. IEEE, 2007, pp. 2394–2401.
- [67] K. Motoi, Y. Yamakoshi, T. Yamakoshi, H. Sakai, N. Tanaka, and K.-i. Yamakoshi, “Measurement of electrocardiograms in a bath through tap water utilizing capacitive coupling electrodes placed outside the bathtub wall,” *Biomedical engineering online*, vol. 16, no. 1, pp. 1–13, 2017.
- [68] J. Xu, P. Cui, and W. Chen, “ECG-based identity validation during bathing in different water temperature,” in *2020 42nd Annual International Conference of the IEEE Engineering in Medicine & Biology Society (EMBC)*. IEEE, 2020, pp. 5276–5279.
- [69] D. Ramaekers, H. Ector, A. Aubert, A. Rubens, and F. Van de Werf, “Heart rate variability and heart rate in healthy volunteers. is the female autonomic nervous system cardioprotective?” *European heart journal*, vol. 19, no. 9, pp. 1334–1341, 1998.

- [70] J. B. Schwartz, W. J. Gibb, and T. Tran, "Aging effects on heart rate variation," *Journal of Gerontology*, vol. 46, no. 3, pp. M99–M106, 1991.
- [71] A. Lochner SPT, P. Crooks, M. Gordon Finlay BA, J. A. Erwin MS, K. Honn Ph.D. *et al.*, "Effect of sleep deprivation and sleep recovery on heart rate and heart rate variability in males versus females," *2020 Symposium Posters. 40*, 2020.
- [72] E. Nagy, H. Orvos, G. Bárdos, and P. Molnár, "Gender-related heart rate differences in human neonates," *Pediatric research*, vol. 47, no. 6, pp. 778–780, 2000.
- [73] H. Bonnemeier, U. K. Wiegand, A. Brandes, N. Kluge, H. A. Katus, G. Richardt, and J. Potratz, "Circadian profile of cardiac autonomic nervous modulation in healthy subjects: differing effects of aging and gender on heart rate variability," *Journal of cardiovascular electrophysiology*, vol. 14, no. 8, pp. 791–799, 2003.
- [74] Y. Yamasaki, M. Kodama, M. Matsuhisa, M. Kishimoto, H. Ozaki, A. Tani, N. Ueda, Y. Ishida, and T. Kamada, "Diurnal heart rate variability in healthy subjects: effects of aging and sex difference," *American Journal of Physiology-Heart and Circulatory Physiology*, vol. 271, no. 1, pp. H303–H310, 1996.
- [75] A. Wilkowska, A. Rynkiewicz, J. Wdowczyk, J. Landowski, and W. J. Cubała, "Heart rate variability and incidence of depression during the first six months following first myocardial infarction," *Neuropsychiatric disease and treatment*, vol. 15, pp. 1951–1956, 2019.
- [76] M. F. Lutfi and M. Y. Sukkar, "Effect of blood pressure on heart rate variability," *Khartoum Medical Journal*, vol. 4, no. 1, pp. 548–553, 2011.
- [77] T. Tombul, O. Anlar, M. Tuncer, N. Huseyinoglu, and B. Eryonucu, "Impaired heart rate variability as a marker of cardiovascular autonomic dys-

-
- function in multiple sclerosis.” *Acta Neurologica Belgica*, vol. 111, no. 2, pp. 116–120, 2011.
- [78] D. Gurses, Z. Ulger, E. Levent, Y. i. Aydinok, and A. R. Ozyurek, “Time domain heart rate variability analysis in patients with thalassaemia major,” *Acta cardiologica*, vol. 60, no. 5, pp. 477–481, 2005.
- [79] M.-Y. Lan, G.-S. Lee, A.-S. Shiao, J.-H. Ko, and C.-H. Shu, “Heart rate variability analysis in patients with allergic rhinitis,” *The Scientific World Journal*, vol. 2013, 2013.
- [80] L. M. DelRosso, M. P. Mogavero, and R. Ferri, “Effect of sleep disorders on blood pressure and hypertension in children,” *Current Hypertension Reports*, vol. 22, no. 11, pp. 1–7, 2020.
- [81] H. Van Praag, “Crossroads of corticotropin releasing hormone, corticosteroids and monoamines,” *Neurotoxicity research*, vol. 4, no. 5-6, pp. 531–556, 2002.
- [82] N. Hjortskov, D. Rissén, A. K. Blangsted, N. Fallentin, U. Lundberg, and K. Sogaard, “The effect of mental stress on heart rate variability and blood pressure during computer work,” *European journal of applied physiology*, vol. 92, no. 1-2, pp. 84–89, 2004.
- [83] O. Kofman, N. Meiran, E. Greenberg, M. Balas, and H. Cohen, “Enhanced performance on executive functions associated with examination stress: Evidence from task-switching and stroop paradigms,” *Cognition & Emotion*, vol. 20, no. 5, pp. 577–595, 2006.
- [84] V. Vuksanović and V. Gal, “Heart rate variability in mental stress aloud,” *Medical engineering & physics*, vol. 29, no. 3, pp. 344–349, 2007.
- [85] Z. Li, H. Snieder, S. Su, X. Ding, J. F. Thayer, F. A. Treiber, and X. Wang, “A longitudinal study in youth of heart rate variability at rest and in re-

- response to stress,” *International Journal of Psychophysiology*, vol. 73, no. 3, pp. 212–217, 2009.
- [86] C. Schubert, M. Lambertz, R. Nelesen, W. Bardwell, J.-B. Choi, and J. Dimsdale, “Effects of stress on heart rate complexity—a comparison between short-term and chronic stress,” *Biological psychology*, vol. 80, no. 3, pp. 325–332, 2009.
- [87] E. Tharion, S. Parthasarathy, and N. Neelakantan, “Short-term heart rate variability measures in students during examinations,” *Natl Med J India*, vol. 22, no. 2, pp. 63–66, 2009.
- [88] H. K. Lackner, I. Papousek, J. J. Batzel, A. Roessler, H. Scharfetter, and H. Hinghofer-Szalkay, “Phase synchronization of hemodynamic variables and respiration during mental challenge,” *International journal of psychophysiology*, vol. 79, no. 3, pp. 401–409, 2011.
- [89] J. Taelman, S. Vandeput, E. Vlemincx, A. Spaepen, and S. Van Huffel, “Instantaneous changes in heart rate regulation due to mental load in simulated office work,” *European journal of applied physiology*, vol. 111, no. 7, pp. 1497–1505, 2011.
- [90] M. Traina, A. Cataldo, F. Galullo, and G. Russo, “heart rate variability in healthy subjects,” *Minerva Psichiatr*, vol. 52, no. 4, pp. 227–231, 2011.
- [91] Z. Visnovcova, M. Mestanik, M. Javorcka, D. Mokra, M. Gala, A. Jurko, A. Calkovska, and I. Tonhajzerova, “Complexity and time asymmetry of heart rate variability are altered in acute mental stress,” *Physiological measurement*, vol. 35, no. 7, p. 1319, 2014.
- [92] R. González-Camarena, S. Carrasco-Sosa, R. Román-Ramos, M. J. Gaitán-González, V. Medina-Bañuelos, and J. Azpiroz-Leehan, “Effect of static and dynamic exercise on heart rate and blood pressure variabilities.” *Medicine and science in sports and exercise*, vol. 32, no. 10, pp. 1719–1728, 2000.

-
- [93] L. Salahuddin, J. Cho, M. G. Jeong, and D. Kim, “Ultra short term analysis of heart rate variability for monitoring mental stress in mobile settings,” in *2007 29th annual international conference of the ieee engineering in medicine and biology society*. IEEE, 2007, pp. 4656–4659.
- [94] R. Costin, C. Rotariu, and A. Pasarica, “Mental stress detection using heart rate variability and morphologic variability of eeg signals,” in *2012 International Conference and Exposition on Electrical and Power Engineering*. IEEE, 2012, pp. 591–596.
- [95] H. Ruediger, R. Seibt, K. Scheuch, M. Krause, and S. Alam, “Sympathetic and parasympathetic activation in heart rate variability in male hypertensive patients under mental stress,” *Journal of human hypertension*, vol. 18, no. 5, pp. 307–315, 2004.
- [96] N. Owen and A. Steptoe, “Natural killer cell and proinflammatory cytokine responses to mental stress: associations with heart rate and heart rate variability,” *Biological psychology*, vol. 63, no. 2, pp. 101–115, 2003.
- [97] F. Custodis, K. Gertz, M. Balkaya, V. Prinz, I. Mathar, C. Stamm, G. Kronenberg, A. Kazakov, M. Freichel, M. Böhm *et al.*, “Heart rate contributes to the vascular effects of chronic mental stress: effects on endothelial function and ischemic brain injury in mice,” *Stroke*, vol. 42, no. 6, pp. 1742–1749, 2011.
- [98] X. Jouven, P. J. Schwartz, S. Escolano, C. Straczek, M. Tafflet, M. Desnos, J. P. Empana, and P. Ducimetière, “Excessive heart rate increase during mild mental stress in preparation for exercise predicts sudden death in the general population,” *European heart journal*, vol. 30, no. 14, pp. 1703–1710, 2009.
- [99] A. Yadav, N. Awasthi, K. Gaur, and K. Yadav, “Comparison of heart rate variability during physical and mental stress in type ‘A’ and type ‘B’ per-

- sonality: An interventional study,” *International Multispecialty Journal of Health (IMJH)*, vol. 5, no. 8, pp. 133–140, 2019.
- [100] I. Papousek, K. Nauschnegg, M. Paechter, H. K. Lackner, N. Goswami, and G. Schuler, “Trait and state positive affect and cardiovascular recovery from experimental academic stress,” *Biological Psychology*, vol. 83, no. 2, pp. 108–115, 2010.
- [101] C. A. Melzig, A. I. Weike, A. O. Hamm, and J. F. Thayer, “Individual differences in fear-potentiated startle as a function of resting heart rate variability: implications for panic disorder,” *International Journal of Psychophysiology*, vol. 71, no. 2, pp. 109–117, 2009.
- [102] M. Hauschildt, M. J. Peters, S. Moritz, and L. Jelinek, “Heart rate variability in response to affective scenes in posttraumatic stress disorder,” *Biological Psychology*, vol. 88, no. 2-3, pp. 215–222, 2011.
- [103] N. Lakusic, K. Fuckar, D. Mahovic, D. Cerovec, M. Majsec, and N. Stancin, “Characteristics of heart rate variability in war veterans with post-traumatic stress disorder after myocardial infarction,” *Military Medicine*, vol. 172, no. 11, pp. 1190–1193, 2007.
- [104] L. Guédon-Moreau, F. Ducrocq, S. Molenda, S. Duhem, J. Salleron, I. Chaudieu, D. Bert, C. Libersa, G. Vaiva *et al.*, “Temporal analysis of heart rate variability as a predictor of post traumatic stress disorder in road traffic accidents survivors,” *Journal of psychiatric research*, vol. 46, no. 6, pp. 790–796, 2012.
- [105] G. A. Alvares, D. S. Quintana, A. H. Kemp, A. Van Zwieten, B. W. Balleine, I. B. Hickie, and A. J. Guastella, “Reduced heart rate variability in social anxiety disorder: associations with gender and symptom severity,” *PloS one*, vol. 8, no. 7, p. e70468, 2013.

-
- [106] E. Martens, I. Nyklicek, B. Szabo, and N. Kupper, “Depression and anxiety as predictors of heart rate variability after myocardial infarction,” *Psychological medicine*, vol. 38, no. 3, pp. 375–383, 2008.
- [107] S. A. Paritala, “Effects of physical and mental tasks on heart rate variability,” *Louisiana State University Master’s Theses*, pp. 1–85, 2009.
- [108] P. Melillo, N. De Luca, M. Bracale, and L. Pecchia, “Classification tree for risk assessment in patients suffering from congestive heart failure via long-term heart rate variability,” *IEEE journal of biomedical and health informatics*, vol. 17, no. 3, pp. 727–733, 2013.
- [109] P. Melillo, R. Izzo, N. De Luca, and L. Pecchia, “Heart rate variability and target organ damage in hypertensive patients,” *BMC cardiovascular disorders*, vol. 12, no. 1, pp. 1–11, 2012.
- [110] D. Herzig, P. Eser, X. Omlin, R. Riener, M. Wilhelm, and P. Achermann, “Reproducibility of heart rate variability is parameter and sleep stage dependent,” *Frontiers in physiology*, vol. 8, pp. 1–10, 2018.
- [111] A. Padole and V. V. Ingale, “Investigating effect of sleep and meditation on HRV and classification using ANN,” in *2019 10th International Conference on Computing, Communication and Networking Technologies (ICCCNT)*. IEEE, 2019, pp. 1–6.
- [112] M. Arslan, M. O. Welcome, and S. Dane, “The effect of sleep deprivation on heart rate variability in shift nurses,” *Journal of Research in Medical and Dental Science*, vol. 7, no. 5, pp. 45–52, 2019.
- [113] Á. R. Súdý, K. Ella, R. Bódizs, and K. Káldi, “Association of social jet-lag with sleep quality and autonomic cardiac control during sleep in young healthy men,” *Frontiers in neuroscience*, vol. 13, pp. 1–10, 2019.

- [114] E. Hynynen, V. Vesterinen, H. Rusko, and A. Nummela, “Effects of moderate and heavy endurance exercise on nocturnal HRV,” *International journal of sports medicine*, vol. 31, no. 6, pp. 428–432, 2010.
- [115] D. V. James, S. C. Munson, S. Maldonado-Martin, and M. B. De Ste Croix, “Heart rate variability: Effect of exercise intensity on postexercise response,” *Research quarterly for exercise and sport*, vol. 83, no. 4, pp. 533–539, 2012.
- [116] K. P. Davy, C. A. Desouza, P. P. Jones, and D. R. Seals, “Elevated heart rate variability in physically active young and older adult women,” *Clinical Science*, vol. 94, no. 6, pp. 579–584, 1998.
- [117] G. Zuanetti, R. Latini, J. M. Neilson, and Schwartz, “Heart rate variability in patients with ventricular arrhythmias: effect of antiarrhythmic drugs,” *Journal of the American College of Cardiology*, vol. 17, no. 3, pp. 604–612, 1991.
- [118] F. Murgia, R. Melotti, L. Foco, M. Gögele, V. Meraviglia, B. Motta, A. Steger, M. Toiff, D. Sinnecker, A. Müller *et al.*, “Effects of smoking status, history and intensity on heart rate variability in the general population: The chris study,” *Plos one*, vol. 14, no. 4, pp. 1–17, 2019.
- [119] H. A. Young, A. L. Cousins, H. T. Watkins, and D. Benton, “Is the link between depressed mood and heart rate variability explained by disinhibited eating and diet?” *Biological psychology*, vol. 123, pp. 94–102, 2017.
- [120] R. Latha, S. Srikanth, H. Sairaman, and N. R. E. Dity, “Effect of music on heart rate variability and stress in medical students,” *International Journal of Clinical and Experimental Physiology*, vol. 1, no. 2, pp. 131–134, 2014.
- [121] J. J. Sollers, T. A. Sanford, R. Nabors-Oberg, C. A. Anderson, and J. F. Thayer, “Examining changes in HRV in response to varying ambient temperature,” *IEEE engineering in medicine and biology magazine*, vol. 21, no. 4, pp. 30–34, 2002.

-
- [122] H. Shin, “Ambient temperature effect on pulse rate variability as an alternative to heart rate variability in young adult,” *Journal of clinical monitoring and computing*, vol. 30, no. 6, pp. 939–948, 2016.
- [123] L. Mourot, M. Bouhaddi, E. Gandelin, S. Cappelle, G. Dumoulin, J.-P. Wolf, J. D. Rouillon, and J. Regnard, “Cardiovascular autonomic control during short-term thermoneutral and cool head-out immersion,” *Aviation, space, and environmental medicine*, vol. 79, no. 1, pp. 14–20, 2008.
- [124] H. C Choo, K. Nosaka, J. J Peiffer, M. Ihsan, C. C Yeo, and C. R Abbiss, “Effect of water immersion temperature on heart rate variability following exercise in the heat,” *Kinesiology*, vol. 50, no. Supplement 1., pp. 67–74, 2018.
- [125] Y. Kataoka and F. Yoshida, “The change of hemodynamics and heart rate variability on bathing by the gap of water temperature,” *Biomedicine & pharmacotherapy*, vol. 59, pp. S92–S99, 2005.
- [126] F. Edelhäuser, S. Goebel, C. Scheffer, and D. Cysarz, “P02. 181. heart rate variability and peripheral temperature during whole body immersion at different water temperatures,” *BMC Complementary and Alternative Medicine*, vol. 12, no. 1, pp. 1–1, 2012.
- [127] V. K. Murthy, T. M. Grove, G. A. Harvey, and L. J. Haywood, “Clinical usefulness of ecg frequency spectrum analysis,” in *The Second Annual Symposium on Computer Application in Medical Care, 1978. Proceedings.* IEEE, 1978, pp. 610–612.
- [128] “Data resource: nippon.com.” URL=<https://www.nippon.com/ja/japan-data/h00623/>, 2020.
- [129] L. S. Lilly, *Pathophysiology of heart disease: a collaborative project of medical students and faculty.* Lippincott Williams & Wilkins, 2012.

- [130] L. Biel, O. Pettersson, L. Philipson, and P. Wide, “ECG analysis: a new approach in human identification,” in *IMTC/99. Proceedings of the 16th IEEE Instrumentation and Measurement Technology Conference (Cat. No. 99CH36309)*, vol. 1. IEEE, 1999, pp. 557–561.
- [131] S. Z. Fatemian and D. Hatzinakos, “A new ECG feature extractor for biometric recognition,” in *2009 16th international conference on digital signal processing*. IEEE, 2009, pp. 1–6.
- [132] C.-C. Chiu, C.-M. Chuang, and C.-Y. Hsu, “A novel personal identity verification approach using a discrete wavelet transform of the ECG signal,” in *2008 International Conference on Multimedia and Ubiquitous Engineering (mue 2008)*. IEEE, 2008, pp. 201–206.
- [133] T. Choudhary and M. S. Manikandan, “A novel unified framework for noise-robust ECG-based biometric authentication,” in *2015 2nd International Conference on Signal Processing and Integrated Networks (SPIN)*. IEEE, 2015, pp. 186–191.
- [134] H.-S. Choi, B. Lee, and S. Yoon, “Biometric authentication using noisy electrocardiograms acquired by mobile sensors,” *IEEE Access*, vol. 4, pp. 1266–1273, 2016.
- [135] F. Porée, A. Gallix, and G. Carrault, “Biometric identification of individuals based on the ECG. which conditions?” in *2011 Computing in Cardiology*. IEEE, 2011, pp. 761–764.
- [136] Y. Gahi, M. Lamrani, A. Zoglat, M. Guennoun, B. Kapralos, and K. El-Khatib, “Biometric identification system based on electrocardiogram data,” in *2008 New Technologies, Mobility and Security*. IEEE, 2008, pp. 1–5.
- [137] W. Louis, M. Komeili, and D. Hatzinakos, “Continuous authentication using one-dimensional multi-resolution local binary patterns (1DMRLBP) in

-
- ECG biometrics,” *IEEE Transactions on Information Forensics and Security*, vol. 11, no. 12, pp. 2818–2832, 2016.
- [138] M.-G. Kim and S. B. Pan, “Deep learning based on 1-d ensemble networks using ECG for real-time user recognition,” *IEEE Transactions on Industrial Informatics*, vol. 15, no. 10, pp. 5656–5663, 2019.
- [139] J. S. Arteaga-Falconi, H. Al Osman, and A. El Saddik, “ECG authentication for mobile devices,” *IEEE Transactions on Instrumentation and Measurement*, vol. 65, no. 3, pp. 591–600, 2015.
- [140] S. J. Kang, S. Y. Lee, H. I. Cho, and H. Park, “ECG authentication system design based on signal analysis in mobile and wearable devices,” *IEEE Signal Processing Letters*, vol. 23, no. 6, pp. 805–808, 2016.
- [141] C.-M. Ting and S.-H. Salleh, “ECG based personal identification using extended kalman filter,” in *10th International Conference on Information Science, Signal Processing and their Applications (ISSPA 2010)*. IEEE, 2010, pp. 774–777.
- [142] F. Agrafioti and D. Hatzinakos, “ECG based recognition using second order statistics,” in *6th Annual Communication Networks and Services Research Conference (cnsr 2008)*. IEEE, 2008, pp. 82–87.
- [143] S. Osowski and T. H. Linh, “ECG beat recognition using fuzzy hybrid neural network,” *IEEE Transactions on Biomedical Engineering*, vol. 48, no. 11, pp. 1265–1271, 2001.
- [144] K. N. Plataniotis, D. Hatzinakos, and J. K. Lee, “ECG biometric recognition without fiducial detection,” in *2006 Biometrics symposium: Special session on research at the biometric consortium conference*. IEEE, 2006, pp. 1–6.
- [145] J. Xu, T. Li, Y. Chen, and W. Chen, “Personal identification by convolutional neural network with ECG signal,” in *2018 International Confer-*

- ence on Information and Communication Technology Convergence (ICTC)*. IEEE, 2018, pp. 559–563.
- [146] T.-H. Yen, C.-Y. Chang, and S.-N. Yu, “A portable real-time ECG recognition system based on smartphone,” in *2013 35th Annual International Conference of the IEEE Engineering in Medicine and Biology Society (EMBC)*. IEEE, 2013, pp. 7262–7265.
- [147] J. S. Arteaga Falconi, “ECG authentication for mobile device,” Ph.D. dissertation, Université d’Ottawa/University of Ottawa, 2013.
- [148] A. F. Hussein, A. K. AlZubaidi, A. Al-Bayaty, and Q. A. Habash, “An iot real-time biometric authentication system based on ECG fiducial extracted features using discrete cosine transform,” *arXiv preprint arXiv:1708.08189*, 2017.
- [149] D. P. Coutinho, A. L. Fred, and M. A. Figueiredo, “One-lead ECG-based personal identification using ziv-merhav cross parsing,” in *2010 20th International Conference on Pattern Recognition*. IEEE, 2010, pp. 3858–3861.
- [150] M. Li and S. Narayanan, “Robust ECG biometrics by fusing temporal and cepstral information,” in *2010 20th International Conference on Pattern Recognition*. IEEE, 2010, pp. 1326–1329.
- [151] A. Lourenço, H. Silva, and A. Fred, “Unveiling the biometric potential of finger-based ECG signals,” *Computational intelligence and neuroscience*, vol. 1, pp. 1–9, 2011.
- [152] I. Odinaka, P.-H. Lai, A. D. Kaplan, J. A. O’Sullivan, E. J. Sirevaag, S. D. Kristjansson, A. K. Sheffield, and J. W. Rohrbaugh, “ECG biometrics: A robust short-time frequency analysis,” in *2010 IEEE International Workshop on Information Forensics and Security*. IEEE, 2010, pp. 1–6.

- [153] B.-H. Kim and J.-Y. Pyun, "ECG identification for personal authentication using lstm-based deep recurrent neural networks," *Sensors*, vol. 20, no. 11, pp. 1–17, 2020.
- [154] H. M. Lynn, S. B. Pan, and P. Kim, "A deep bidirectional gru network model for biometric electrocardiogram classification based on recurrent neural networks," *IEEE Access*, vol. 7, pp. 1–11, 2019.
- [155] P. Melillo, M. Bracale, and L. Pecchia, "Nonlinear heart rate variability features for real-life stress detection. case study: students under stress due to university examination," *Biomedical engineering online*, vol. 10, no. 1, pp. 1–13, 2011.